SEISMIC PERFORMANCE OF TIMBER-STEEL HYBRID SYSTEMS WITH INFILLED PLYWOOD SHEAR WALLS

Darren Kho

A Thesis in partial fulfilment of the requirements for the Degree of Masters of Engineering

September 2018

This thesis is dedicated to my parents and my sister.

"Who dares wins." – NZSAS

ABSTRACT

Timber-steel hybrid structures provide a viable solution to strengthen lateral load resisting systems in multi-storey light timber framed buildings. This thesis investigated cyclic behaviour of one type of timber-steel hybrid wall systems consisting of steel moment resisting frames infilled with plywood shear walls. A detailed finite element model was developed to model the hybrid wall behavior under cyclic loading. The hysteretic parameters of critical connection elements were calibrated by experimental testing results. Using the validated hybrid wall model, a parametric study was further conducted to investigate the effect of nail size, plywood thickness, bolt size and steel moment frame section sizes on the hybrid wall behavior. Overall, the hybridization of the steel moment frame and the plywood infill walls can provide significantly better performance compared with conventional plywood shear walls. Based on the results of the parametric studies, a brief design guide with a worked example was developed to assist structural engineers to use this type of timber-steel hybrid shear walls in muilti-storey timber buildings.

ACKNOWLEDGEMENTS

Many people have contriuted to the successful completion of this research. First among them is my advisor, Dr. Minghao Li, who shared the idea for this thesis, and gave guidance along the way. I am grateful for the many opportunities Dr. Li afforded to me to present and publish our research along the way.

The support of Alan Poynter, Russell McConchie and the Department of Civil & Natural Resources for the laboratory time, procuring test materials and a source of wonderful enthusiasm.

My friend and mentor Wenchen Dong, who painstakingly tutored me in numerical modelling, illuminating my way through the rigamaroles of computer coding. Your support and suggestions were a treasure.

The leadership of Tim and Laura Bateman, for providing an invaluable tool for work-life balance (a sensory deprivation float tank), and arguably the best part-time job I could ask for. Thank you for reminding me of the importance of pursuing one's dreams.

The podcasts of Joe Rogan, Jocko Willink and Dr. Jordan B. Peterson, which I consumed voraciously, while for providing much wisdom, inspiration and entertainment along the way.

Lastly, I am forever grateful to my parents, Kho Bok Choon and Bernice Chew for instilling my moral values and character; teaching me the value of hard work and education. My sister for her patient 'mentorship' both in our childhood and now.

To my friends, who took me surfing, and practiced brazilian jiu jitsu with me. The social interaction combined with physical exertion was paramount in keeping my mental game sharp.

Funding for this research was provided by the EQC Earthquake Commission.

CONTENTS

LIST OF TABLES

LIST OF FIGURES

LIST OF ABBREVIATIONS AND ACRONYMS

μ	=	Structural ductility
CLT	=	Cross laminated timber
E	=	Modulus of Elasticity
E_{diss}	=	Total energy dissipation
E_{lb}	=	Lower bound Modulus of Elasticity
E_{loop}	=	Energy dissipated by the actual non-linear wall
E_{so}	=	Strain energy of the linear-elastic system at the target displacement
E_x	=	Modulus of Elasticity in the x-direction
E_y	=	Modulus of Elasticity in the y-direction
EYM	=	European Yield Model
$F_{1\text{-}3}$	=	Percentage of strength degradation under cyclic testing
f_b	=	Bending strength
f_c	=	Compression strength parallel to grain
F_{est}	=	Estimated maximum force resisted
F_{max}	=	Maximum force resisted
F_o	=	Y-intercept of post-yield stiffness line
f_p	=	Compression strength perpendicular to grain
f_{pb}	=	Bending strength
f_{pc}	=	Compression strength parallel to grain
f_{pp}	=	Compression strength perpendicular to grain
f_{pr}	=	Rolling shear strength
f_{ps}	=	Panel shear strength
f_t	=	Tension strength
f_{ult}	=	Ultimate force resisted
F_y	=	Yield Force
GPa	=	Gigapascals
k_1	=	Initial stiffness
k_2	=	Post-yield stiffness

k_3 = Degradation stiffness

k_4 = Unloading stiffness

k_{hybrid} = Initial stiffness of hybrid system

k_{infill} = Infill wall stiffness

kN = Kilonewton

k_{rot} = Rotational stiffness

K_s = Secant stiffness

L_4 = Distance between supports an Four-point bending test

LTF = light-timber frame

MPa = Megapascals

M_y = Yield moment

Nm = Newton meters

OSB = orientated strand board

P_I = Pinching force

$P_{infill,\ peak}$ = Peak load resisted by infill wall

P_{peak} = Peak load resisted by hybrid system

P_{yield} = Yield force of the timber-steel hybrid shear wall

R = Relative infill-to-frame stiffness ratio

T_1 = Fundamental natural period

t_p = Thickness of panel/sheathing

v_{ult} = Ultimate displacement in connection testing

Z = Section Modulus

α_{LD} = Reloading degradation factor

α_{UN} = Unloading degradation factor

β = Stiffness degradation factor

Δ_{fail} = Displacement at failure

Δ_{max} = Maximum displacement

Δ_t = Target displacement

Δ_{ult} = Ultimate displacement for walls

Δ_y = Yield displacement

δ_{yield} = Yield displacement

ε_p = Plastic strain

ξ_{el} = Elastic viscous damping

ξ_{eq} = Equivalent viscous damping

ξ_{hyst} = Hysteretic viscous damping

ρ = Density

σ_y = Yield stress

σ_{yp} = Plastic strain

LIST OF APPENDICES

1 INTRODUCTION

In New Zealand, current standard NZS3604:2011 for timber-framed buildings only allows light timber framed (LTF) buildings up to a maximum of 2 or 3 storeys. Due to limited strength and stiffness of conventional LTF shear walls braced by gypsum boards or plywood, LTF construction is uncommon to build multi-storey residential buildings in New Zealand. The introduction of timber-steel hybrid structural system however, can provide a viable and efficient solution for lateral load resisting systems for multi-storey timber buildings for seismic regions.

The timber-steel hybrid system studied in this thesis combines conventional steel moment frames and plywood shear walls, producing a stronger, stiffer, and more ductile lateral load resisting system, when compared to conventional LTF construction. This hybridization uses a relatively simple construction technology by using existing construction materials in the New Zealand market. Therefore, in theory, the timber-steel hybrid shear walls can be effectively integrated into New Zealand's existing LTF construction methods without much construction difficulty.

Furthermore, the increased use of timber materials in taller building systems will improve the sustainability of the built environment while also benefiting New Zealand's forestry industry.

1.1 Research Motivation and Objectives

The key objective of this research is to deliver a hybrid shear wall solution for multi-storey timber buildings for seismically active regions such as New Zealand. This will be achieved by meeting the following objectives.

- Undertake an experimental testing campaign to assess the performance of the critical connections in the timber-steel hybrid shearwall system.
- Develop a finite element model of the timber-steel hybrid shear wall system and conduct a parametric study of the system's response under cyclic loading.
- Provide a design example to demonstrate the application of the hybrid systems in multi-storey LTF buildings.

1.2 Organisation

Chapter 2 presents literature survey of previous experimental and numerical research efforts on timber-steel hybrid systems and key findings are summarised.

Chapter 3 describes experimental testing of critical connections in the timber-steel hybrid shear wall system. Details of the construction and fabrication of the joints are given. Results of the testing campaign are presented, and observed behaviour of each joint is given in-detail. Key details of each joint's performance are determined in terms of strength, stiffness, and ductility etc.

Chapter 4 describes the numerical modelling of the timber-steel hybrid shear wall system. In addition, a parametric study has been undertaken to study the performance of the hybrid shear wall with various design parameters such as the connection types and steel frame sizes.

Chapter 5 presents a design example of the hybrid system within multi-storey timber buildings. Force based and dispalcement-based seismic design approaches are followed.

Chapter 6 concludes the thesis with a summary.

2 LITERATURE REVIEW

This chapter introduces the concept of a timber-steel hybrid shear wall and previous research conducted on the hybrid system.

2.1 The case for multi-storey timber buildings

Global demand for multi-storey LTF buildings is increasing (Carradine, 2014). In North America, allowable heights for LTF have been increased to 6 storeys within seismic regions. Several reasons exist for the increased use of timber in buildings, with environmental and economic advantages at the forefront. Another driving factor pushing the height of LTF buildings to a new limit is to meet the rising housing demand - caused by increased populations in big cities. In New Zealand, particularly in Auckland, the gap between housing demand and supply is also increasing.

Observations following the 2010 and 2011 Canterbury earthquakes have provided ample evidence that most of low-rise LTF houses can provide adequate strength to resist severe earthquake loading without collapse (Buchanan et al, 2011). In New Zealand, the forestry industry through plantation forests provides large amounts of cost-effective contruction materials and is the 3rd largest export earner. (MPI, 2018). Thus, LTF construction also has great potential for meeting the increased housing demand for multi-storey residential buildings in New Zealand, as long as the structural limitations of the conventional LTF systems can be overcome.

Other countries such as the U.S. and Canada have provided design guidance and specifications on LTF buildings up to six storeys. But due to different design practices and legislation requirements, they cannot be directly translated to the New Zealand building context. If mid-rise LTF buildings are to satisfy building regulations in New Zealand, solutions to enhance the lateral capacity of conventional LTF buildings need to be provided. To address this challenge, researchers have proposed solutions that combine timber with other materials through proper hybridization, allowing for a stronger lateral-load resisting system.

2.2 Timber-steel hybrid shear walls: taking the solution one step further

One hybridization method to enhance the lateral capacity of conventional LTF shear walls is through the incorporation of steel moment frames. The hybrid system studied in this thesis consists of these two subsystems; a steel moment frame and plywood infill shear walls (Figure 2-1). This thesis focuses on the cyclic behaviour of this type of hybrid shear wall.

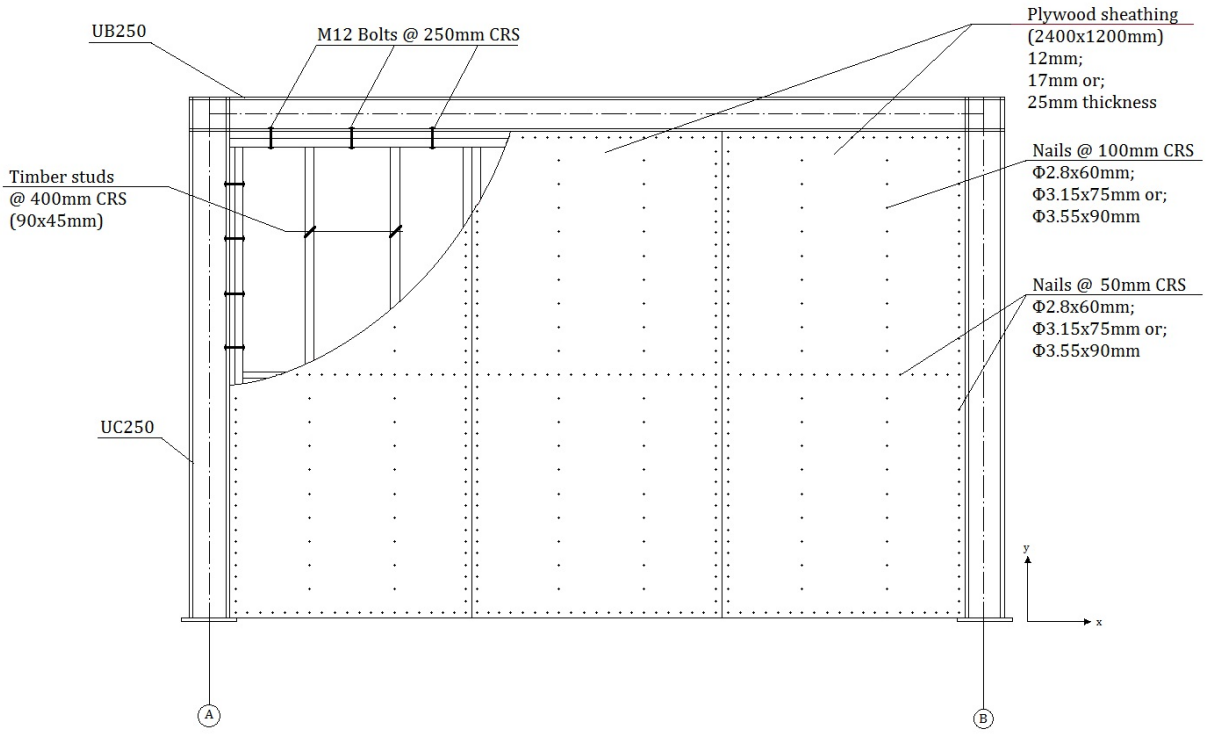

Figure 2-1: Structural configuration of a timber-steel hybrid shear wall with plywood infill walls

Within the hybrid system, two key structural connections exist: timber-sheathing connections and timber-steel connections. The timber-sheathing connections are comprised of plywood and timber framing members connected by nail fasteners. These connections provide ductility and energy dissipation for the infill wall, via nail yield bending and wood embedment deformation. The timber-steel connections, on the otherhand, are comprised of timber framing members joined to steel framing members, via bolts or screws. These connections facilitate shear transfer between the steel frame and the infill wall and ensure the load-sharing mechanism between the timber and steel subsystems.

2.3 General behaviour of timber-steel hybrid shear walls

Two different types of timber-steel hybrid shear walls have been investigated in literature: one with CLT panels and the other with OSB sheathing in the infill walls. (Dickof, 2013, He et al, 2014).

He et al (2014) conducted full-scale experimental testing on a single-storey hybrid shear wall, consisting of OSB sheathing and steel moment frames (Figure 2-2). Static pushover and reversed cyclic tests have been conducted along with subsequent parametric studies (Li et al, 2014a, 2014b). This hybrid system is quite similar to the proposed hybrid system in this study, with exception of sheathing type (OSB vs. plywood). It is therefore useful to present the findings of He et al (2014).

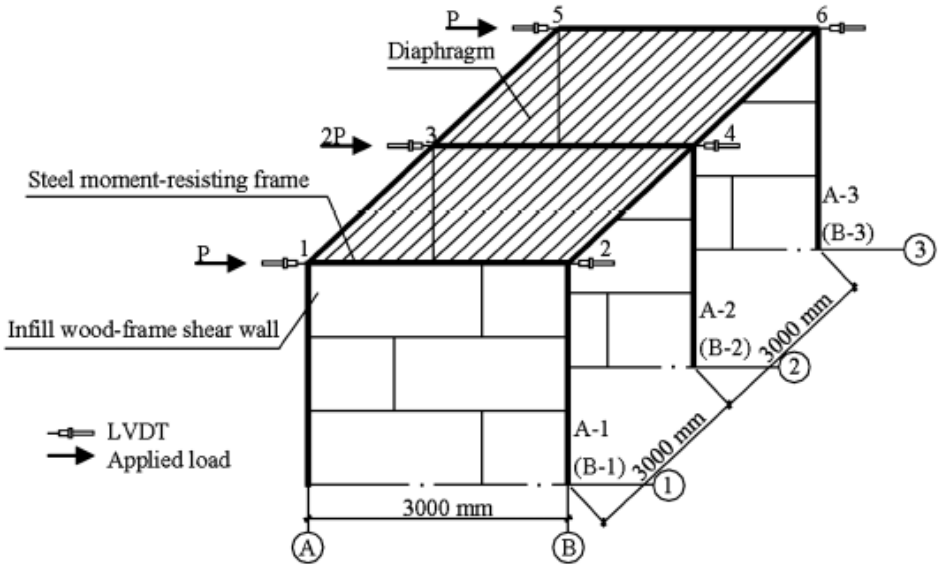

Figure 2-2: Experimental setup of the timber-steel hybrid shear wall system studied by He et al (2014)

It was found that the hybrid systems had significantly higher lateral capacity and initial stiffness than the bare steel moment frame or the infill wall working on its own. Inelastic deformation was concentrated in the nailed connections which provided seismic energy dissipation. Following failure of the LTF wall, the steel moment frame resisted the lateral load and plastic hinges formed, given that appropriate detailing was undertaken.

However, OSB sheathing is not a popular material in New Zealand. Plywood panels manufactured from Radiata Pine are widely used in New Zealand (MPI, 2014). Also other types of mechanical fasteners such as nails, bolts and screws are used in New Zealand market. Their applications in timber-steel hybrid systems have not been investigated previously and therefore are included in the research project.

2.3.1 Load-sharing and modes of failure

An example of the cyclic response of the timber-steel hybrid shear wall system obtained by the full-scale experiments conducted by He et al (2014) is shown in Figure 2-3. Percentage of load-sharing in the two subsystems throughout testing is shown in Figure 2-4.

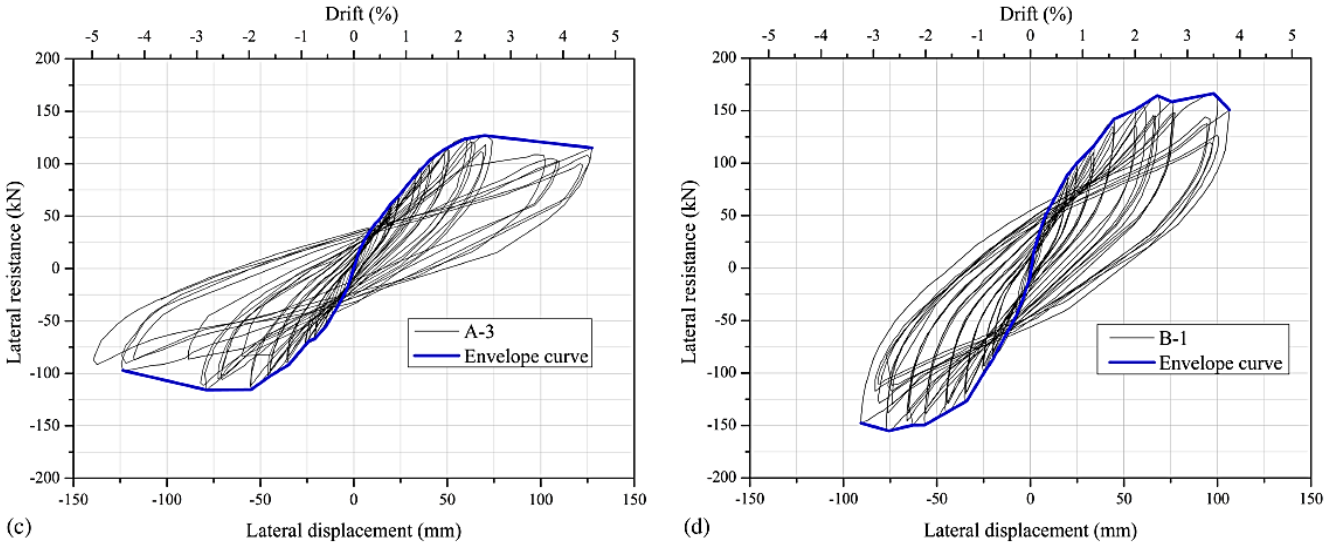

Figure 2-3: Experimental test results on full scale, single-storey timber-steel hybrid system, Li et al (2014)

The general behaviour of the hybrid system can be divided into three stages:

- Stage I: In initial stages of loading, the infill walls experience linear-elastic shear deformations and resist the majority of the lateral load. As the applied load is increased, the nailed connections of the edge on the sheathings begin to behave in a non-linear fashion. As the edge nails yield, the hybrid system experienced a level of stiffness degradation and the load carried by the infill wall decreased.
- Stage II: As greater loads are applied, more damage accumulates in the infill shear wall, resulting in further stiffness degradation of the hybrid system. The infill wall carries even less lateral load and as a consequence, more lateral load is carried by the steel frame. After the occurrence of the first yield points in the steel frame (at 0.6-0.8% drift), the infill walls became less effective.
- Stage III: Steel frame response becomes non-linear, and the structure dissipated significant amounts of energy. Failures of the nail connections spread out in the infill wall and plastic hinges formed in the steel frame members, and the steel frame carried most of the lateral loads when the drift ratio exceeded 2%.

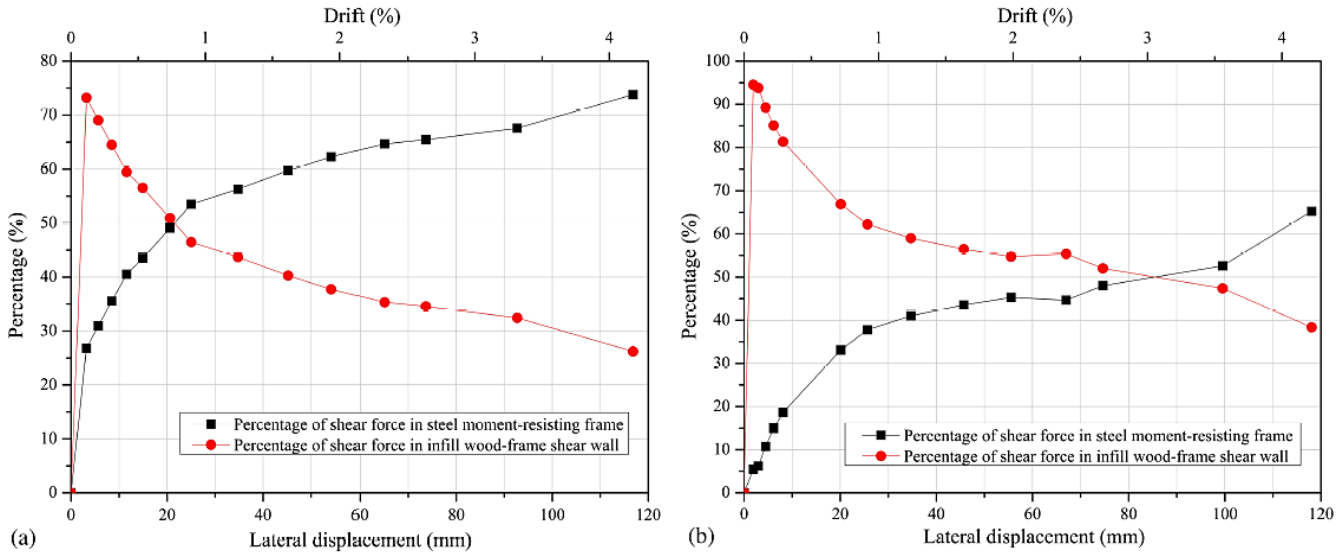

Figure 2-4: Percentage of shear force in the two subsystems: (a) structure with single sheathed infill wood-frame shear walls, (b) structure with double-sheathed infill wood-frame shear walls, He et al (2014)

Little relative displacement between timber and steel subsystems was observed. The timber-steel connections were in good condition after cyclic loading up to the specimen's ultimate limit state. No failure was found in the wood frame during the whole period of the test. Tight bolt connections between the timber and steel subsystems guaranteed them to resist lateral load together.

2.4 Parametric studies on timber-steel hybrid systems

Dickof (2012) developed a numerical model of a hybrid system consisting of steel moment frames and CLT infill walls in a commercial software package called SAP2000. Li et al (2014) developed a numerical model of a hybrid system consisting of steel moment frame and OSB-sheathed infill walls in a commercial software package called ABAQUS. Dong (2017) developed a numerical model of a hybrid system consisting of steel moment frames and plywood infill walls, also in ABAQUS software. Due to the similarities in structural configuration (particularly the interface connections) of the hybrid models developed by Li et al (2014) and Dong (2017).

2.4.1 Li et al (2014a, 2014b)

An FE Model of the experimental setup of the hybrid walls adopted by He et al (2014) was developed by Li et al (2014a, 2014b). A user-defined element based on the concept of so called pseudo-nail method was used to model the infill wall behaviour. The model predictions under cyclic displacement control loading agreed well with the experimental test data.

It was found that increases in lateral stiffness of the OSB sheathed infill wall led to proportional increases in the lateral stiffness of the hybrid system. Investigations revealed that in terms of energy dissipation, the relative infill-to-frame stiffness ratio (R ratio) should be no less than 1.0. Other important structural parameters influencing performance were investigated such as wall aspect ratio and rotational stiffness of steel beam-column joints. The hybrid system was found to have relatively high ductilty, which was observed in

both experimental and numerical tests. Results indicate that during minor earthquake loads can be carried by the infill walls within small drift ratio (0.5%). During severe earthquakes, the infill walls will carry a certain part of the shear forceand dissipate sigificant energy via irrecoverable nail deformations. Plastic hinges may also form in the steel frame.

2.4.2 Dong (2017)

Dong (2017) conducted experimental studies on 2/3 scale timber-steel hybrid shear walls which also consisted of steel moment frames and OSB infill walls.

A detailed FE model of the hybrid walls was developed in ABAQUS based on the experimental setup. The sawn timber studs and OSB sheathing were modelled as a linear elastic material. Nailed connections between the timber members and the OSB sheathing were modelled as non-linear springs using user-defined elements. The timber framing joints were modelled as hinged joints. Timber-steel connections were modelled as elastic connections. The model predictions were found to be in good agreement with the experimental test data. An investigation into cost-effectiveness and structural efficiency based on structural weight and material pricing was conducted. A six storey steel moment frame and a six storey timber-steel hybrid shear wall with the same dimensions were both subjected to the same lateral load. Based on this design load, required structural sections were calculated and the weight of materials was evaluated. It was found that under the same load, the the required steel weighed 43% less when compared to the required steel in the hybrid system. Considering that steel prices are generally higher than that of wood, this study suggests that timber-steel hybrid shear walls provide more cost-effective and structurally efficient solutions.

2.5 Connection behaviour

Key aspects of the critical connection components, behaviour and function are outlined below. Previous efforts to predict and model connection behaviour for the purposes of structural design are presented. Current test methods and standards are reviewed and the most appropriate testing protocol is selected.

2.5.1 Timber-steel interface connections

Timber-steel interface connections allow the two subsystems to work together, creating a hybrid system. An example for a bolted timber-steel connection is shown in Figure 2-5. Shear force transfer between the two subsystems is facilitated through dowel action. The more efficient the timber-steel interface connections are, the better the two subsystems will work together (He et al, 2014).

A typical load-deformation curve for a timber-steel joint is similar to the nailed connection except for the different magnitude of forces and displacements. Ideally, such a hybrid system should fully engage the load carrying capacity of the plywood infill wall. This is achieved by strong timber-steel connections in the system. In accordance with capacity design principles, these connections should not fail before the failure of ductile nailed timber-plywood connections.

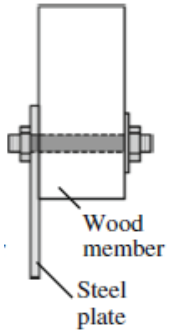

Figure 2-5: A typical timber-steel interface connection

Previous researchers have modelled timber-steel connections in timber-steel hybrid shear walls. Li et al (2014) used monotonic load-displacement data to calibrate multilinear spring elements in ABAQUS. Dong (2017) also assumed an elastic spring element based on high strength bolts such that only the elastic stage of loading was considered. For a more robust FE model, this thesis proposes to incorporate the nonlinear cyclic behavior of timber-steel connections, based on empirical data. The load-displacement curves under cyclic loading is described by the Q-Pinch model developed by Judd (2005) and is introduced to the FE model in ABAQUS as a user-defined element.

2.5.2 Timber-sheathing connections

In plywood shear walls, nailed timber-plywood connections can provide excellent ductility, allowing the wall to have inelastic deformations and dissipate energy (Timber Design Guide, Buchanan, 2007). A typical nailed timber-sheathing joint is shown in Figure 2-6. In the shear walls, deformations within the panel sheets is usually very small compared with the nail slips under shear loads.

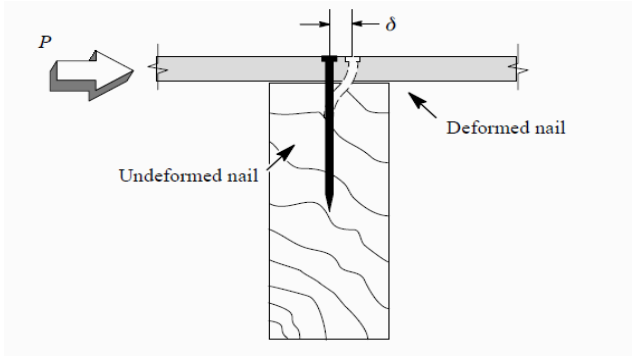

Figure 2-6: Typical nailed timber joint and mode of deformation when subjected to lateral load

Numerous investigations have been conducted into the behaviour of nailed connections in timber shear walls (Judd, 2005). The behavior of nailed connections is governed by various parameters including nail sizes, coating and penetration depth, timber density and moisture content, grain direction with respect to loading, creep effect, etc. (Steward, 1987).

2.5.3 General monotonic and cyclic response of dowel-type connections

The European Yield model (EYM) (Eurocode 5: Design of timber structures, Part 1-1: General - Common rules and rules for buildings, 1995) is widely used for the design of bolted wood connections and nailed connections , attributed to its simplicity and accuracy (Heine and Dolan, 2000). EYM is derived from general dowel – embedment internation equations and was proposed by Johansen (1949).

NZS3603:1993 on the other hand, prescribes characteristic strengths for each connection type. However, the prescribed characteristic strengths are based on a testing standard which has been superseded and only provides testing protocol for monotonic experiments, not cyclic. When loaded monotonically or cyclically, the load deformation curves of typical nailed or bolted connections are shown in Figure 2-7.

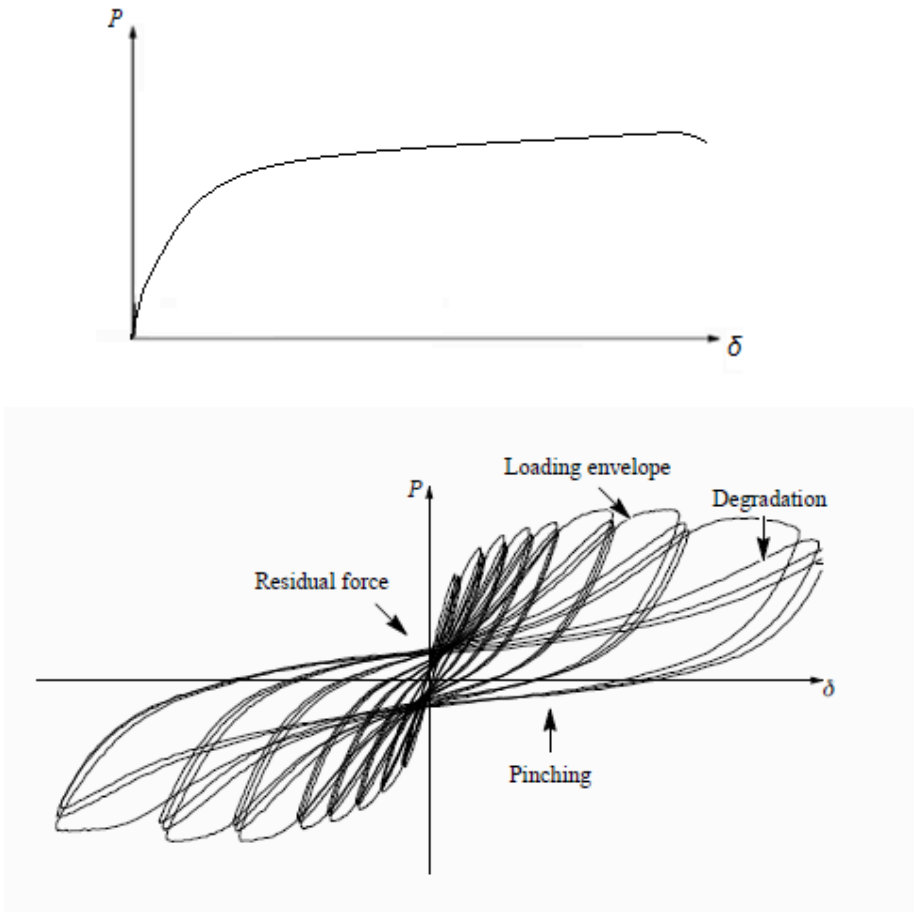

Figure 2-7: Typical load-deformation curves for laterally loaded dowel-type steel fastener under monotonic loading (above) and under cyclic loading (below). *P* = Load (kN or N), *δ* = deformation (mm).

The load-deformation response of a dowel-type connections experiences stiffness and strength degradation and pinched hysteresis behaviour under cyclic loading (Dolan and Madsen 1992). In detailed connection models, the metal connector can be modelled as an elastoplastic beam (e.g. steel nail) embedded in a layered nonlinear foundation (e.g. sheathing or framing). This approach is versatile and is capable of capturing the detailed cyclic response of a connector, however, it is computationally demanding (Folz and Filiatrault, 2001). A simpler and more efficient approach is to develop a specific hysteretic model based on a minimum number of path-following rules that can reproduce the response of the connector under general cyclic loading. A

comprehensive discussion of hysteresis models for sheathing-to-framing connections and bolted connection has been previously discussed by Foliente (1995; 1997) and Heine and Dolan (2001) respectively.

2.5.4 Analytical representations for dowel-type connections

Many researchers have proposed analytical tools to simulate the response of timber connections (Heine and Dolan, 2000). A number of input parameters are required to accurately describe a load-displacement curve. These parameters are typically derived from experimental data. Appropriate hysteresis models to describe connection behaviour has been discussed by Judd (2005). Building on previous models, Judd developed the "Q-Pinch" hysteresis model, shown in Figure 2-8. A brief explanation of the connector model and input requirements are given here.

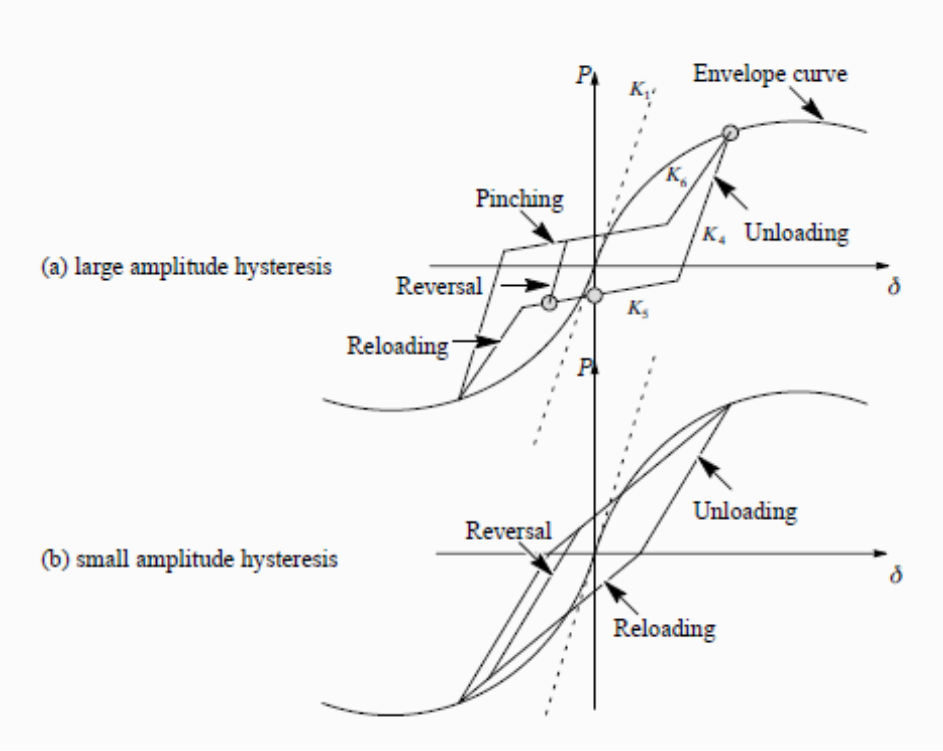

Figure 2-8: Characteristics of the Q-Pinch connector model (a) model behaviour in large amplitudes, (b) model behaviour in small amplitudes (Judd, 2005)

The model accurately reproduces the load-displacement curves of dowel-type connectors under cyclic loading. The Q-Pinch model has two modes of modelling, depending on the amplitudes of displacement protocols. For small amplitudes, the model is identical to the Q-Hyst model, developed by Saiidi and Sozen (1979), shown in Figure 2-9.

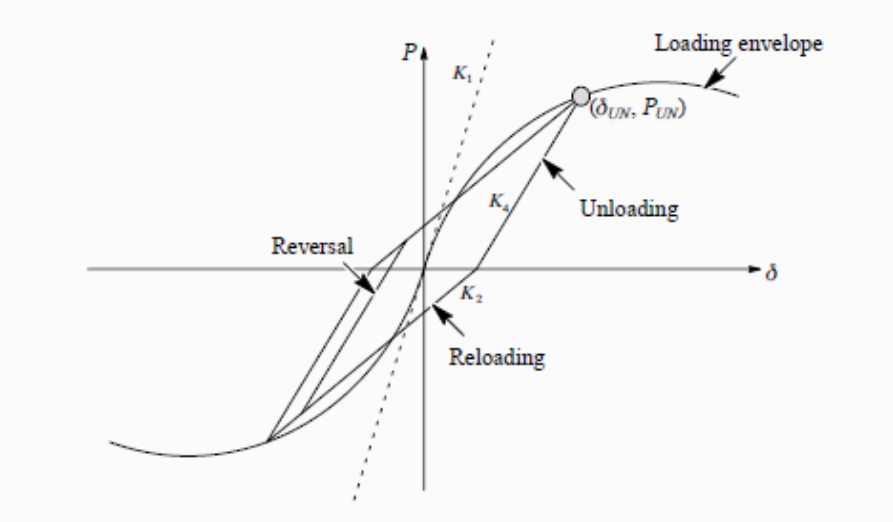

Figure 2-9: Characteristics of the Q-Hyst model (Saiidi and Sozen, 1979)

The Q-Hyst model takes into account degradation of the unloading stiffness of a connection. The Q-Hyst model requires three input parameters and uses these three to calculate the unloading and reloading stiffness of the hysteresis curve (k_4 and k_2):

k_1 = initial stiffness

δ_{yield} = yield displacement

α_{UN} = unloading degradation factor

For large amplitudes, the Q-Pinch model is adapted from the modified Stewart model, proposed by Folz and Filiatrault (2001). The modified Steward model is built upon an exponential curve used by Dolan (1989) to include the hysteretic features of a model developed my Steward (1987) to model wood frame shear walls. The modified Steward model takes into account the pinching phenomena, where a pinching force P_I corresponds to zero displacement, and the reversal load path follows the unloading stiffness.

In the Q-Pinch model, the loading first follows the envelope curve, and then unloading is defined as in the Q-Hyst model. Reloading consists of a slipping (pinching) branch and a reloading branch, like the modified Steward model. The reloading stiffness k_6 is defined by the unloading points, where $k_1 \geq k_6 \geq F_{LD}/\delta_{LD}$. The slipping branch is defined by the crossing point and the zero displacement load intercept. Degradation of the unloading and reloading stiffness (k_4 and k_6) are calculated based on the previous k_4 and k_6 values with unloading and reloading degradation factors (α_{UN}, β, and α_{LD}) applied.

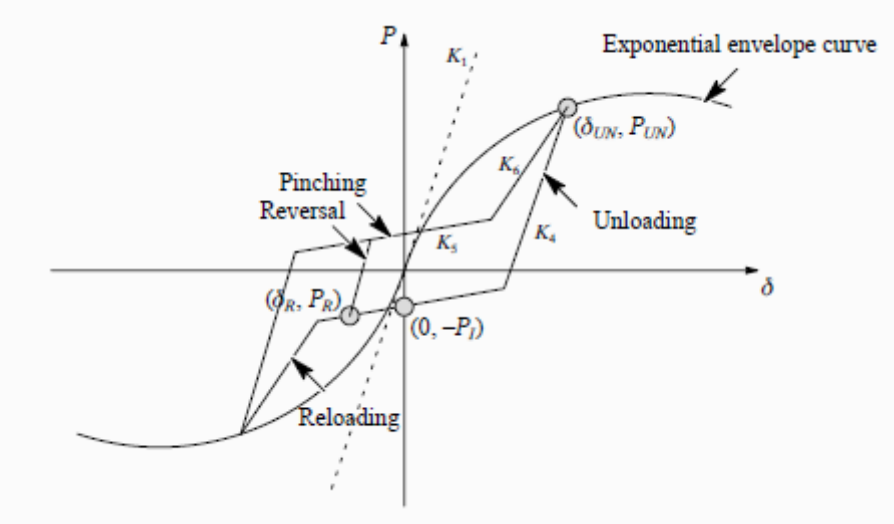

Figure 2-10: Q-Pinch hysteresis model (Judd, 2005)

The Q-Pinch model therefore requires seven input parameters:

k_1 = *initial stiffness*

k_4 = *unloading stiffness*

α_{UN} = *unloading degradation factor*

δ_{yield} = *yield displacement*

P_l = *pinching force*

β = *stiffness degradation factor*

α_{LD} = *reloading degradation factor*

This connector model has been successful implemented in ABAQUS software as a user-defined element (written in Fortan language) to accurately model the behaviour of a timber-steel hybrid system by Dong (2017). More information on the derivation of the connector models can be found in Judd (2005).

2.5.5 Connection test methods

Limited cyclic data exists for the timber-steel and timber-plywood connections required of the proposed hybrid wall system. NZS3603:1993 specifies a superseded standard AS1649 (Standards New Zealand, 1974) (*'Determination of Basic Working Loads for Metal Fasteners for Timber*,), which only provides a testing protocol for monotonic assessment of timber joints. International Standard ISO16670 (International Organization for Standardization, 2003) *('Timber Structures – Joints made with mechanical fasteners – Quasi-static reversed-cyclic test method*'), however, provides a cyclic test procedure as a basis for the development of characteristics of joints for use in seismic design.

2.6 Research Needs

Based on the literature review, it was found that limited data on the connections used in the proposed hybrid system exist. Also the experimental data with New Zealand materials, mainly Radiata pine timber and plywood, are also very limited. This study aims to develop a detailed FE model of the proposed timber-steel hybrid system using New Zealand construction materials. Therefore, there is a need to conduct experimental research to evaluate the behavior of the critical connecitons: nailed timber-plywood connecitons and steel-timber interface connections. The experimental data will be used to calibrate the model input parameters for the FE hybrid wall model. In particular, three tasks are required:

1. Cyclic testing of the timber-steel connections and nailed timber-sheathing connections in accordance with ISO16670:2003.
2. Processing the experimental data to calibrate parameters of the Q-Pinch model.
3. Incorporate the calibrated Q-Pinch model into the FE hybrid shear wall model in ABAQUS.

Based on the literature review, the existing FE model developed by Dong (2017) can be built upon to investigation the effect of variations in interface connections on the structural performance of the hybrid system. Four tasks are required to fulfil the numerical modelling needs of this research:

- Revise the FE model developed by Dong (2017) to consider typical NZ materials dimensions and configurations;
- Revisions to the base connections of the steel frame and plywood infill wall to calculate shear load contributions from the two subsystems;
- Revisions to the timber-steel and timber-sheathing connections (non-linear spring elements) to incorporate cyclic behaviour based on experimental data.
- Conduct a parametric analysis investigating the effect of plywood thickness, nail size, bolt and coach screw size, and end-stud thickness.

3 EXPERIMENTAL TESTING

This chapter describes the experimental testing campaign evaluating the performance of the critical connections in the timber-steel hybrid shearwall system. It gives details of test specimens, experimental setups and testing protocols. Test observations and experimental results are presented and discussed.

3.1 Introduction

The primary objective of this experimental campaign was to evaluate the structural performance of the critical connections in the timber-steel hybrid shearwall system under reversed cyclic loading. Critical connections include timber-steel interface connections and nailed timber-sheathing connections. Based on the load-displacement relationship, the connection behavior was assessed in terms of strength, stiffness, ductilty and strength degradation. Test matrices are presented in Tables 3-1, 3-2, and 3-3.

Three sets of experiments were conducted:

- Bending tests on bolts and coach screws. The true yield strength was determined and compared to manufacturer's documents,
- Lateral load tests on timber-steel interface connections. The study focused on the effect of variations in bolt size and stud thickness on connection performance.
- Lateral load tests on nailed timber-sheathing connections using common nails in the New Zealand market. The study focused on the effect of plywood thickness, nail diameter and nail length on connection performance.

Table 3-1: Test matrix of three-point bending tests on fasteners

Fasteners	Thread	Three-point bending test
4.6 Bolts	M10	x4
	M12	x5
4.6 Coach screws	M10	x3
	M12	x4

Table 3-2: Test matrix of timber-steel interface connections.

Fasteners (timber-steel interface)	Thread	Double Studs		Triple Studs	
		Mono	Cyclic	Mono	Cyclic
4.6 Bolts	M10	x5	x6	x5	x6
	M12	x5	x6	x5	x6
4.6 Coach screws	M10	x5	x6	x5	x6
	M12	x5	x6	x5	x6

Table 3-3: Test matrix of nailed timber-sheathing connections

Nail type (dia. x length, mm)	Parallel to grain						Perpendicular to grain					
	Mono			Cyclic			Mono			Cyclic		
	Plywood thickness			Plywood thickness			Plywood thickness			Plywood thickness		
	12mm	17mm	25mm	12mm	17mm	25mm	12mm	17mm	25mm	12mm	17mm	25mm
2.8 x 60	x5	x5	-	x6	x6	-	x5	x5	-	x6	x6	-
3.15 x 75	x5	x5	x5	x6	x6	x6	x5	x5	x5	x6	x6	x6
3.55 x 90	x5	x5	x5	x6	x6	x6	x5	x5	x5	x6	x6	x6

3.2 Bolted and coach screwed timber-steel connections

Two type of tests were conducted for the timber-steel connections: bending tests on the metal fasteners and connection tests. In this study, the considered fasteners suitable for the timber-steel interface connections were hexagon head bolts and coach screws. Figure 3-1 shows an example of the bolted interface connections to connect the flange of the steel frame members and the boundary timber framing members of the infill plywood walls.

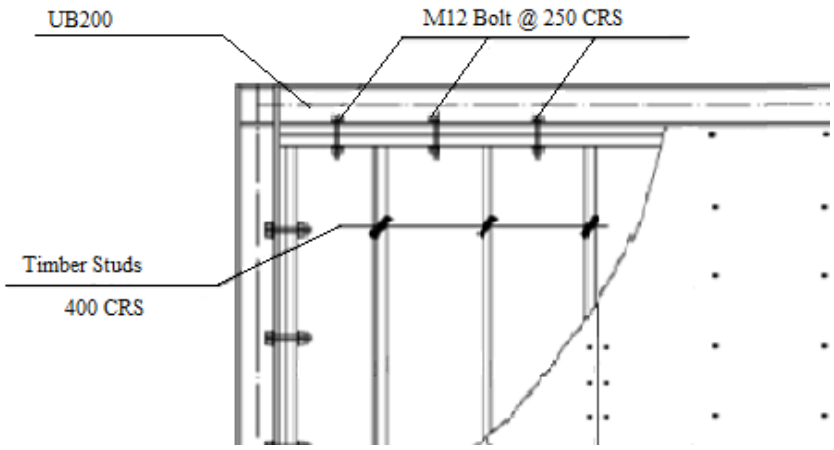

Figure 3-1: Timber-steel bolted connection in a timber-steel hybrid shearwall

3.2.1 Materials

The following bolts and coach screws (Figure 3-2) were purchased from New Zealand market.

- Grade 4.6 Mild Steel M10x180mm Bolts
- Grade 4.6 Mild Steel M12x180mm Bolts
- Grade 4.6 Mild Steel M10x180mm Coach Screws
- Grade 4.6 Mild Steel M12x180mm Coach Screws

The bolts are described as standard commercial hexagon head bolts with ISO metric threads, manufactured to the NZS/AS 1111 standard (Standards New Zealand, 1980). The coach screws are standard commercial hexagon head coach screws with ISO metric threads, manufactured to the AS/NZS 1393 standard (Standards New Zealand, 1996). The bolts and screws have Grade (or Class) 4.6 and have an average yield strength of 400MPa according to manufacturer's report. In addition, the bolts and coach screws tested were galvanized finished to the standard AS/NZS 1214 (Standards New Zealand, 2016).

Figure 3-2: Bolts and coach screws tested

Radiata Pine timber studs with Grade SG8 were sourced from New Zealand market. In New Zealand, SG grade timber are manufactured according to AS/NZS 1748 Standard (Standards New Zealand, 2011).

Table 3-4 shows the design properties of SG8 structural timber.

Table 3-4: Structural properties of Grade SG8 timber.

Bending	Compression parallel	Tension	Compression perpendicular	Modulus of Elasticity (MoE)	Lower bound MoE
f_b (MPa)	f_c (MPa)	f_t (MPa)	f_p (MPa)	E (GPa)	E_{lb} (GPa)
14.0	18.0	6.0	8.9	8.0	5.4

Moisture contents were measured with an electronic moisture gauge, and ranged from 10.0% to 14.0%. The measured average density of the timber specimens were approximately 545kg/m^3.

3.2.2 Bending tests of bolts and coach screws

The aim of the bending tests is to experimentally determine the bending yield strengths of steel fasteners used in the hybrid system.

3.2.2.1 Test method

AS/NZS/ISO 10984.1 (Standards New Zealand, 2015) prescribes two methodologies to determine the yield stress using standard bending moment tests – Method A and Method B. In this study, Method B was used and is shown in Figure 3-3.

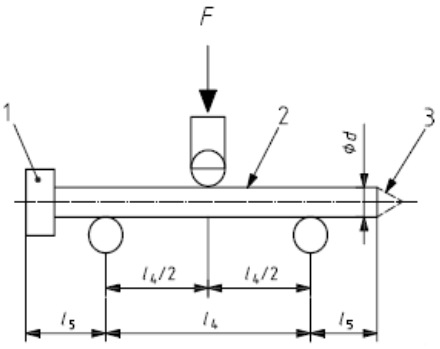

Key
1 fastener head
2 dowel-type fastener
3 pointed tip for nails and screws

Figure 3-3: Three-point bending test as per Method B (AS/NZS/ISO 10984)

As shown in Figure 3-4, the test standard determines the bending yield moment of the fastener using so called "offset yield point technique". The offset yield point is determined by fitting a straight line to the initial linear portion of the load-deformation curve, offsetting the line by 5% of the fastener diameter, and selecting the point at which the offset line intersects with the load-deformation curve.

The bending plastic yield moment of the fastener M_{yp}, is calculated by Equation (1).

$$M_{yp} = \frac{F_y l_4}{4} \quad (1)$$

Where:

F_y = Yield Force determined by the offset point technique. L_4 = the support span.

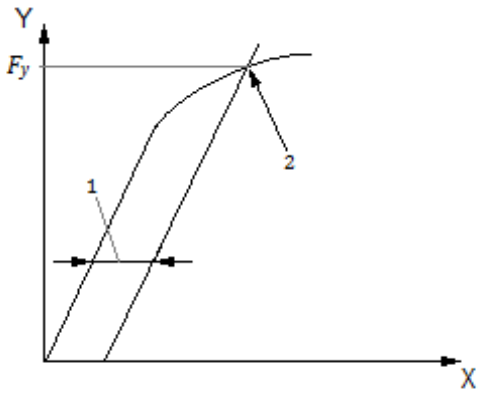

Key

X	Deformation, mm
Y	Load, N
1	5% of fastener diameter
2	Offset yield point

Figure 3-4: Typical load versus deformation curve obtained from Method B.

The yield strength, σ_y, for each fastener was determined by Eq. (2):

$$\sigma_y = \frac{M_{yp}}{Z_P} \quad (2)$$

Where:

Z_p = Plastic Section Modulus, $d^3/6$ (for circular sections)

NB: pitch diameter is used for the calculation of yield stress for coach screws.

For coach screws, the pitch diameter was applied in the calculation of the Section Modulus. For formula for pitch diameter is as follows:

$$Pitch\ diameter\ (mm) = Outer\ diameter\ (D) - depth\ of\ thread\ (h) \quad (3)$$

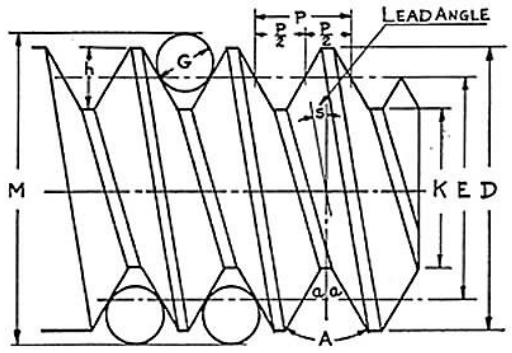

Figure 3-5: Thread dimensions in a coach screw.

The diameters of the bolts and the coach screws were meas ured at the location of loading with a digital veneer and are reported in Table 3-5 and Table 3-6 respectively.

Table 3-5: 4.6 Mild Steel M10 and M12 Bolts tested – measured diameters at the point of load

Bolt no.	M10 Bolt Measured diameter (mm)	M12 Bolt Measured diameter (mm)
1	9.92	11.89
2	9.71	11.85
3	9.95	11.83
4	9.95	11.93
5	-	11.91

Table 3-6: Mild Steel M10 and M12 Coach Screws tested – measured diameters at the point of load

Bolt no.	M10 Coach Screw			M12 Coach Screw		
	Outer diameter (mm)	Inner diameter (mm)	Pitch diameter (mm)	Outer diameter (mm)	Inner diameter (mm)	Pitch diameter (mm)
1	10.06	7.30	8.78	12.11	8.92	10.52
2	9.85	7.33	8.59	12.06	8.94	10.50
3	9.95	7.60	8.68	12.15	8.93	10.54
4	-	-	-	12.14	9.03	10.59

Figure 3-6 and Figure 3-7 show the bending tests of the coach screws. The test span was 90mm between both supports. The weak portion of the fasteners with smaller cross sections were tested in bending. Therefore, the bolts were loaded on the smooth shaft and the coach screws were loaded on the threaded section. A constant loading rate of 2mm/min was applied. The test was considered complete once the deflection of 10mm was achieved.

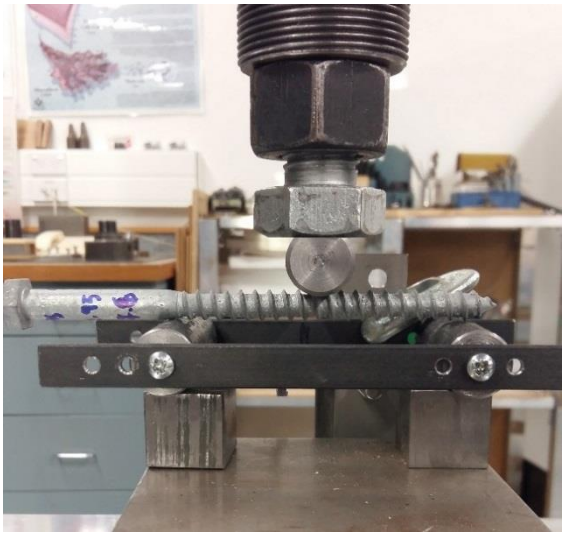

Figure 3-6: Location of loading point on coach screw.

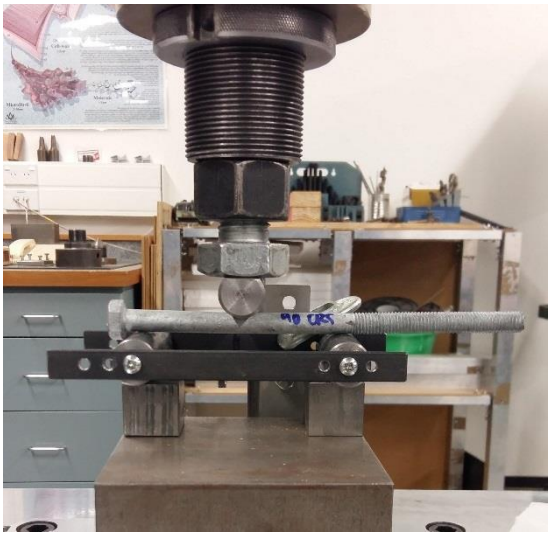

Figure 3-7: Location of loading point on bolt.

Test Results

3.2.2.2 Typical bending deformations of the bolts and screws are shown in Figure 3-8. Load-deformation plots obtained from the testing are presented in Figure 3-9 and Figure 3-10. Structural properties such as Yield Force (F_y), Yield Moment (M_{yp}) and Yield strength (σ_{yp}) of the metal fasteners summarised in

Table **3-7** - Table 3-10. A graphical comparison of Yield strengths (σ_{yp}) of each fastener is presented in Figure 3-11**.**

Figure 3-8: M12 bolt and M10 soach screw - post-test.

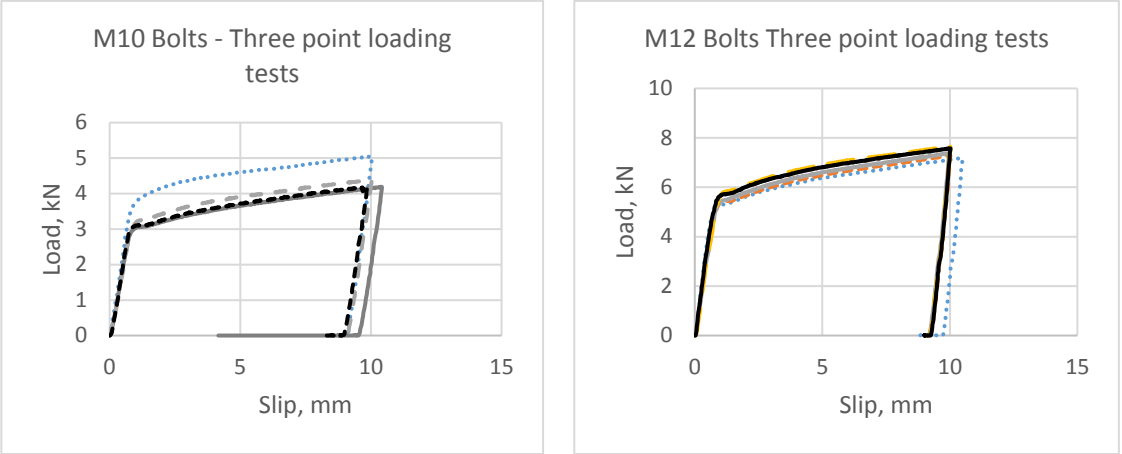

Figure 3-9: Load-deflection curve of M10 and M12 bolts

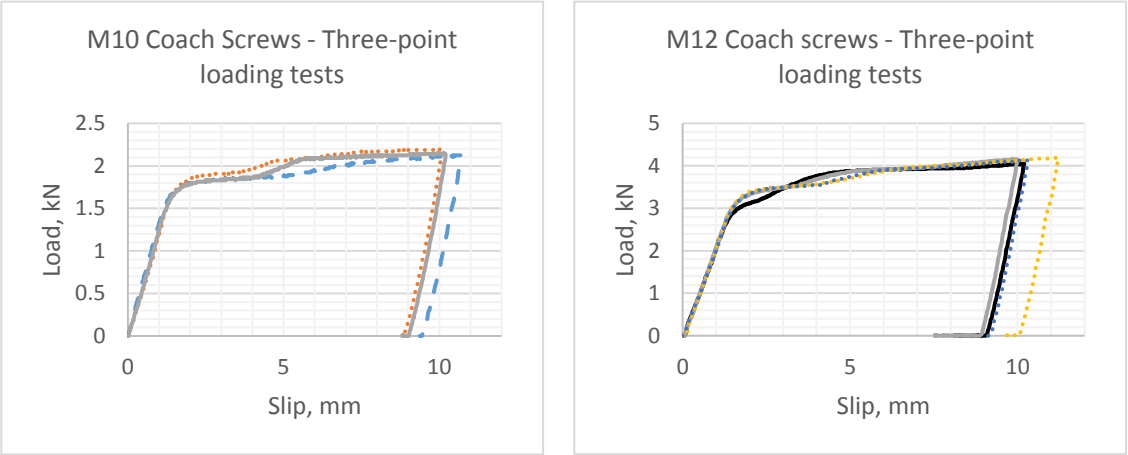

Figure 3-10: Load-deformation curves of M10 and M12 coach screws under monotonic loading

Table 3-7: Structural properties of M10 Bolts obtained through experiments.

Bolt no.	**Diameter (mm)**	**Section Modulus (Z, mm³)**	**Yield Force (F_y, kN)**	**Yield Moment (M_y, Nmm)**	**Yield strength (σ_y, MPa)**
1	9.92	162.70	3.87	87,075	535
2	9.71	152.58	3.01	67,725	444
3	9.95	164.18	3.24	72,900	444
4	9.95	164.18	3.10	69,525	424
Average*	9.87	160.91	3.12	70,050	437

**Bolt #1 is considered an outlier and as a result is not included in the calculation of the average values*.

Table 3-8: Structural properties of M12 Bolts obtained through experiments.

Bolt no.	Diameter (mm)	Section Modulus (Z, mm^3)	Yield Force (F_y, kN)	Yield Moment (M_y, Nmm)	Yield strength (σ_y, MPa)
1	11.89	280.15	5.25	118,125	422
2	11.85	277.33	5.33	119,925	432
3	11.83	275.93	5.46	122,783	445
4	11.93	275.93	5.90	132,840	481
5	11.91	275.93	5.67	127,575	462
Average	**11.88**	**277.05**	**5.52**	**124,250**	**448**

Table 3-9: Structural properties of M10 Coach Screws obtained through experiments.

Bolt no.	Diameter (mm)	Section Modulus (Z, mm^3)	Yield Force (F_y, kN)	Yield Moment (M_y, Nmm)	Yield strength (σ_y, MPa)
1	8.78	112.61	1.88	42,300	376
2	9.85	105.64	1.83	41,175	390
3	9.95	109.00	1.77	39,825	365
Average	**9.53**	**109.08**	**1.83**	**41,100**	**377**

Table 3-10: Structural properties of M12 Coach Screws obtained through experiments.

Bolt no.	Diameter (mm)	Section Modulus (Z, mm^3)	Yield Force (F_y, kN)	Yield Moment (M_y, Nmm)	Yield strength (σ_y, MPa)
1	10.52	193.77	3.73	83,925	433
2	10.50	192.94	3.40	76,388	396
3	10.54	195.15	3.36	75,488	387
4	10.59	197.66	3.11	69,975	354
Average	**10.54**	**194.88**	**3.40**	**76,444**	**393**

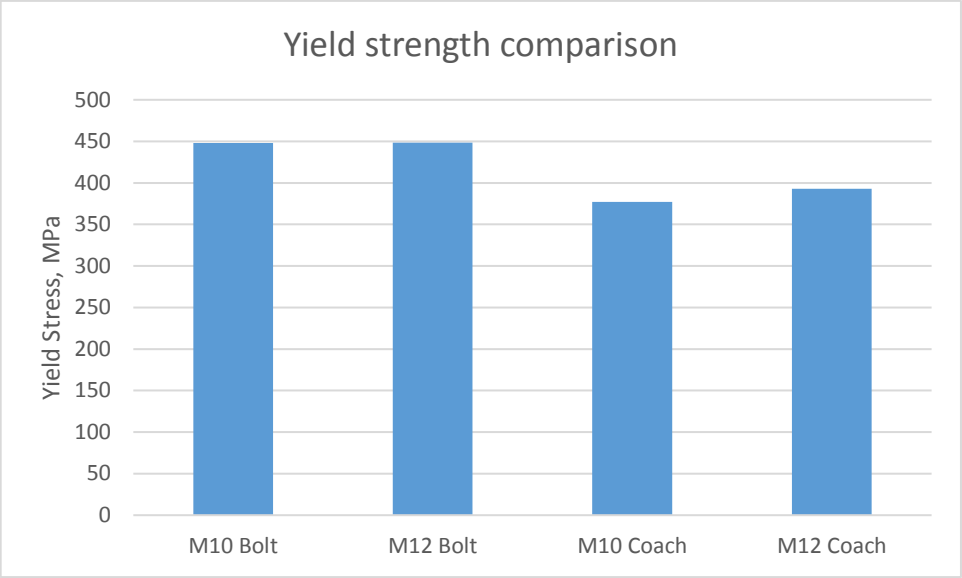

Figure 3-11: Experimentally determined Yield Stress (MPa) of commonly available steel fasteners.

Discussion

3.2.2.3 Experimentally determined yield strengths for both metal fasteners were in good agreement with the manufacturer's report. The report states yield strength of 400 MPa for the Class 4.6 Bolts and Coach Screws. The average yield strength of the tested bolts was 12% larger (448MPa) while the average yield strength of the tested coach screws was 5% smaller (393MPa). Usually, manufacturers may provide metal fasteners at slightly higher yield strengths in order to introduce a factor of safety into their products. So, it is not unsurprising to see the bolts yield at slightly larger stresses. However, the tested coach screws had a slightly lower average yield strength. It should be noted that a limited number of sample size was used in the bending tests.

3.2.3 Lateral load tests (Monotonic and Cyclic)

The monotonic and cyclic tests on the timber-steel connections are described in-detail in this section. Under the ISO16670 standard (International Organization for Standardization, 2003) , the specific cyclic

3.2.3.1 displacement-based protocol is derived from two key connection parameters: peak load (F_{max}) and ultimate displacement (v_{ult}) obtained from the monotonic testing first.

Test method

The definitions for these peak load (F_{max}) and ultimate displacement (v_{ult}) under monotonic loading are illustrated in Figure 3-12 below.

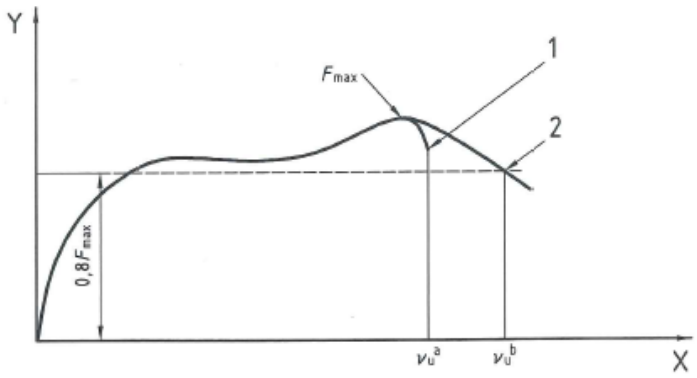

Key

X Displacement, v
Y Load, F
1 case a
2 case b
a Displacement at failure (case a).
b Displacement at $0,8F_{max}$ in the descending portion of the load-displacement curve (case b).

Figure 3-12: Typical load-displacement curve and definitions of peak load and ultimate displacement (ISO6891).

The ultimate displacement (Δ_{ult}) is defined as either the displacement at failure (i.e. brittle failure), or the displacement corresponding to $0.8F_{max}$ on the the post-peak load-displacement curve. The initial stiffness k_i is defined as:

$$k_i = {}^{0.4F_y}\Big/_{\Delta_{0.4Fy}} \qquad (4)$$

where F_y = yield force (kN); and $\Delta_{0.4Fy}$= displacement corresponding to a load of $0.4F_y$ (mm).

Once Δ_{ult} has been established under monotonic loading, the cyclic displacement protocol is derived based on that. Under ISO16670:2003, the loading protocol consists of a number of cycle groups and the groups with large amplitudes contain three idential cycles with a specific displacement amplitude. The displacement amplitudes are percentages of Δ_{ult}. As testing progresses, the displacement ampitude increases, as shown in Figure 3-13. An example of the testing protocol is also given in tabular form (

Table **3-11**). Testing is complete when the capacity of the connection reaches 50% of it's maximum load under cyclic loading, or brittle failure is observed.

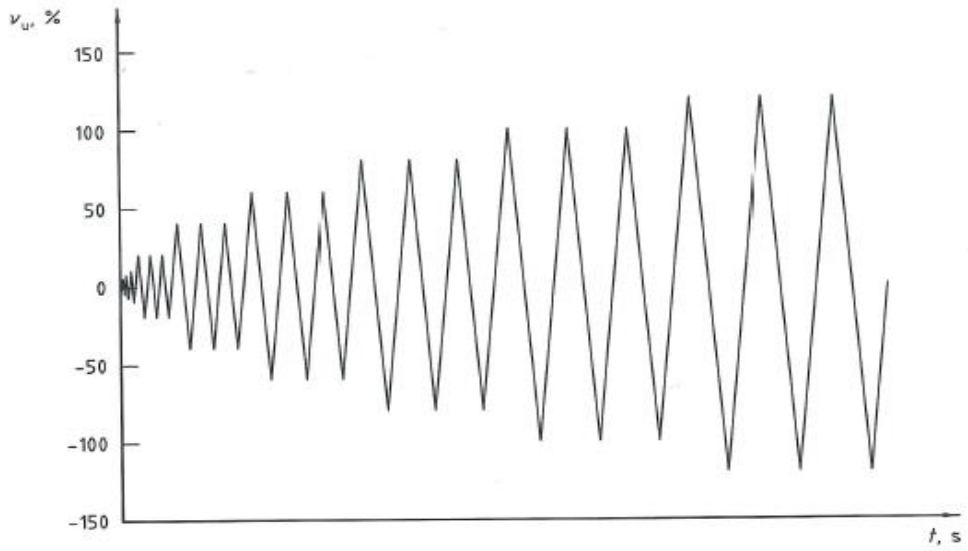

Figure 3-13: Cyclic Protocol for mechanical joints as per ISO 16670, to be applied as a function of Δ_{ult}, as determined from monotonic testing

Table 3-11: Example of a displacement-based cyclic protocol as per ISO16670:2003

Steps	**No. of cycles**	**Amplitude**	
1	1	1.25%	-0.6 mm
2	1	2.5%	1.3 mm
3	1	5%	-2.6 mm
4	1	7.5%	3.9 mm
5	1	10%	-5.2 mm
6	3	20%	10.2 mm
7	3	40%	-20.6 mm
8	3	60%	30.9 mm
9	3	80%	-41.2 mm
10	3	100%	51.5 mm
11	3	increments of 20% v_{ult}	

Figure 3-14 shows the test setup in which, a 10 mm thick steel plate was used as the flange of steel beams or columns and the timber studs were pre-drilled to match the diameter of the steel fastener. The steel plate was rigidly fixed to the loading machine. To construct the timber-steel connection, the timber studs were first clamped together using a G-clamp and then placed in line with the steel flange below the load cell, so that the steel fastener could connect the two elements. The fastener was then tightened to a torque of 25Nm, forming the timber-steel connection.The constructed joint was then held in place with a clamping mechanism

comprising of smaller steel plates and threaded screws. The steel flange was then subjected to a tension and/or compression load at a constant loading rate. Figure 3-15 and Figure 3-16 show the test photos.

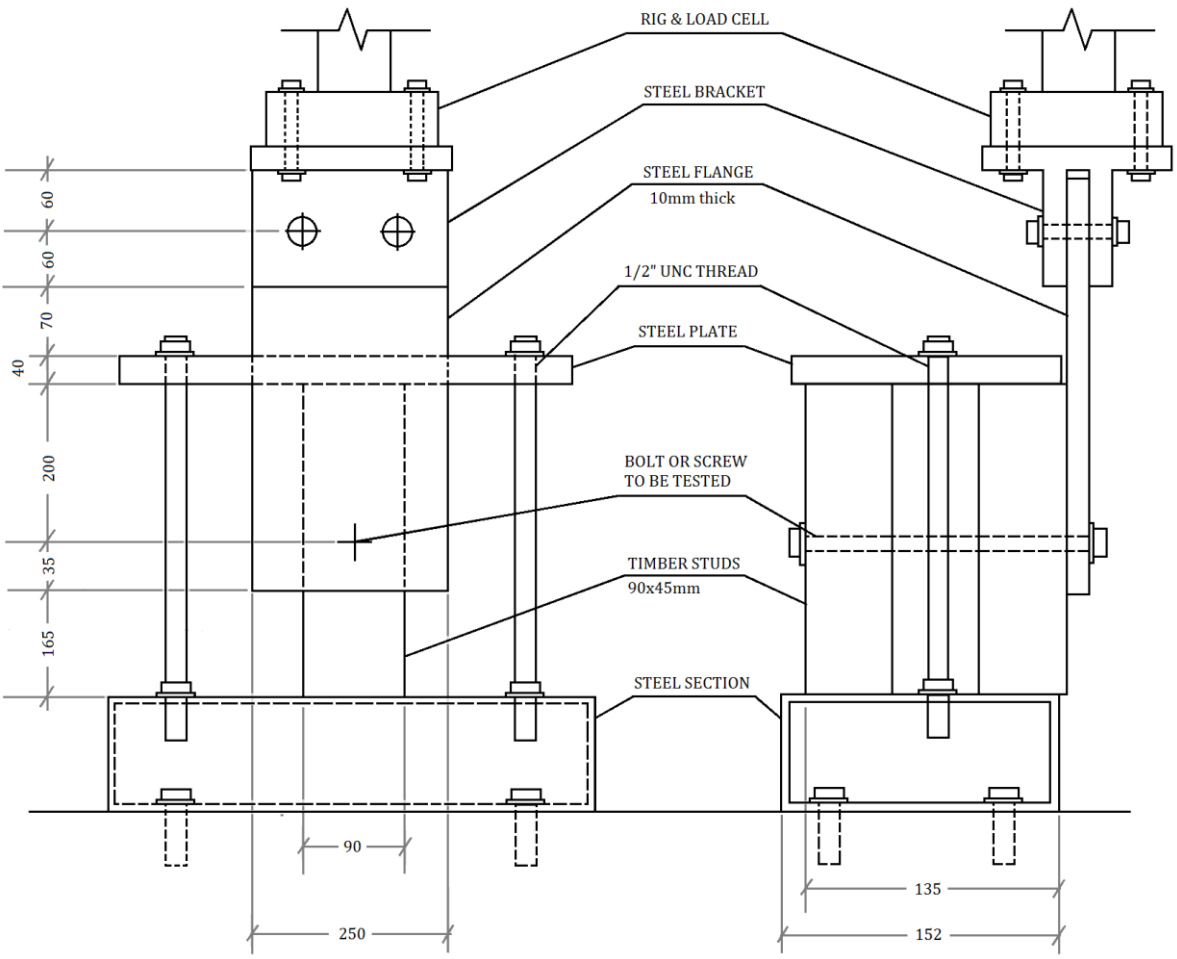

Figure 3-14: Dimensions of the Timber-Steel experimental setup. Front and Side view.

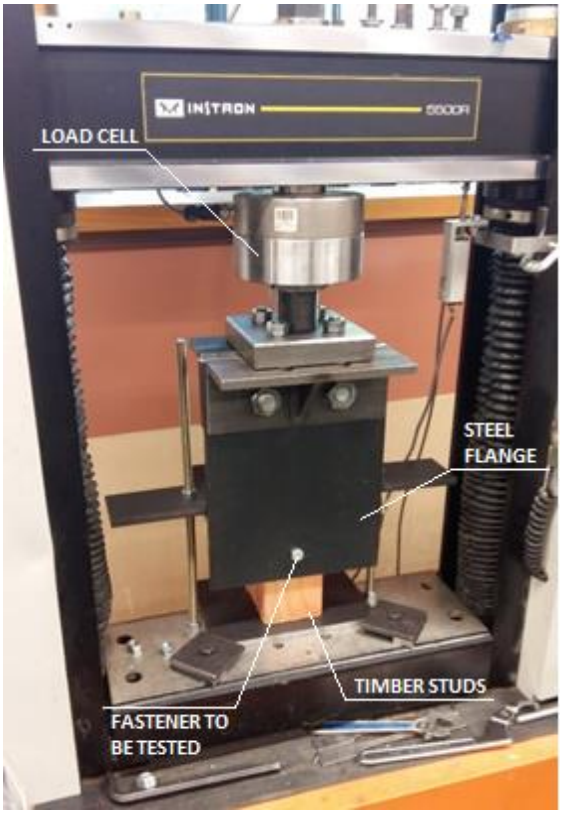

Figure 3-15: Test setup for Timber-Steel connections. Front view.

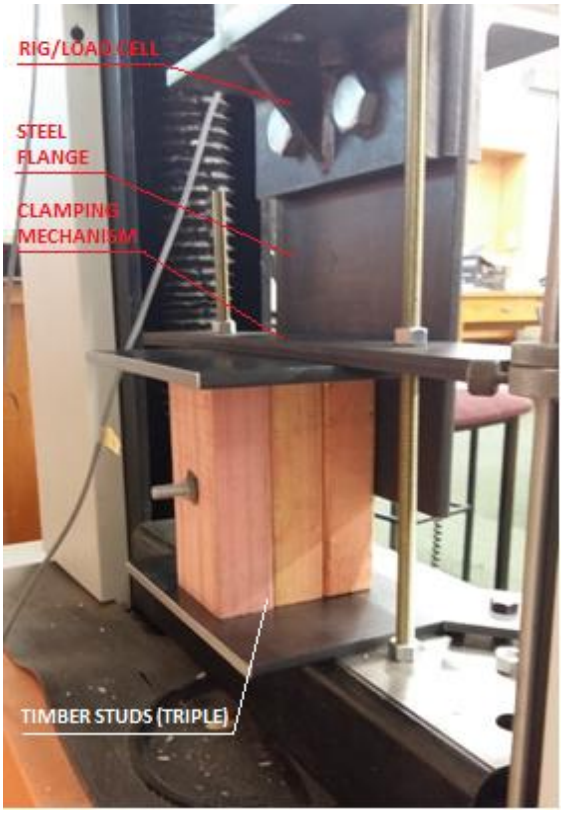

Figure 3-16: Test setup for Timber-Steel connections. Rear view.

The monotonic loading protocol is displacement controlled. The loading rate was maintained at 2mm/min until 70% of estimiated peak load and then increased to 5mm/min till failure. The data sampling rate was 2 Hz. The test was considered complete once the ultimate displacement (v_{ult}) was reached. The load displacement curve was recorded and the following key parameters were derived:

- Maximum Load, $F_{max,}$ kN
- Ultimate Displacement (or slip), $v_{ult,}$ mm
- Initial Stiffness, k_i, kN/mm

Because the ultimate displacement (v_{ult}) obtained from the monotonic testing was required to define the amplitudes of the cyclic protocol, the cyclic displacement protocol was unique to each connection type.

A number of critical connection parameters were derived from the backbone curves and the load-displacement hysteretic loops. These parameters include initial stiffness ($k_{i,}$ kN/mm), yield force (f_y, kN), maximum force (f_{max}, kN), ultimate force (f_{ult}, kN), yield displacement (Δ_y, mm), maximum displacement (Δ_{max}, mm), ultimate displacement (v_{ult}, mm), ductility (μ) and strength degradation ($F_{(1\text{-}3\%)}$). The ultimate force (f_{ult}, kN) is taken as $0.8F_{max}$ or is equal to F_{max} if a brittle failure is observed. the ultimate displacement (v_{ult}, mm) is the displacement correponding to f_{ult}.

Initial stiffness (k_i) is defined in ISO16670 as the following:

$$k_i = \frac{0.3F_{max}}{\Delta_{0.4Fmax} - \Delta_{0.1Fmax}} \qquad (5)$$

Ductility (μ) is given by:

$$\mu = \frac{v_{ult}}{\Delta_y} \quad (6)$$

The strength degradation ($F_{1\text{-}3}$) was determined by calculating the differences between the peak loads on the backbone curves of the first, second and third cycle within the cycle groups. The strength degradation is reported in the form of a percentage of the peak load on the first backbone curve. The displacement schedule was carried out with a loading rate starting at 1mm/min and as the testing progressed, was slowly increased to 50mm/min to control the total testing time. A data sampling rate of 2 Hz was also adopted. The test was considered complete once the load dropped to at least half of its peak load or brittle failure was observed.

Monotonic test results

The load-displacement plots obtained from monotonic tests and failure modes are presented from Figure 3-17 through Figure 3-21. Structural properties such as strength, stiffness and ductility are presented in tabular form (Table 3-12 - Table 3-13) and a description of connection behaviour under monotonic loading is provided. The full sets of the test results and each cyclic loading protocol for the timber-steel connections under monotonic loading are provided in Appendix A.

3.2.3.2

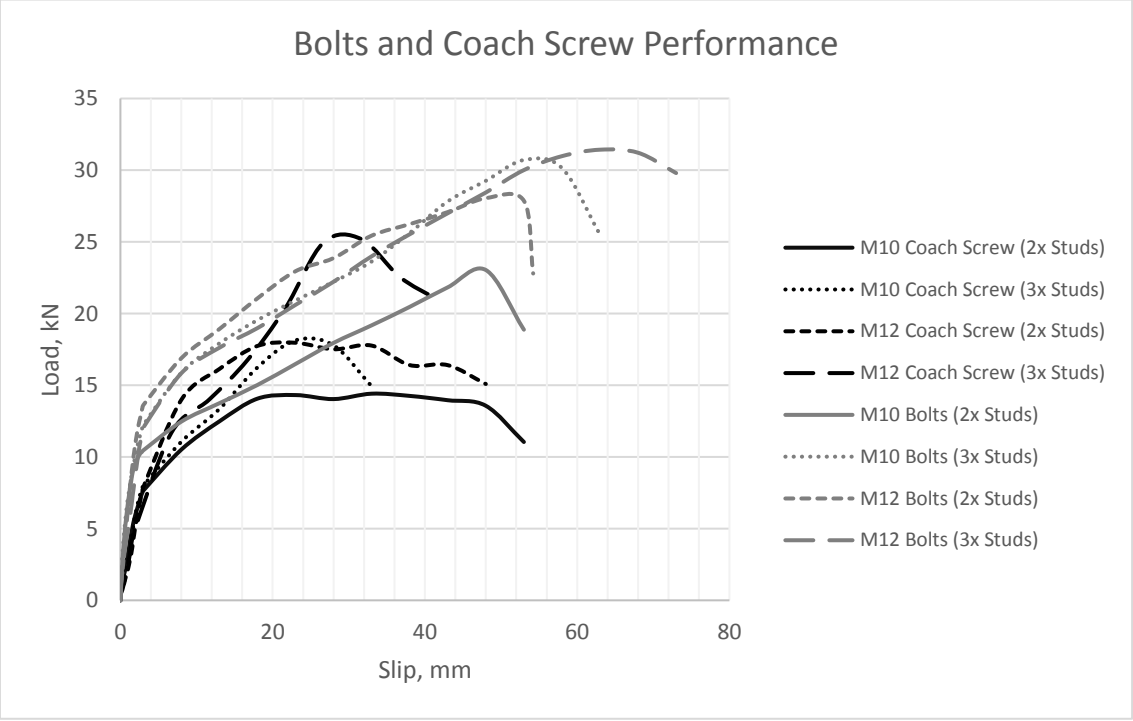

Figure 3-17: Average monotonic load-slip curves of each connection type

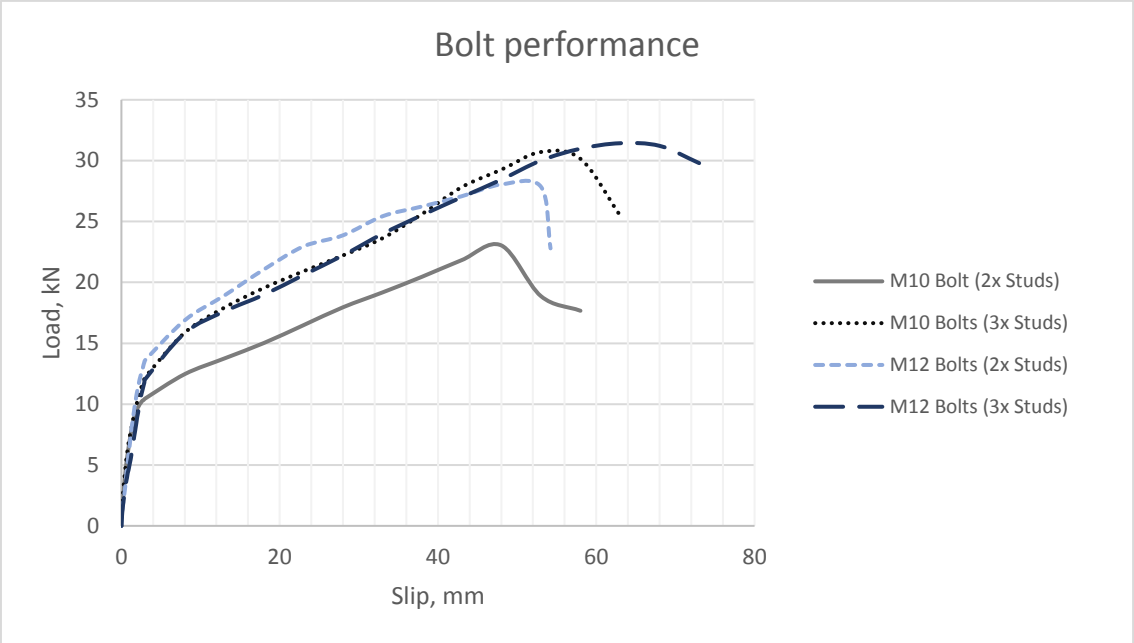

Figure 3-18: Average monotonic load-slip curves for bolted connections

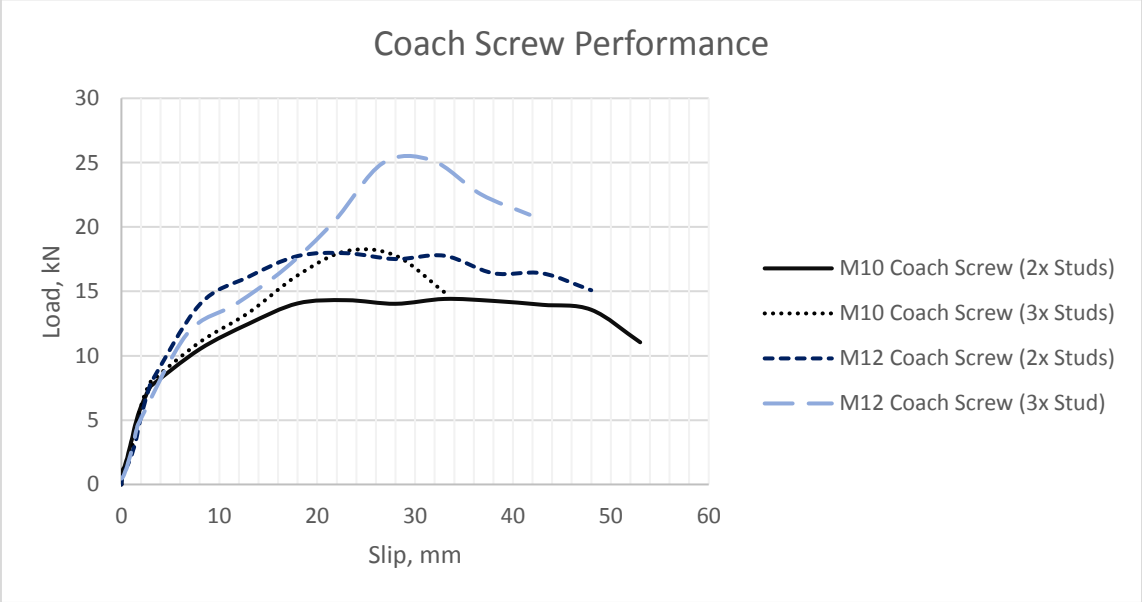

Figure 3-19: Average monotonic load-slip curves for coach screwed connections

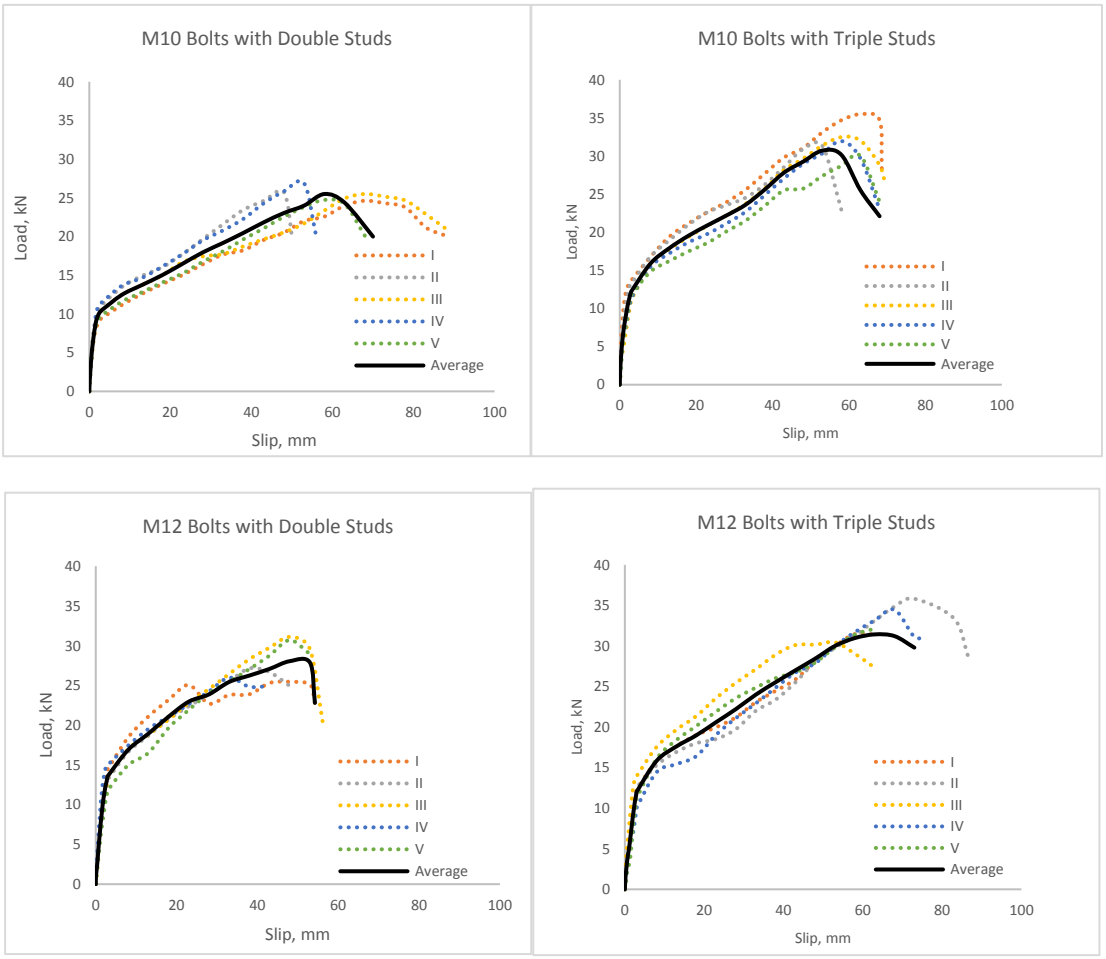

Figure 3-20: Monotonic load-slip curves of individual bolted connections

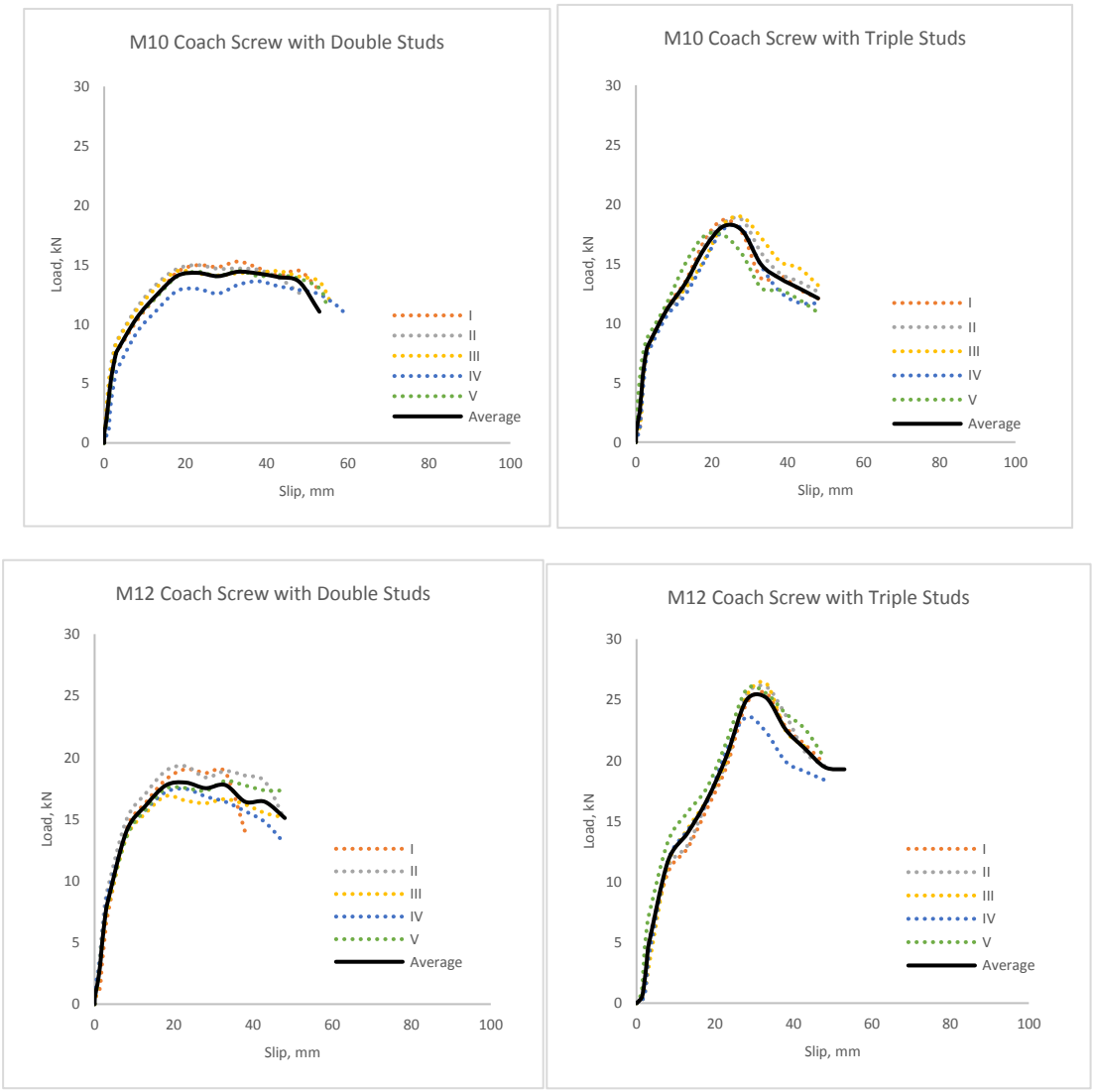

Figure 3-21: Monotonic load-slip curves of individual coach screwed connections

As the load increased, the fastener began to bend. Beyond the elastic range, the fastener started yielding and embedded further into the surrounding wood medium. Eventually, at large displacement, timber splitting occurred and ocassionally, the fasterner head was sheared off, as shown in Figure 3-22 and Figure 3-23. For the bolted connections, wood crusing under the washer and nut was observed due to the significant rope effect. Table 3-12 and Table 3-13 show the average values for each type of connection in terms of maximum load F_{max}, ultimate displacement Δ_{ult} and initial stiffness k_i.

Figure 3-22: Wood splitting failure

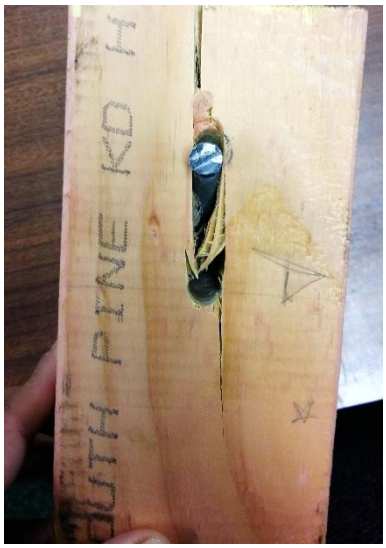

Figure 3-23: Wood embedment crushing and fastener head shear-off

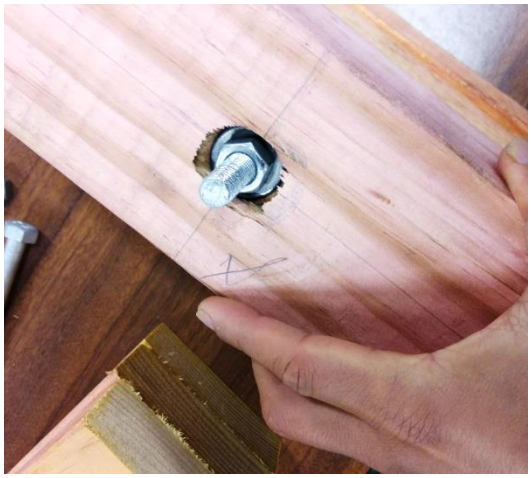

Figure 3-24: Wood bearing failure under washer and nut

At the end of each test, most of the fasteners exhibited the development of two plastic hinges, one below the head of the fastener (which was sheared off in Figure 3-25) and the other along the shaft. Therefore the failure mode for the fastener can be conceptualized in Figure 3-26.

Figure 3-25: Fastener deformation with two plastic hinges highlighted

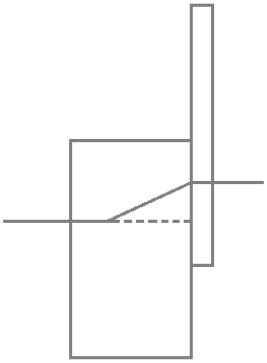

Figure 3-26: Idealised failure mechanism with two plastic hinges

Table 3-12: Summary of peak load, F_{max} (kN), ultimate displacements, v_{ult} (mm) and initial stiffnesses, k_i(kN/mm) obtained from testing (Bolts).

Fastener no.	M10 Bolts						M12 Bolts					
	Double Studs			Triple Studs			Double Studs			Triple Studs		
	F_{max} (kN)	v_{ult} (mm)	k_i (kN/mm)	F_{max} (kN)	v_{ult} (mm)	k_i (kN/mm)	F_{max} (kN)	v_{ult} (mm)	k_i (kN/mm)	F_{max} (kN)	v_{ult} (mm)	k_i (kN/mm)
1	24.7	85.5	2.53	35.9	68.2	3.39	26.3	54.2	6.58	31.6	63.1	4.08
2	26.1	52.9	4.96	32.6	52.7	4.65	26.7	50.0	4.75	36.1	86.4	2.29
3	25.7	88.8	3.67	32.7	69.5	3.00	31.5	55.8	4.50	31.0	64.0	5.90
4	27.0	57.3	5.14	32.1	68.1	2.23	26.6	46.2	8.18	34.8	76.2	2.36
5	25.1	57.3	2.87	30.2	65.2	2.87	31.3	53.8	4.04	32.3	66.5	1.00
Average	25.7	70.5	3.84	32.7	64.7	3.23	28.7	51.3	5.61	33.1	71.5	3.13

Table 3-13: Summary of peak load, F_{max} (kN), ultimate displacements, v_{ult} (mm) and initial stiffnesses, k_i(kN/mm) obtained from testing (Coach Screws).

Fastener no.	M10 Coach Screws						M12 Coach Screws					
	Double Studs			Triple Studs			Double Studs			Triple Studs		
	F_{max} (kN)	v_{ult} (mm)	k_i (kN/mm)	F_{max} (kN)	v_{ult} (mm)	k_i (kN/mm)	F_{max} (kN)	v_{ult} (mm)	k_i (kN/mm)	F_{max} (kN)	v_{ult} (mm)	k_i (kN/mm)
1	15.3	54.7	3.06	18.8	31.1	2.79	19.1	36.7	2.31	25.9	44.3	1.58
2	15.0	48.2	4.01	18.9	34.3	2.90	19.4	47.0	3.10	26.6	41.7	1.57
3	14.5	56.0	4.15	19.0	38.0	2.54	17.2	53.6	2.46	26.8	39.7	1.58
4	13.6	55.9	2.10	18.6	32.9	2.48	17.6	45.4	2.93	23.6	43.8	1.70
5	14.6	54.5	2.91	17.7	31.1	4.29	18.1	57.9	2.59	26.0	47.1	1.68
Average	14.6	53.9	3.25	18.6	33.5	3.00	18.3	48.1	2.68	25.8	43.3	1.62

Cyclic test results

The cyclic load-displacement plots are presented in Figure 3-27 and Figure 3-28. The full cyclic test results are provide in Appendix B.

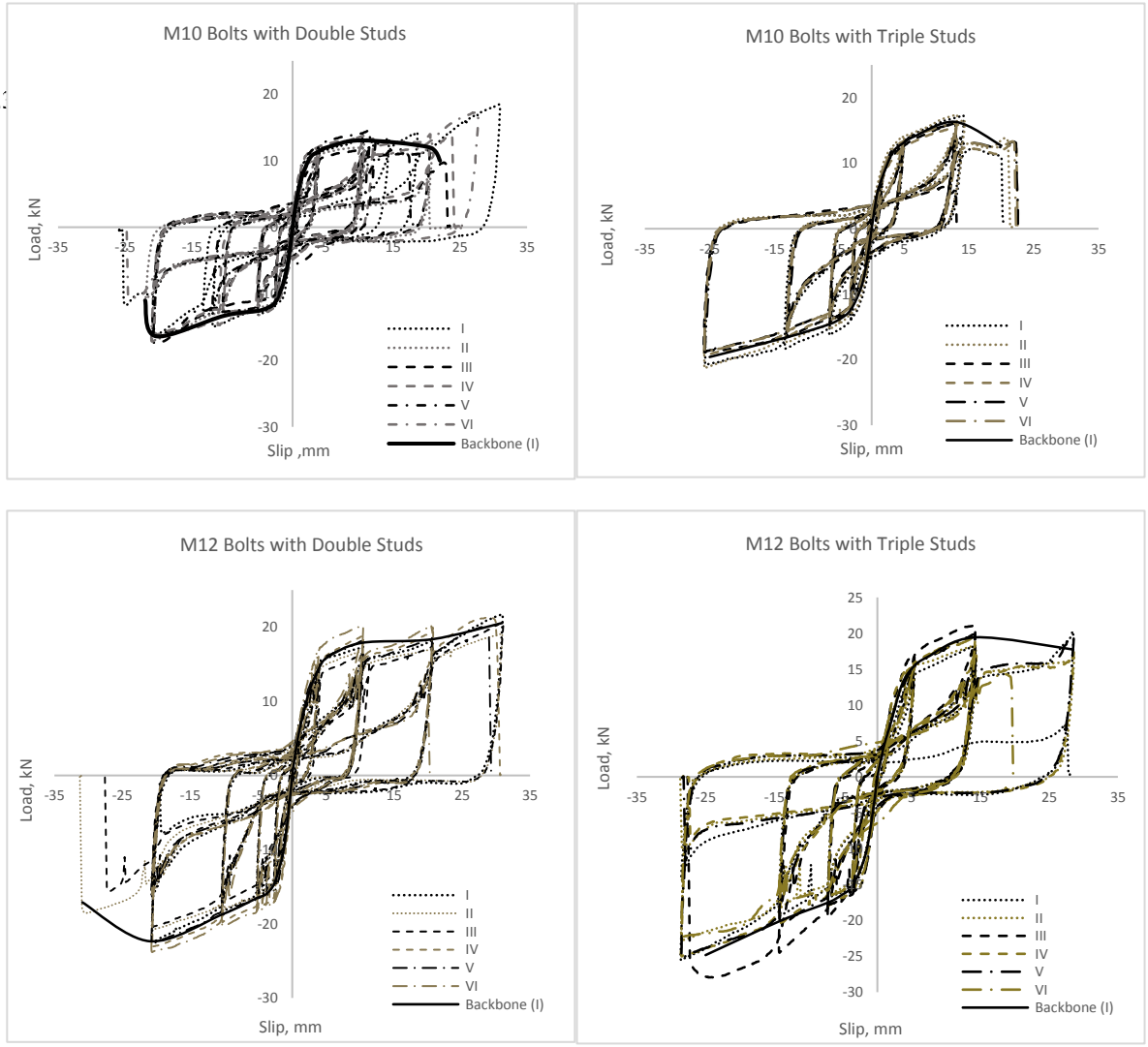

Figure 3-27: Hysteresis curves and backbone curves obtained for Bolted Timber-Steel Connections.

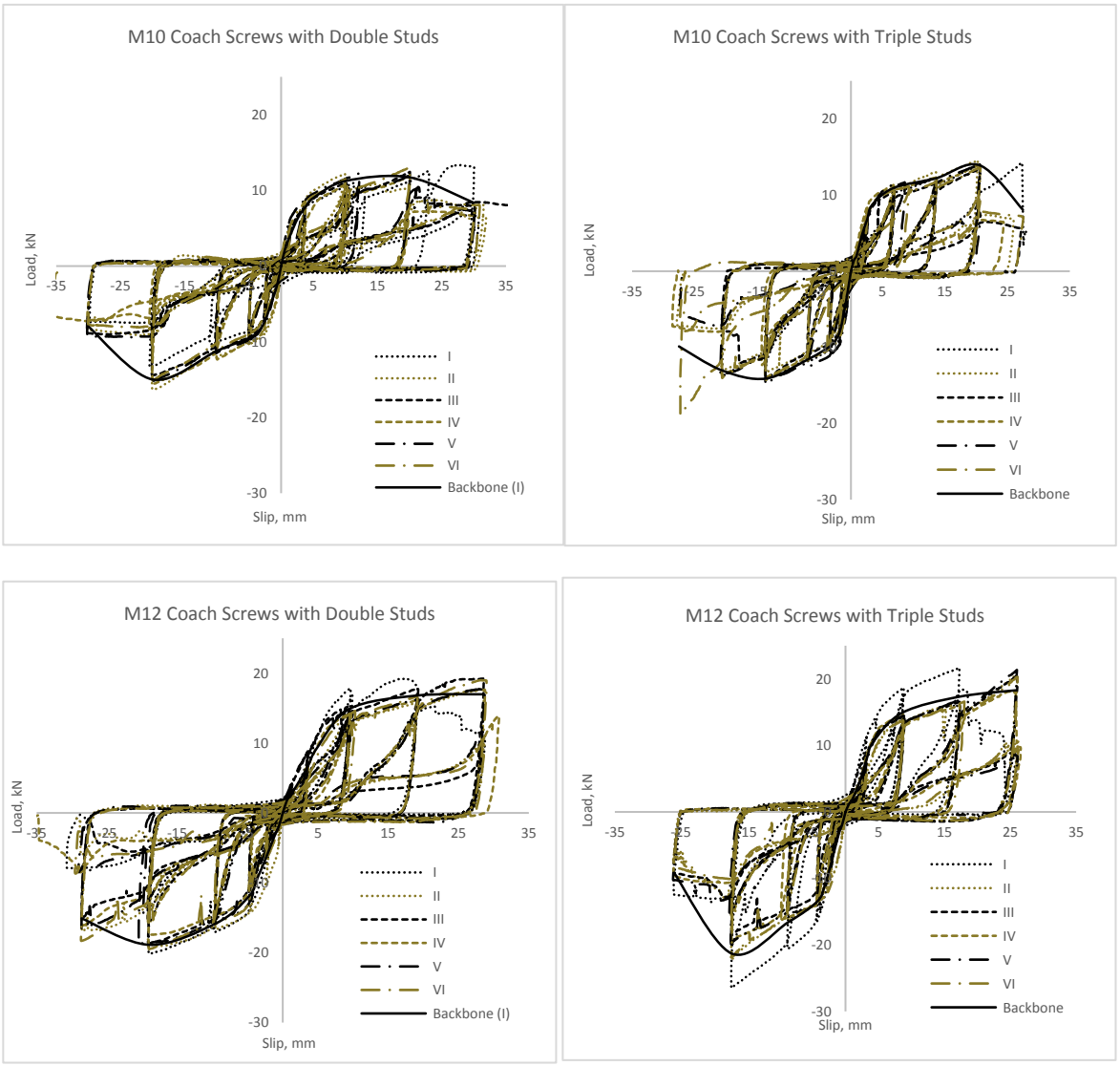

Figure 3-28: Hysteresis curves and backbone curves obtained for Coach Screw Timber-Steel Connections

All the connections had ultimate brittle failure modes after significant plastic deformation. Fastener head shear-off was observed at large displacement (Figure 3-29). A small number of the bolted connections also failed due to wood splitting. As these connections were cyclically loaded, the fasteners were observed to withdraw signicantly (Figure 3-30).

Figure 3-29: Fastener head shear-off in bolted and coach screw connections

Figure 3-30: Fastener withdrawal

Table 3-14 and Table 3-15 give the summary of test results in terms of stiffness, yield strength, peak loads, ultimiate loads and the correponding displacements. The ratios of strength degradation caused by the repeated cycles are also provided.

Table 3-14: Average structural properties for Bolted Timber-Steel connections tested under cyclic loading.

	M10 Bolts				M12 Bolts			
	Double Studs (n=2)		Triple Studs (n=3)		Double Studs (n=2)		Triple Studs (n=3)	
	Mono	Cyclic	Mono	Cyclic	Mono	Cyclic	Mono	Cyclic
k_i (kN/mm)	3.48	6.01	3.23	5.33	5.61	6.11	3.13	4.70
F_y (kN)	9.4	9.3	9.5	10.1	13.2	14.0	12.6	13.2
F_{max} (kN)	25.7	15.9	32.7	18.0	28.7	21.4	31.5	22.3
F_{ult} (kN)	22.7	14.3	23.9	15.6	27.1	19.8	29.8	16.9
Δ_y (mm)	3.2	1.6	3.1	2.2	2.7	2.9	3.0	4.1
Δ_{max} (mm)	61.2	21.8	49.7	19.5	46.2	24.6	67.0	24.7
Δ_{ult} (mm)	70.5	23.0	67.4	23.0	51.3	26.0	71.5	27.5
u	22.0	14.4	21.7	10.5	19.0	9.0	23.8	6.7
$F_{(1-3)}$	-	47.9 - 92.5%	-	56.0 - 73.2%	-	59.7 - 88.3%	-	46.6 - 79.2%

Table 3-15: Average structural properties for Coach Screw Timber-Steel connections tested under cyclic loading.

	M10 Coach Screws				M12 Coach Screws			
	Double Studs (n=2)		Triple Studs (n=3)		Double Studs (n=2)		Triple Studs (n=3)	
	Mono	Cyclic	Mono	Cyclic	Mono	Cyclic	Mono	Cyclic
k_i (kN/mm)	3.35	2.85	3.00	3.45	2.68	2.23	1.62	3.26
F_y (kN)	7.5	7.4	8.5	8.0	11.7	12.1	10.1	11.4
F_{max} (kN)	14.6	13.8	18.6	14.5	18.2	18.7	25.8	20.9
F_{ult} (kN)	11.7	8.2	14.9	10.4	14.6	12.4	20.6	10.1
Δ_y (mm)	2.9	2.9	3.3	2.4	4.7	5.8	6.4	3.8
Δ_{max} (mm)	28.6	19.3	24.9	20.0	26.1	23.0	30.5	20.9
Δ_{ult} (mm)	53.9	31.1	33.5	24.9	48.1	28.7	43.3	26.0
u	18.6	10.7	10.2	10.4	10.2	4.9	6.8	6.8
$F_{(1-3)}$	-	41.4 - 61.7%	-	33.6 - 65.6%	-	29.6 - 74.1%	-	35.1 - 73.1%

Discussion

The connections exhibited typical elastoplastic behavor with initial stiffness in the linear range followed by yield plateau with much lower stiffness. Some brittle failure modes such as fastener head shear-off and wood splitting were observed at the ultimate stage with continued loading.

The bolted connections generally have higher peak loads, initial stiffness and ductility than coach screwed connections. Depending on the number of studs, the bolted connections had 10 - 76% larger peak loads, 6.7 – 107% higher initial stiffness and up to 2.5 times larger ductilty factor than the coach screwed connections with the same fastener diamater.

3.2.3.4

The general response of the bolted and coach screwed connections under cyclic loading were similar to the properties under monotonic loading. However, under cyclic loading, the load carrying capacity and displacements (yield, ultimate, etc) were lower, due to the more demanding loading protocol and the low cycle fatigue caused by cyclic loading. Strength degradation properties for bolted and coach screwed connections were very similar. Strength degradation remained relatively constant across the two variables (fastener thread and number of studs) examined. One aspect that was noted is that bolted connections had slightly more strength degradation than coach screws (6.5 – 30% more degradation) in the second and third loading cycles.

Within the bolted connections, fastener thread size (M10 or M12) and the number of timber studs both show a positive correlation with peak load (F_{peak}), maximum load, (F_{max}) and ultimate load (F_{ult}). The connections with M12 bolts had 11.7 – 40.4% higher peak loads (F_{max}) than the connections with M10 bolts, depending on the number of studs the fastener. The yield displacement (Δ_y), ductilty (μ) and initial stiffness (k_i) of the bolted connection is a function of both fastener size and the number of timber studs. Specimens with double studs had 15.6 – 26.7% smaller yield displacements when the bolt size increased from M10 to M12. Increasing the bolt size from M10 to M12 also reduced ductility factors by 38.7%. However, the connections with triple studs, the opposite trend occurred: the yield displacements increased by 31.7 – 34.8% and ductilty increased by 22.5%.

Within the coach screwed connections, fastener thread size (M10 or M12) and the number of timber studs in the connection (n), both showed a positive correlation on peak load (F_{max}) and yield displacements (Δ_y). Depending on the number of studs the fastener, the connections with M12 coach screws had 18.8 to 56.0% higher peak loads (F_{max}) than the connections with M10 coach screws, and also had 62.0 to 93.9% larger yield displacements (Δ_y). However, the coach screw size had a negative correlation with initial stiffness (k_i), substantialy reduced by 22.2 – 87.5% when the screw size increased. Ductilty has a negative correlation with both coach screw thread and number of timber studs. When coach screw thread is increased, ductility drops by 32 – 44.3%. Similarly, when number of studs is increased from double to triple, ductility drops by 32.7 – 45.8%

Maximum and ultimate displacements of the coach screwed connection were dependent upon both the screw size and the number of timber studs. In the specimens with double studs, increasing screw size from M10 to M12 resulted in maximum and ultimate displacements decrease by 8.8% and 10.8%, respectively. In specimens with triple studs, the opposite trend occurred: maximum and ultimate displacements increased by 31.7 – 34.8% and ductilty increased by 22.5%.

3.3 Nailed timber-plywood connections

This section describes the monotonic and reversed cyclic tests on the timber-plywood connections.

3.3.1 Materials

The similar SG8 Radiata Pine timber studs used in the timber-steel interface connection tests were used in the nailed timber-plywood connection tests. The 2.4 x 1.2m plywood sheets were sourced from New Zealand market. Moisture contents of the plywood were measured with an electronic moisture gauge, and ranged from 9.1% to 13.7%. They had F8 grade and were manufactured to AS/NZS2269 (Standards New Zealand, 2012), thus having the structural properties listed in Table 3-16:

Table 3-16: Structural properties of Radiata Pine plywood, Grade F8.

Bending	Tension	Panel shear	Rolling shear	Compression		MoE	Shear Modulus
f_{pb}, MPa	f_{pt}, MPa	f_{ps}, MPa	f_{pr}, MPa	(in-plane) f_{pc}, MPa	(normal-to-plane) f_{pp}, MPa	E, MPa	G, MPa
22.5	13.5	4.2	1.7	16.9	8.6	9100	455

Galvanized flat head nails with smooth shanks were also sourced from New Zealand market. Table 3-2 shows the test matrix in terms of nail sizes, plywood thickness, loading-grain orientations and number of replicates. Design strengths for the nailed connections can be found in Timber Design Guide (Buchanan, 2007), as given in Table 3-17.

Table 3-17: Nail Strength reported in the Timber Design Guide, 2007

Nail diameter (mm)	2.8	3.15	3.55
Strength (N)	917	1148	1438

3.3.2 Methodology

The connection test setup is shown in Figure 3-31. Front and rear views of the experiment is shown in Figure 3-32.

The nailed plywood-to-stud connection consisted of two identical nails. Therefore each nail carried half of the total load. To connect the plywood to the timber stud, the nails were hand-driven into the plywood and timber stud. The nail spacing and edge distance were determined as per NZS3603 (Figure 3-33 - Figure 3-35).

To test the the nailed plywood-stud connection, it was placed on the testing platform, and lined up with the steel flange connected to the load cell. The plywood was clamped tight to the steel flange using two small steel plates and a M12 bolted connection.. Sufficient contact between the steel plates and the plywood was required to achieve enough friction and to avoid slip. The timber stud was clamped in place onto the test table using

threaded rods, steel plates and nuts. The nailed connection was then loaded vertically, in tension and/or compression, depending on whether a monotonic or cyclic test was being undertaken.

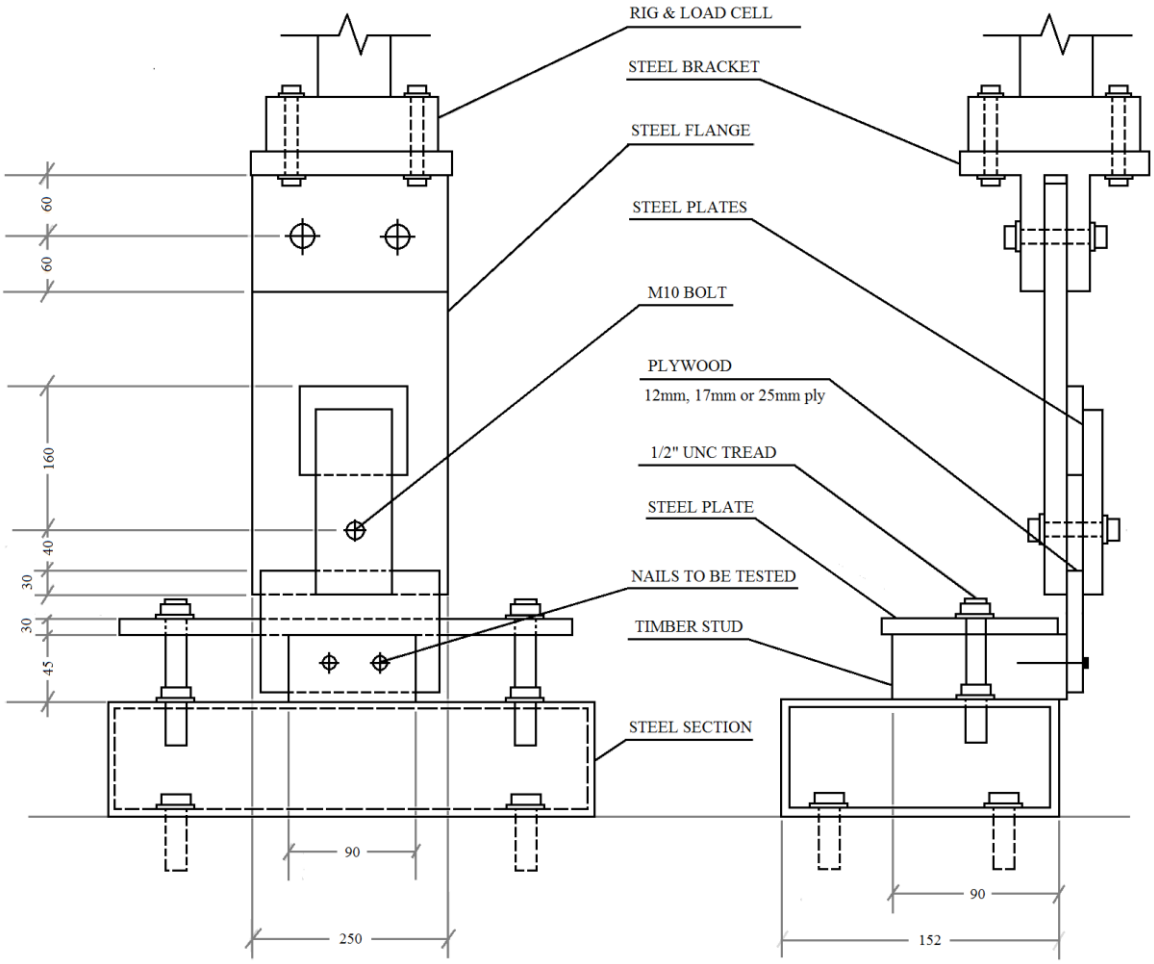

Figure 3-31: Dimensions and test setup of nailed timber-plywood connections

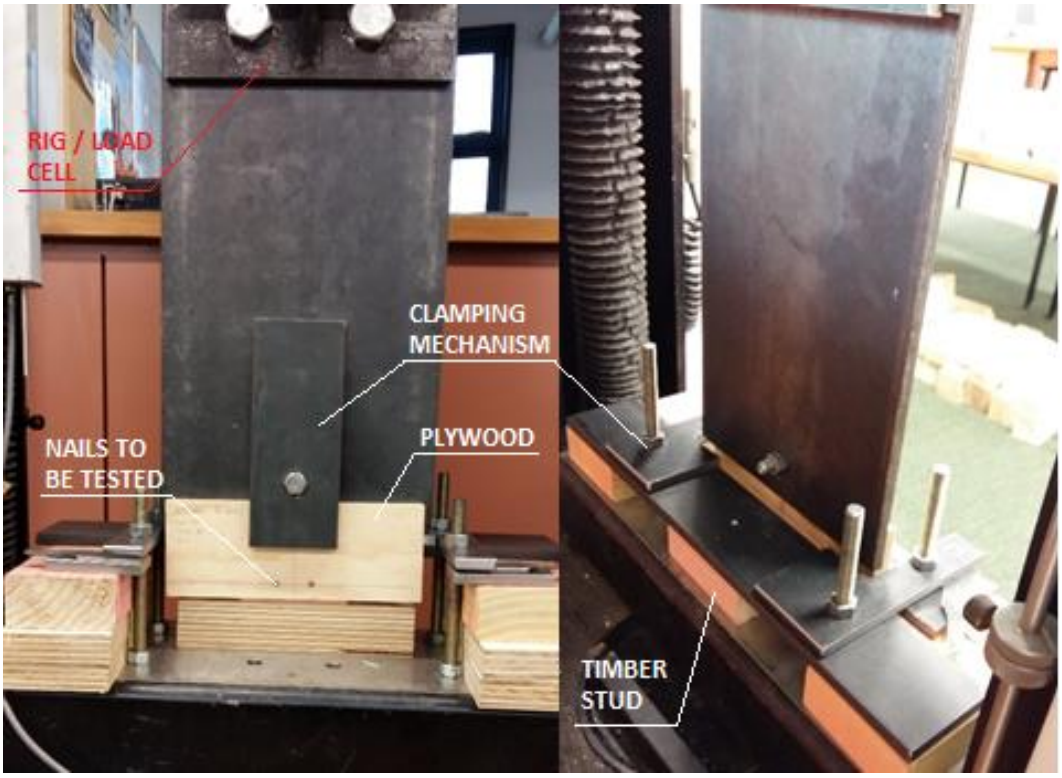

Figure 3-32: Timber-plywood connection test setup. Front and Rear view.

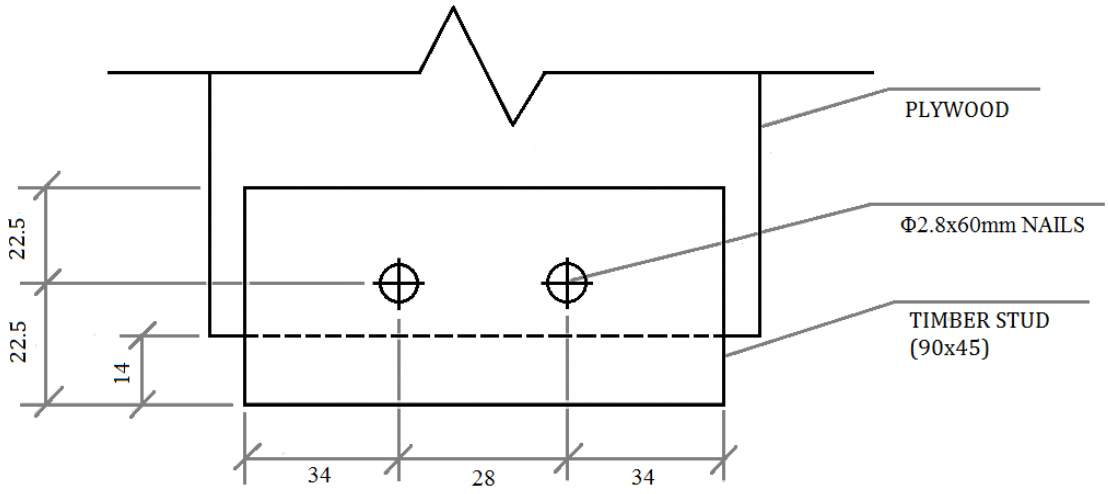

Figure 3-33: Spacing requirements for φ2.8x60mm nails

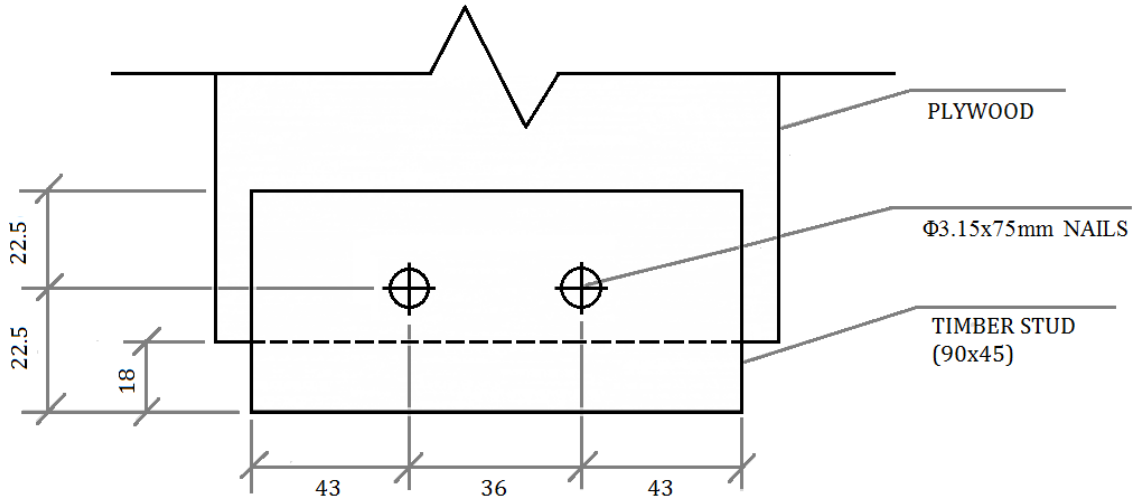

Figure 3-34: Spacing requirements for φ3.15x75mm nails

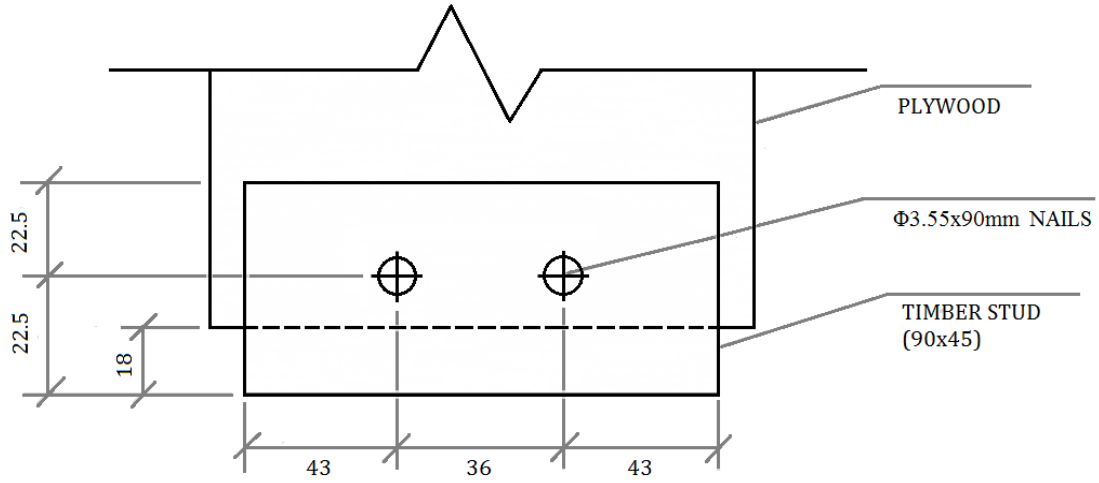

Figure 3-35: Spacing requirements for φ3.55x90mm nails

In the monotonic testing, a data sampling rate of 2 Hz was adopted. The test was considered complete once the ultimate displacement (v_{ult}) was reached. The load displacement curve was recorded and processed to obtain the ma ximum load, F_{max}, ultimate displacement, v_{ult} and the initial stiffness, k_i. From these parameters, the unique cyclic loading protocol for each connection was also derived in accordance with both ISO6891 and ISO16670.

In the cyclic testing, each connection was subjected to the displacement protocol (Figure 3-13) in accordance with ISO16670, which is derived from the results of the monotonic experiments. The displacement schedule was carried out with a loading rate starting at 1mm/min and as the testing progressed, was slowly increased to 50mm/min to control total testing time.

During the testing, the connection was constantly monitored and the test was considered complete once the load fell to at least half of its peak load or brittle failure mechanism was observed.

3.3.3 Monotonic tests

Figure 3-36 through Figure 3-41 show the average load-displacement curves of the nailed connections with diffirent combinations of nail sizes, plywood thicknesses and load-grain directions. Table 3-18 through Table 3-20 show the summary of the nailed connections properties in terms of peak loads, ultimate displacement and intial stiffness. Based on the monotonic response, the unique cyclic displacement protocol for each connection was derived.

For the full sets of test results of the nailed timber-plywood connections under monotonic loading, see Appendix C.

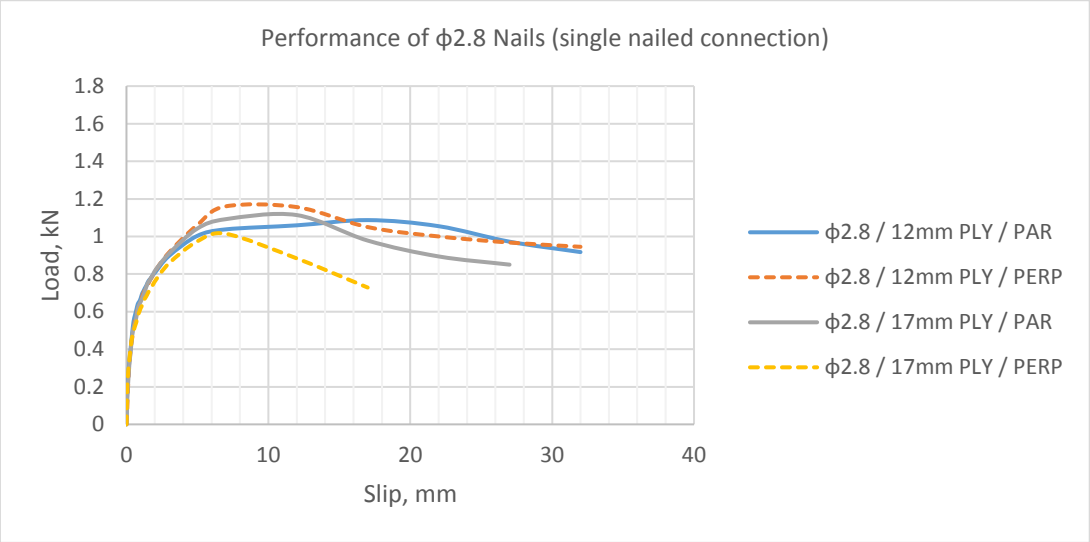

Figure 3-36: Load-displacement curves for Φ2.8 nails with various ply thicknesses under monotonic loading (single nail)

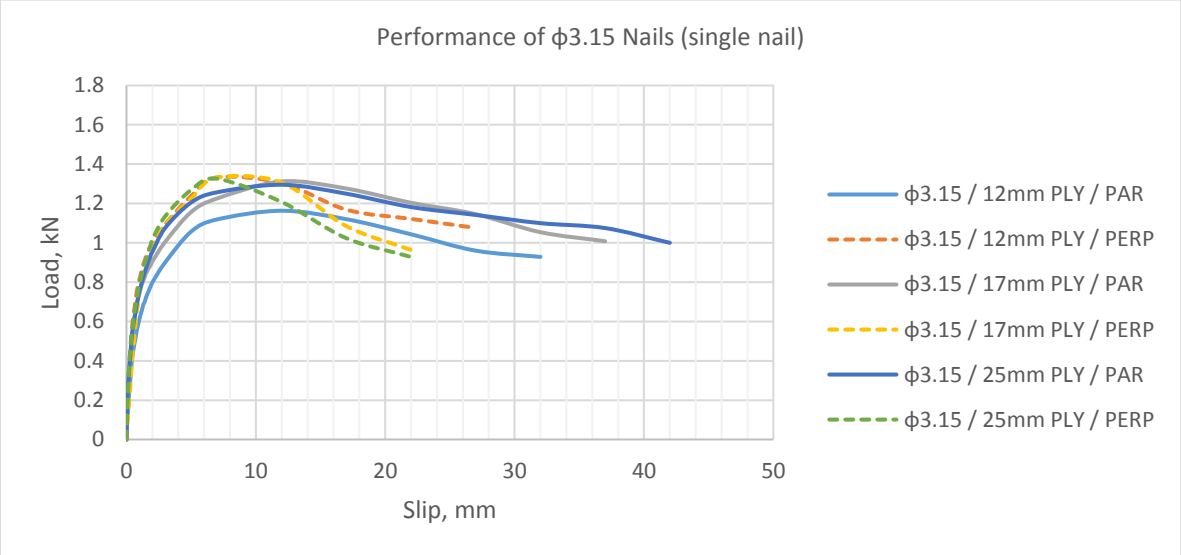

Figure 3-37: Load-displacement curves for Φ3.15 nails with various ply thicknesses under monotonic loading

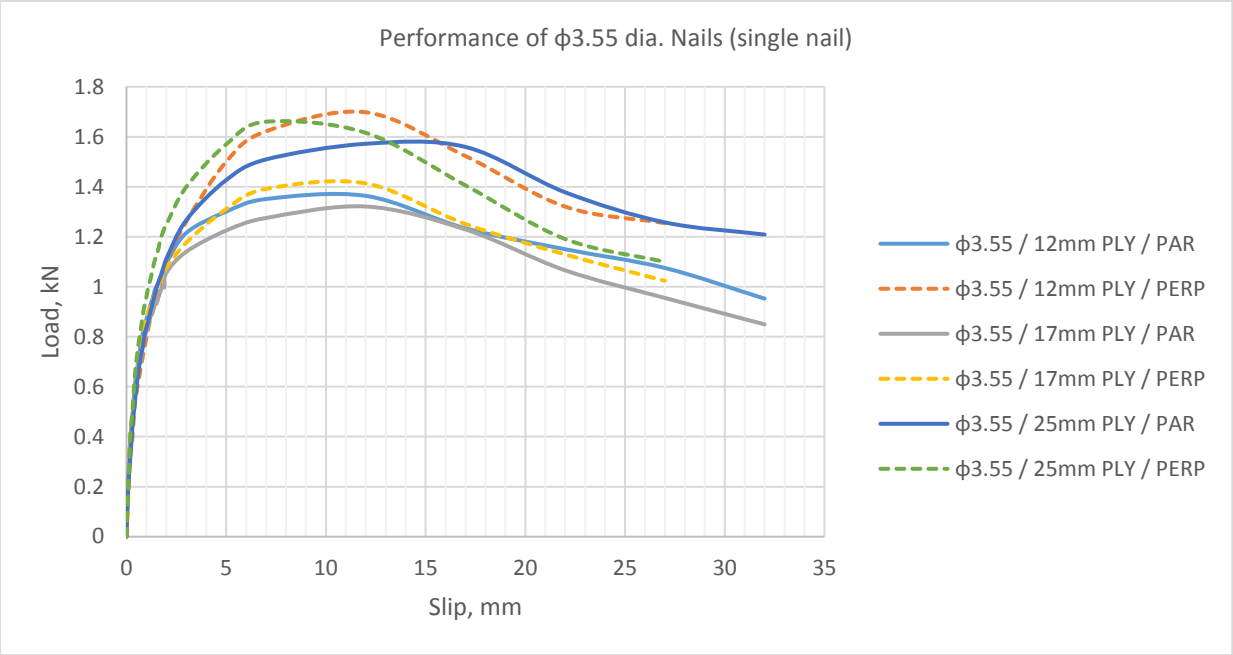

Figure 3-38: Load-displacement curves for Φ3.55 nails with various ply thicknesses under monotonic loading

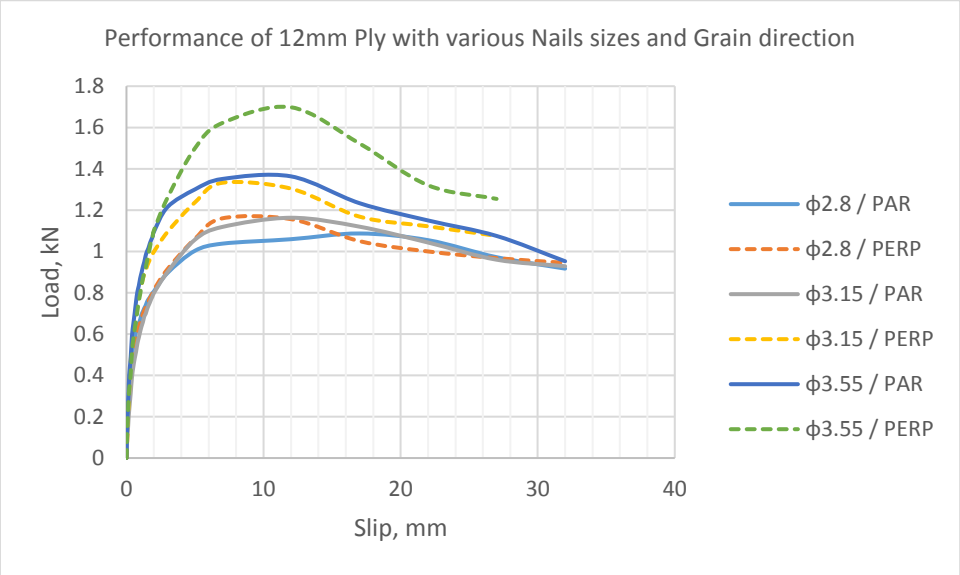

Figure 3-39: Load-displacement curves for 12mm ply with various nail sizes under monotonic loading

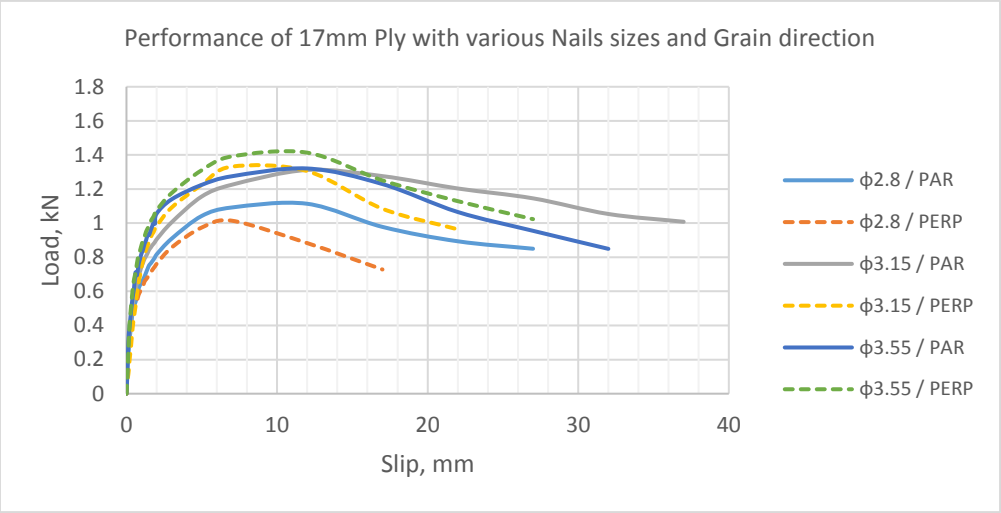

Figure 3-40: Load-displacement curves for 17mm ply with various nail sizes under monotonic loading

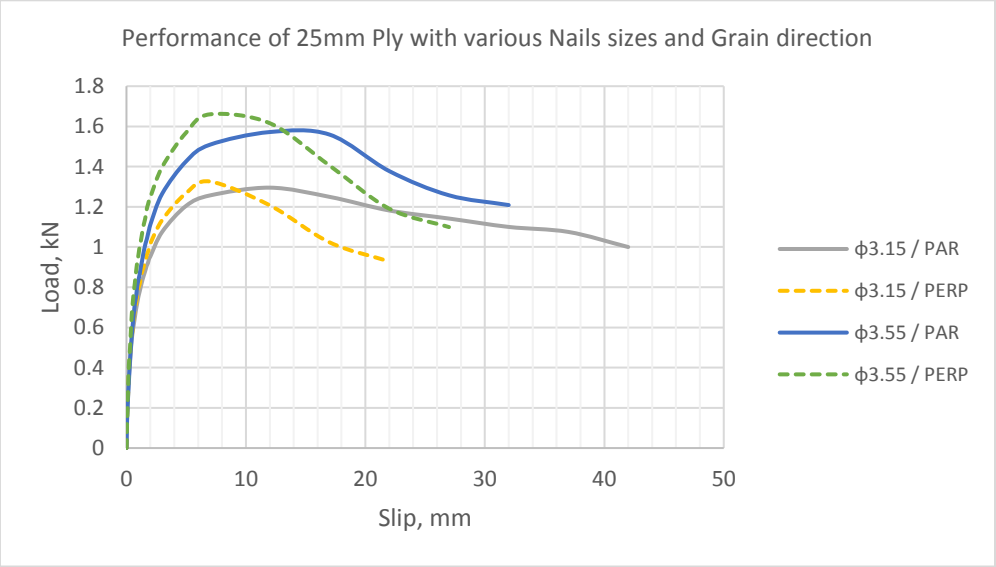

Figure 3-41: Load-displacement curves for 25mm ply with various nail sizes under monotonic loading

Table 3-18: Structural properties derived for Timber-Sheathing connections with 12mm Plywood (single nail)

12mm Ply	Φ2.8 Nails		Φ3.15 Nails		Φ3.55 Nails	
	Parallel	Perpendicular	Parallel	Perpendicular	Parallel	Perpendicular
F_{max} (kN)	1.15	1.22	1.19	1.40	1.46	1.73
v_{ult} (mm)	27.7	20.5	32.4	18.4	22.5	21.1
k_i (kN/mm)	1.13	1.65	1.02	1.30	1.69	1.30

Table 3-19: Structural properties derived for Timber-Sheathing connections with 17mm Plywood (single nail).

17mm Ply	Φ2.8 Nails		Φ3.15 Nails		Φ3.55 Nails	
	Parallel	Perpendicular	Parallel	Perpendicular	Parallel	Perpendicular
F_{max} (kN)	1.14	1.04	1.32	1.45	1.33	1.46
v_{ult} (mm)	20.3	13.4	31.1	18.2	23.0	21.3
k_i (kN/mm)	1.12	1.43	1.30	1.01	1.44	1.58

Table 3-20: Structural properties derived for Timber-Sheathing connections with 25mm Plywood (single nail).

25mm Ply	Φ3.15 Nails		Φ3.55 Nails	
	Parallel	Perpendicular	Parallel	Perpendicular
F_{max} (kN)	1.34	1.37	1.61	1.72
v_{ult} (mm)	32.5	14.8	25.7	18.0
k_i (kN/mm)	1.21	1.09	1.24	1.40

Figure 3-42 through to Figure 3-44 showed the typical failure modes of the nailed connections. As the load increased, the nail began to bend and crush the surrounding wood medium and plywood. Beyond the elastic range, the nail began to yield and the nail embedded further into timber stud. The ductile connection behavior was in part, due to the fact that the nail underwent withdrawal as the load increased. As the nail started to withdraw, the location of the maximum bending moment along the nail shank also changed, resulting in very ductitle behavior. No splitting of the plywood or timber studs were observed which indicates sufficent nail spacing and edge distances.

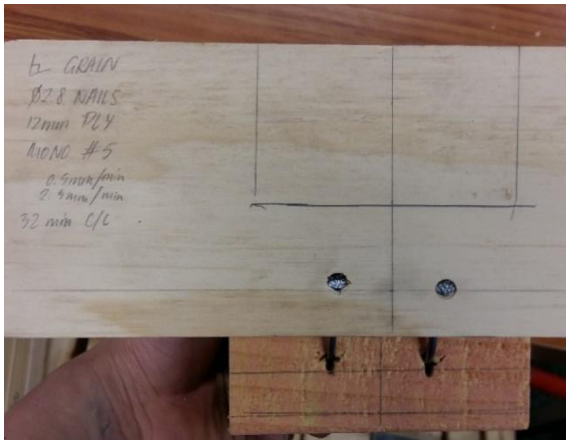

Figure 3-42: Withdrawal, lateral deformation and crushing of the timber stud and plywood observed post-test.

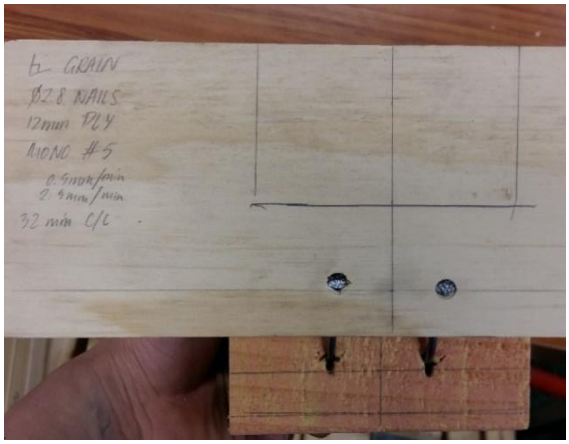

Figure 3-44: Withdrawal, lateral deformation and crushing of the timber stud and plywood observed post-test.

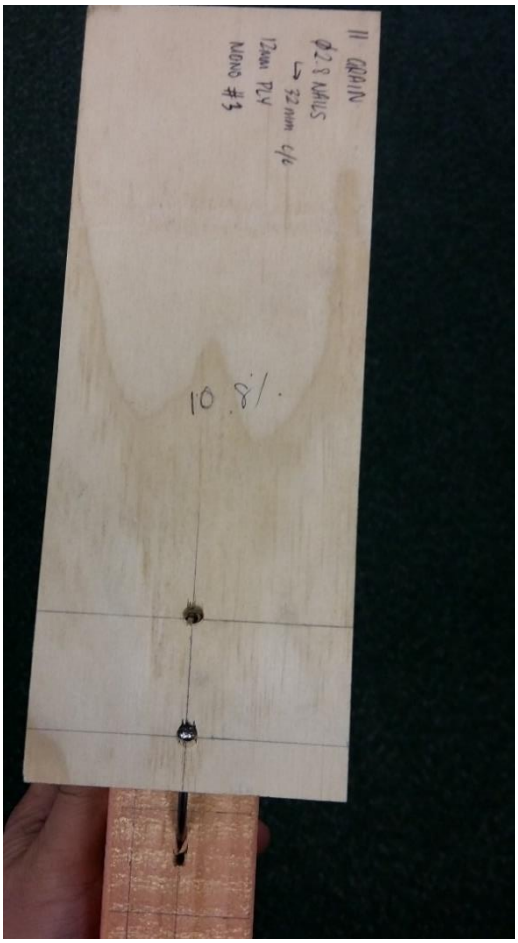

Figure 3-43: Withdrawal, lateral deformation and crushing of the timber stud and plywood observed post-test.

3.3.4 Cyclic test results

Figure 3-45 through Figure 3-47 show the load-displacement curves obtained from the cyclic tests. Structural properties such as strength, stiffness and ductility are presented in tabular form (Table 3-21 to Table 3-23) and a description of connection behaviour under cyclic loading is provided. For the full cyclic tests results for the timber-sheathing, see Appendix D.

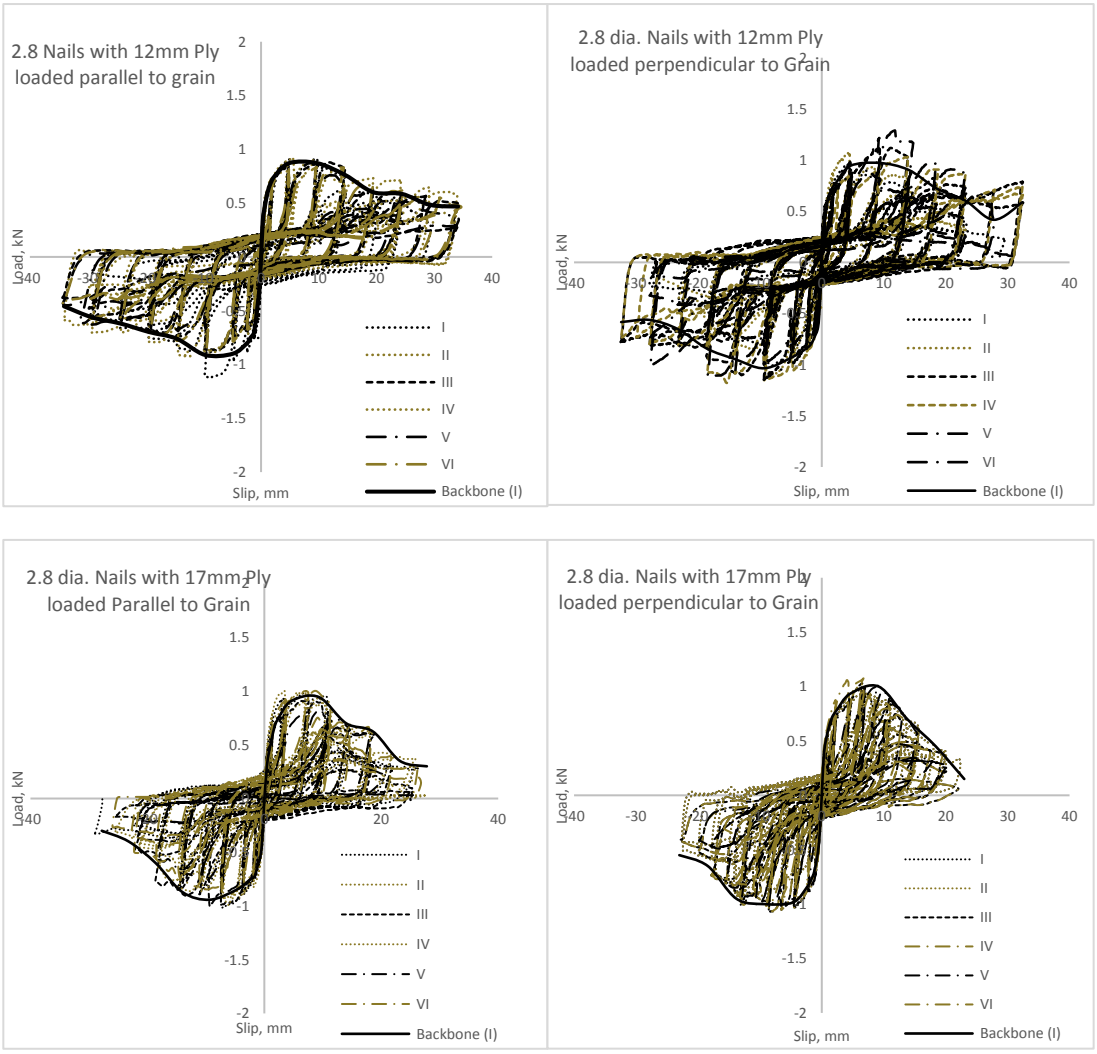

Figure 3-45: Hysteresis curves for φ2.8 Nails with varying plywood thickness (single nail).

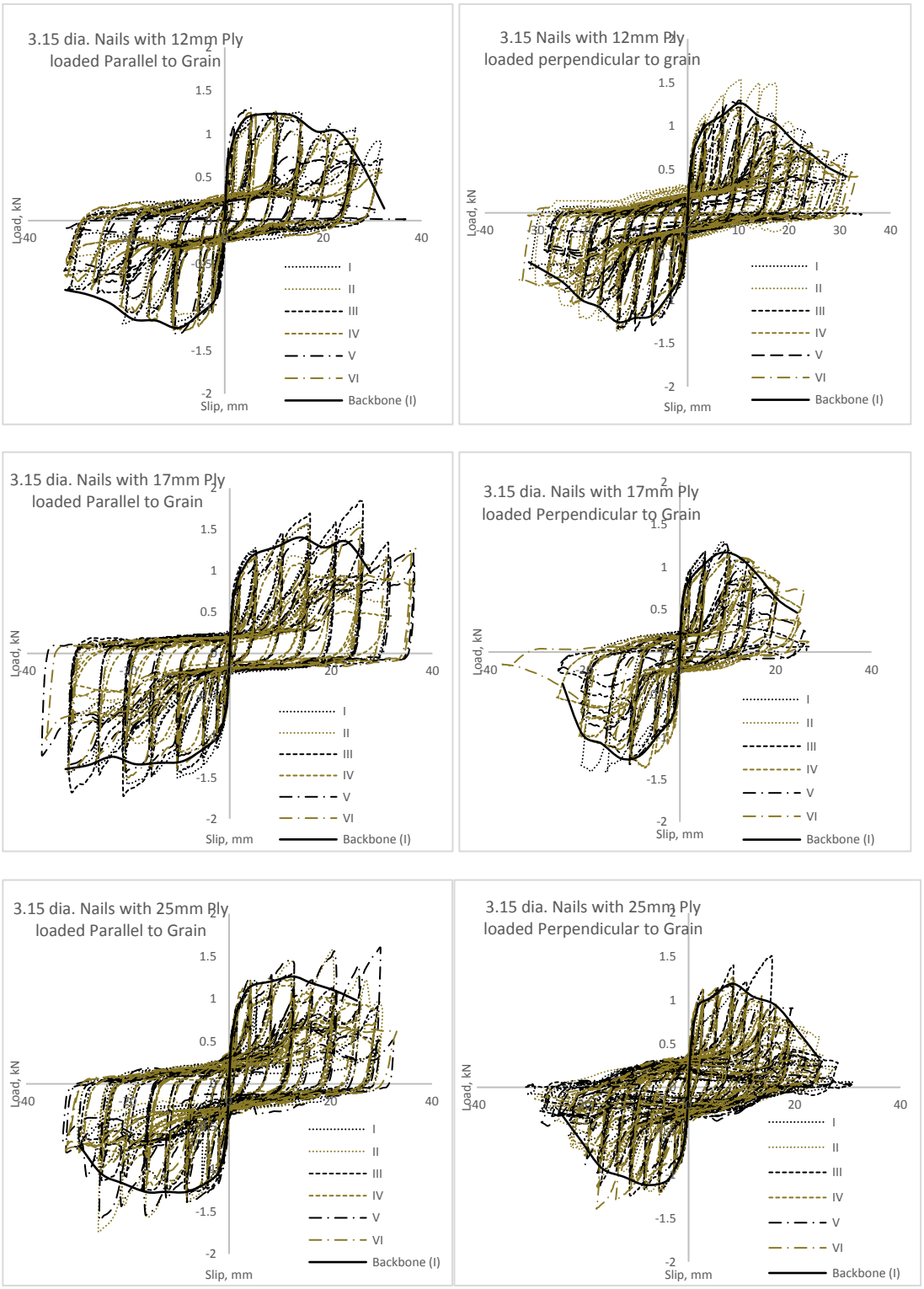

Figure 3-46: Hysteresis curves for φ3.15 Nails with varying plywood thickness (single nail).

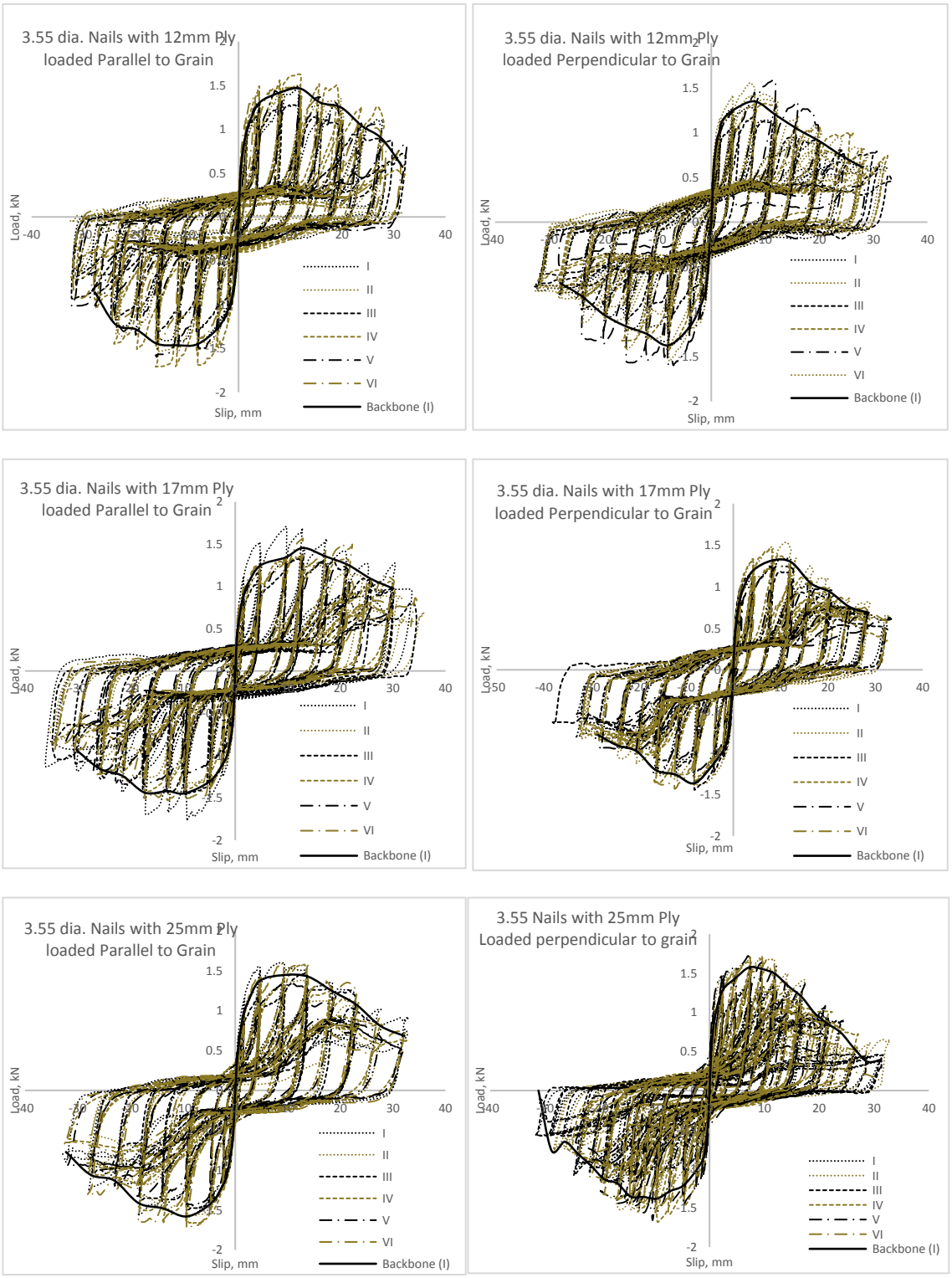

Figure 3-47: Hysteresis curves for φ3.55 Nails with varying plywood thickness (single nail).

Table 3-21: Average properties for φ2.8 nailed connections (single nail) with varying plywood thicknesses tested under both montonic and cyclic loading.

φ2.8 NAILS	12mm Ply				17mm Ply			
	Parallel		Perpendicular		Parallel		Perpendicular	
	Mono	Cyclic	Mono	Cyclic	Mono	Cyclic	Mono	Cyclic
k_i (kN/mm)	1.13	0.90	1.65	1.20	1.11	1.25	1.43	0.91
F_y (kN)	0.66	0.65	0.60	0.68	0.58	0.66	0.47	0.58
F_{max} (kN)	1.15	0.91	1.22	1.09	1.14	0.96	1.04	1.10
F_{ult} (kN)	0.88	0.73	1.00	0.87	0.91	0.76	0.83	0.88
Δ_y (mm)	0.9	1.8	0.8	1.2	0.7	1.3	0.4	1.9
Δ_{max} (mm)	14.2	10.4	11.7	8.5	10.8	8.3	6.7	8.2
Δ_{ult} (mm)	27.7	19.4	20.5	16.9	20.3	13.3	13.4	14.8
u	30.8	10.8	25.6	14.1	29.0	10.2	33.5	7.9
$F_{(1-3)}$	-	21.3 - 46.5%	-	19.7 - 36.3%	-	12.3 - 33.3%	-	6.1 - 13.9%

Table 3-22: Average properties for φ3.15 Nailed connections (single nail) with varying plywood thicknesses tested under cyclic loading.

φ3.15 NAILS	12mm Ply				17mm Ply				25mm Ply			
	Parallel		Perpendicular		Parallel		Perpendicular		Parallel		Perpendicular	
	Mono	Cyclic	Mono	Cyclic	Mono	Cyclic	Mono	Cyclic	Mono	Cyclic	Mono	Cyclic
k_i (kN/mm)	1.02	1.04	1.30	0.89	1.30	1.07	1.01	1.42	1.21	1.42	1.09	1.63
F_y (kN)	0.65	0.86	0.85	0.73	0.77	0.81	0.87	0.73	0.91	0.91	0.87	0.85
F_{max} (kN)	1.19	1.34	1.41	1.28	1.32	1.46	1.45	1.28	1.34	1.39	1.37	1.22
F_{ult} (kN)	0.85	1.07	1.13	1.03	1.06	1.17	1.12	1.03	1.07	1.11	1.10	0.98
Δ_y (mm)	1.1	3.2	1.1	1.2	1.5	1.2	1.3	1.1	1.7	1.3	1.3	1.5
Δ_{max} (mm)	11.5	12.7	10.4	11.6	12.7	15.2	9.3	10.5	15.4	12.7	7.9	8.8
Δ_{ult} (mm)	32.4	22.1	18.4	18.4	31.1	28.4	18.2	17.3	32.5	23.2	14.8	15.4
u	29.5	7.0	16.7	15.3	20.7	23.7	14.0	15.7	19.1	17.9	11.4	10.3
$F_{(1-3)}$	22 - 46.7%		-	22 - 46.7%	-	19.9 - 31.2%	-	14.5 - 30.5%	-	22 - 36.4%	-	14.6 - 29.5%

Table 3-23: Average properties for φ3.55 nailed connections (single nail) with varying plywood thicknesses tested under both monotonic and cyclic loading.

φ3.55 NAILS	12mm Ply				17mm Ply				25mm Ply			
	Parallel		Perpendicular		Parallel		Perpendicular		Parallel		Perpendicular	
	Mono	Cyclic	Mono	Cyclic	Mono	Cyclic	Mono	Cyclic	Mono	Cyclic	Mono	Cyclic
k_i (kN/mm)	1.69	0.74	1.30	1.61	1.44	1.22	1.58	1.17	1.24	1.21	1.40	1.66
F_y (kN)	0.84	0.95	0.98	0.97	0.88	0.93	0.90	0.90	0.91	1.00	1.01	1.05
F_{max} (kN)	1.46	1.49	1.73	1.41	1.33	1.46	1.46	1.36	1.61	1.54	1.72	1.54
F_{ult} (kN)	1.11	1.19	1.38	1.12	1.14	1.17	1.15	1.09	1.29	1.23	1.37	1.23
Δ_y (mm)	0.9	1.2	1.5	2.2	1.0	1.5	1.1	1.4	1.4	1.6	1.2	1.8
Δ_{max} (mm)	10.5	11.6	10.0	9.1	10.3	12.5	10.3	9.5	14.2	10.0	11.1	9.9
Δ_{ult} (mm)	22.5	22.6	21.1	16.9	23.0	24.0	21.3	17.2	25.7	20.3	18.0	18.2
u	25.0	18.8	14.1	7.7	23.0	16.0	19.4	12.3	19.0	12.7	15.6	10.1
$F_{(1-3)}$	-	13.8 - 33%	-	14.3 - 27.5%	-	13 - 24.4%	-	12.8 - 24%	-	8 - 15%	-	7.6 - 15.5%

The nailed connections under cyclic loading showed similar ductile behavior compared with the connections under monotonic loading. The failure modes included nail bending yielding, nail withdrawal, low cycle fatigue failure, and wood embedment crushing, as shown in Figure 3-48.

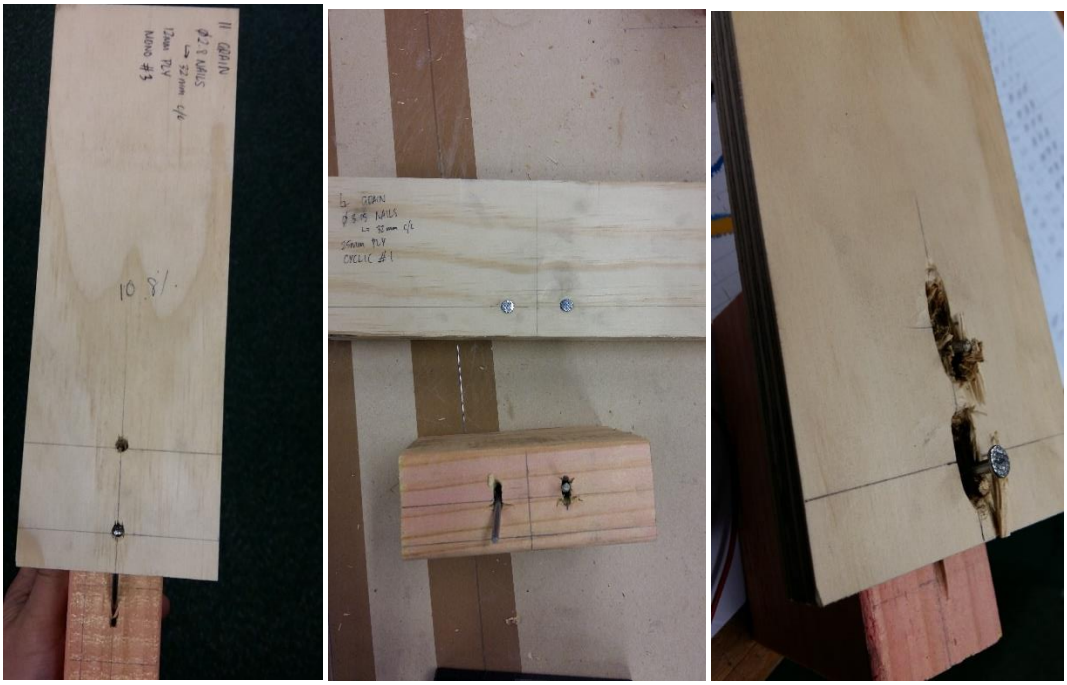

Figure 3-48: Failure modes observed in cyclic testing of nailed connections.

3.3.5 Discussion

Nail size was shown to have positive correlation with the connection strength (yield, peak and ultimate). Depending on the thickness of plywood in the connection, incremental increases in nail size led to 10 - 53% higher capacity. Nail size also showed weak negative correlation with strength degradation in the second and third cycles of loading: increasing nail size led to 1.3 – 14% less strength degradation in the second cycles, and 1.2% to 21% less strength degradation in the third loading cycles. Generally speaking, nail size showed positive correlation with ductility, when in combination with thinner plywood (12mm and 17mm), and increasing nail size led to 22 – 139% larger ductility factors. However, ductility began to drop as nail size was increased in thicker plywood (25mm), decreasing by 30% for Φ3.55x90mm nails compared with Φ3.15x75mm nails.

Compared to the two other plywood thicknesses, 17mm thick plywood was observed to provide a connection with largest displacements (and ductility) when combined with larger nails (Φ3.15x75mm and Φ3.55x90mm). Of particular interest is the fact that mid-size nails (Φ3.15x75mm) used in combination with mid-thickness plywood (17mm), produced the most ideal structural performance in terms of peak loads and ductility.

Plywood thickness was not found to have correlation with connection strength or initial stiffness. As the plywood thickness increased, the effect on the peak load and initial stiffnes was negligible. However, the effect of increasing plywood thickness on ultimate displacements (and ductility) is dependent on the nail size. For example, the results showed minor increases in ultimate displacement for Φ3.55x90mm nails, while with Φ2.8x60mm nails, increases in plywood thickness show large reductions in ultimate displacements,.and the

effect of ultimate displacement on Φ3.15x75mm nails as the plywood thickness increased was negligible. It is important to note that nail embedment depth is an important design parameter. Greater nail embedment depth is correlated with higher peak strengths and greater ductility factors.

The influence of load-grain direction on the connection capacity was found not significant. However, the connections loaded perpendicular to grain had significantly lower ultimate displacement due to the tendancy of wood splitting, thus leading to 12 – 45% lower ductility than the connections loaded parallel to grain.

3.4 Conclusions

In this chapter, two types of critical connections in the hybrid shear wall sytems: timber-steel interface connections and timber-plywood connections were experimentally tested. Fastener bending yield strength was evcaluated by three-point bending tests, and monotonic tests and reversed cyclic tests were conducted to evaluate the connection behavior.

In the timber-steel interface connection tests, the effect of fastener sizes and timber stud thickness (i.e. of number of timber studs) on the connection behavior was evaluated. In the timber-plywood connection tests, the effect of nail size, plywood thickness and load-grain orientation was evaluated.

The main findings are presented as follow:

- All the connections showed ductile behavior and reliable load carrying capacity.
- In general, the bolted timber-steel interface connections had better performance in terms of strength and ductility. Given similar connection configurations, the bolted steel-timber interface connections, compared to the coach screwed connections, had 10 - 76% higher yield strengths, 6.7 – 107% greater initial stiffness (k_i). The bolted connections also exhibited higher ductility, up to 2.5 times larger than the coach screwed connections.
- The timber-plywood connections in combination of Φ3.15x75mm nails with 17mm plywood showed most favorable overall performance in terms of strength and ducility among all the combinations of nails sizes and plywood thicknesses. The combination of smaller nails (Φ2.8x60mm) with thicker ply (25mm) was not recommended because of relatively insufficient nail embedment depth leading to relativley poor performance.

4 NUMERICAL MODELLING

This chapter describes finite element modeling of the hybrid shear wall using software package ABAQUS (Dassualt Systemes, 2018). The model input parameters for the critical connections were calibrated by the connection test database. A parametric study was further conducted to study the influence of various design parameters on the cyclic performance of the hybrid walls.

4.1 Introduction

The primary objective of this numerical campaign was to simulate the behaviour of the timber-steel hybrid wall under cyclic loading. The construction of the hybrid wall model, along with the curve-fitting process for experimental connection data is first described in Section 4.2. Section 4.3 presents the parametric study on a total of 70 different hybrid wall configurations considering the following the effect of various plywood thickness, nail size, interface connection types, and steel member sizes. Wall configurations in the parametric study are summarised in Table 4-1 and Table 4-2.

Table 4.3 lists of the dimensions of the steel beams and columns used in this study. Based on the load-drift curves of the walls, the wall performance was assessed in terms of strength, stiffness, ductilty and strength degradation. The effect of each variable is discussed in Section 4.4.

Based on the simulation data, a hybrid wall ductilty factor for structural design was also suggested (Section 4.4). The viscous damping ratio (required for displacement-based design), was evaluated for the proposed timber-steel hybrid wall system (Section 4.6). The chapter concludes with a summary of main research findings, as well as the limitations of the numerical investigation.

Table 4-1: Wall configurations with various nail sizes, plywood thicknesses, and timber-steel interface connections (note: steel framing members kept constant, UB250 and UC250).

	12mm Ply			17mm Ply			25mm Ply	
	Φ2.8	**Φ3.15**	**Φ3.55**	**Φ2.8**	**Φ3.15**	**Φ3.55**	**Φ3.15**	**Φ3.55**
M10 Coach (2x Studs)	*Wall #01*	*Wall #02*	*Wall #03*	*Wall #04*	*Wall #05*	*Wall #06*	*Wall #07*	*Wall #08*
M10 Coach (3x Studs)	*Wall #09*	*Wall #10*	*Wall #11*	*Wall #12*	*Wall #13*	*Wall #14*	*Wall #15*	*Wall #16*
M12 Coach (2x Studs)	*Wall #17*	*Wall #18*	*Wall #19*	*Wall #20*	*Wall #21*	*Wall #22*	*Wall #23*	*Wall #24*
M12 Coach (3x Studs)	*Wall #25*	*Wall #26*	*Wall #27*	*Wall #28*	*Wall #29*	*Wall #30*	*Wall #31*	*Wall #32*
M10 Bolt (2x Studs)	*Wall #33*	*Wall #34*	*Wall #35*	*Wall #36*	*Wall #37*	*Wall #38*	*Wall #39*	*Wall #40*
M10 Bolt (3x Studs)	*Wall #41*	*Wall #42*	*Wall #43*	*Wall #44*	*Wall #45*	*Wall #46*	*Wall #47*	*Wall #48*
M12 Bolt (2x Studs)	*Wall #49*	*Wall #50*	*Wall #51*	*Wall #52*	*Wall #53*	*Wall #54*	*Wall #55*	*Wall #56*
M12 Bolt (3x Studs)	*Wall #57*	*Wall #58*	*Wall #59*	*Wall #60*	*Wall #61*	*Wall #62*	*Wall #63*	*Wall #64*

Table 4-2: Wall configurations #65 to #70 with various steel frame member sizes (Note: other wall parameters kept constant M12 bolts with double studs, Φ3.55x90mm nails and 25mm thick plywood.

	Steel column		
Steel beam	**UC200**	**UC250**	**UC310**
UB150	*Wall #65*	-	-
UB180	*Wall #66*	-	-
UB200	-	*Wall #67*	*Wall #69*
UB250	-	*Wall #68*	*Wall #70*

Table 4-3: Steel member section sizes as per Easy Steel design charts*. All dimensions given are in mm.*

Steel designation	Depth	Flange		Web thickness
		Width	Thickness	
UB150	155	75	9.5	5.99
UB180	175	90	8.0	5.0
UB200	203	133	7.82	5.84
UB250	252	146	8.64	6.1
UC200	203	203	11.0	7.32
UC250	254	254	14.2	8.64
UC310	308	305	15.4	9.91

4.2 Finite element model overview

The FE hybrid wall model was built upon a similar hybrid wall model developed by Dong (2017). It has three key components:framing elements, panel elements, and connection elements. The framing elements represent steel frame members and timber frame members. The panel elements represent the plywood sheathing and the connection elements represent the connections including the critical timber-plywood and timber-steel interface connections investigated in Chapter 3, and the steel frame base connections. A screenshot of the FE model is given in Figure 4-1. A comprehensive summary of the structural components, material properties, section properties and their element type designation in ABAQUS can be found in Table 4-4. Numerical behaviour of the interface connections was simulated using the Q-Pinch model, and calibrated with the connection test results presented in Chapter 3.

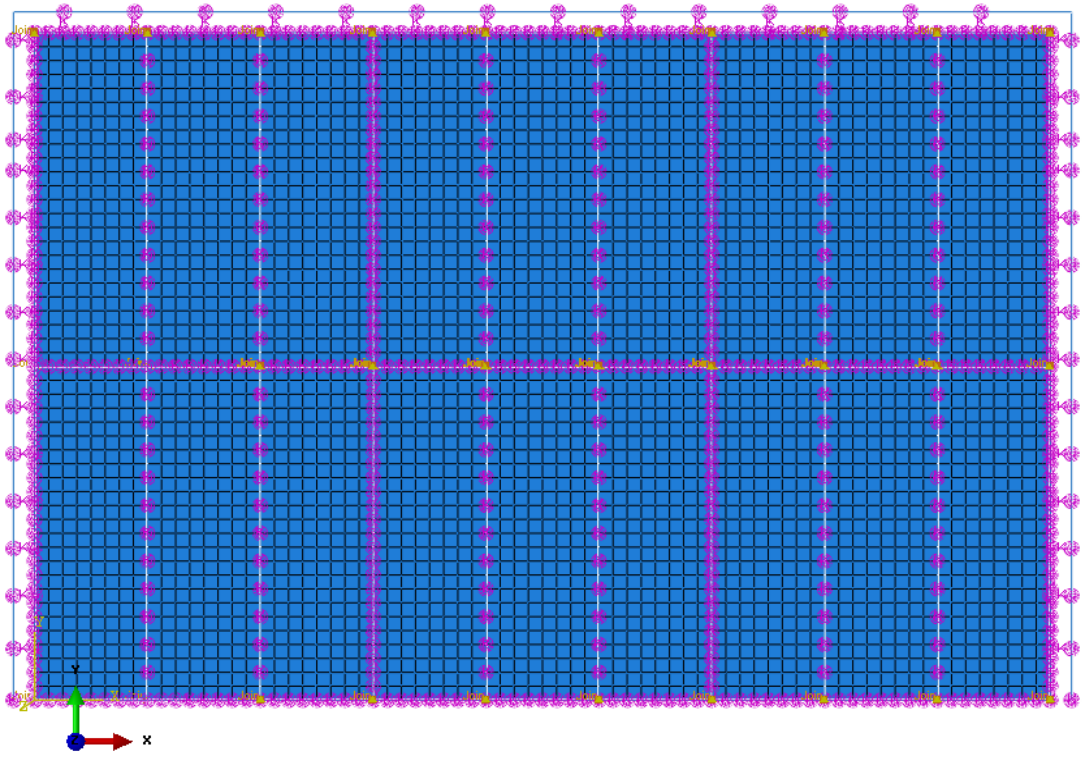

Figure 4-1: Timber-steel hybrid shear wall FE model in ABAQUS (2018)

Table 4-4: Finite element representation of structural components in ABAQUS

Structural Component	Finite-Element representation (ABAQUS)	Material and Section properties
Steel framing	Beam element: 2-node (B21)	E = 210GPa, ρ = 7850 kg/m^3, σ_y = 300MPa, σ_{yp} = 301MPa, ε_p = 0.001
Timber framing	Beam element: 2-node (B21)	E = 8.0GPa ρ = 450 kg/m^3 Cross-sectional area = 90x45mm
Sheathing	Solid element: 8-node plain stress, reduced integration (CPS8R)	E_x = 1.9GPa, E_y = 9.1GPa, G = 455MPa, ρ = 650 kg/m^3 Plywood thicknesses (t_p) = 12mm, 17mm, 25mm
Timber-sheathing connections	User defined element pair: 2-node, non-linear (U1)	Nail sizes = Φ2.8x60mm, Φ3.15x75mm, Φ3.55x90mm Plain shank, Q-Pinch parameters
Timber-steel connections	User defined element pair: 2-node, non-linear (U1)	Q-Pinch parameters

4.2.1 Framing and panel elements

As shown in Table 4-4, the material properties of the steel beam elements were defined as elastic-perfectly plastic with structural steel 300 grade. Beam-column joints of the steel frame were modelled as rigid

connections. Material properties of plywood and timber members were assumed to be linear elastic. The average elastic modulus for plywood was taken both directions (parallel and perpendicular to face grain). Steel frame base connections were modelledas pin connections.

4.2.2 Critical connection elements

The critical interface connections were experimentally tested in Chapter 3. The test results were used to calibrate the parameters of the Q-Pinch model (Judd, 2005). The Q-Pinch model was incorporated into the FE model as a user-defined, non-linear spring element. This section presents the calibration of the Q-Pinch model parameters to replicate the cyclic load-displacement behaviour of the connections tested in Chapter 3. The calibrated Q-Pinch parameters of different conneciton configurations are listed in Table 4-5 and Table 4-6.

Q-Pinch model calibration

4.2.2.1 The Q-Pinch model was implemented in a simple FE connection model in ABAQUS to replicate the experimental results. The FE model was subjected to the same ISO16670:2003 displacement protocol as the experimental tests.

In Chapter 3, each nailed timber-plywood connection type was tested along both parallel to grain and perpendicular to the face grain directions. Since the load-grain directions had no sigficant influence on the conneciton behavior, for simplicity, the average load-deformation curves along those two directoins were used for the Q-Pinch model calibration.

Figure 4-2 shows one example of the calibrated Q-Pinch model predictions compared with the experimental results. The model showed good agreement with the experimental response.

4.2.2

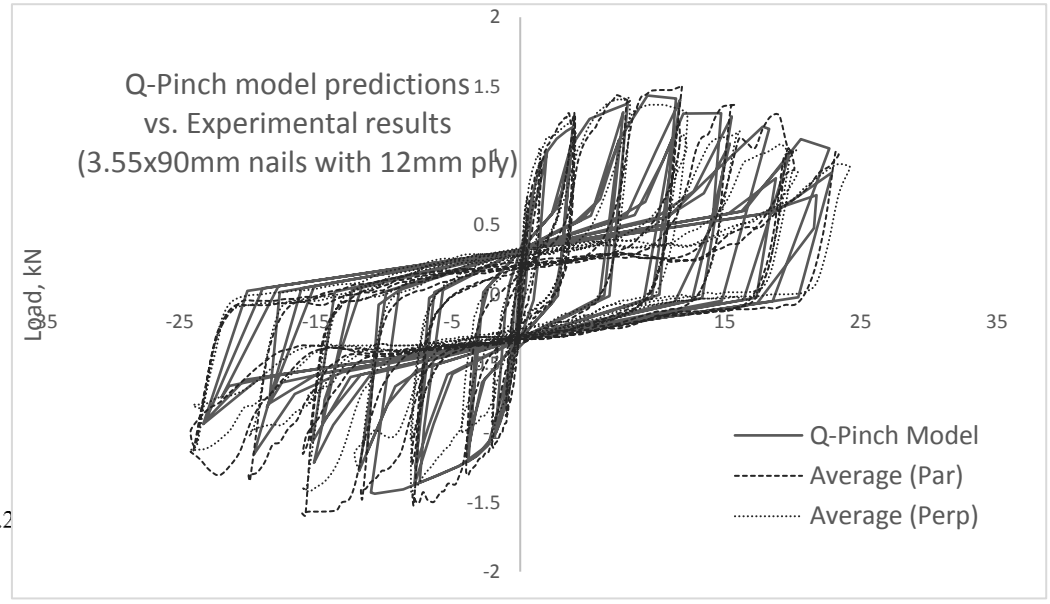

Figure 4-2: Model validation for interface connections using the Q-Pinch model (Judd, 2005)

Q-Pinch connection model parameters

The calibrated Q-Pinch parameters of the critical connections are summarised in

Table **4-5** and Table 4-6. The definitions of the model parameter can be found in the footnote of Table 4-6.

Table 4-5: Calibrated parameters of timber-plywood connections

Nail size	t_p	k_1 N/mm	k_2 N/mm	k_3 N/mm	k_4 N/mm	F_0 N	F_1 N	Δ_y mm	Δ_{ult} mm	Δ_{fail} mm	α	β
ϕ2.8x60	**12mm**	846	25	38.5	920	783	175	1.1	9.9	16	0	1.1
ϕ3.15 x75	**12mm**	625	20	20	675	1120	250	2.0	7.3	21	0	1.05
ϕ3.55 x90	**12mm**	1243	39	33	1950	1070	320	1.1	10	20	0	1.1
ϕ2.8x60	**17mm**	850	35	60	1050	750	150	1.1	8.2	14	0	1.1
ϕ3.15x75	**17mm**	1094	25	31.5	1450	1025	220	1.6	18.3	24	0	1.1
ϕ3.55x90	**17mm**	970	27	35	1000	1090	305	1.1	12.6	25	0	1.1
ϕ3.15x75	**25mm**	1131	34	35	1231	935	310	1.1	8.2	15	0.35	1.1
ϕ3.55x90	**25mm**	1303	53	50	1903	1175	280	1.1	10	17	0.2	1.1

Table 4-6: Calibrated parameters of timber-steel interface connections

Fastener	No. of studs	k_1 N/mm	k_2 N/mm	k_3 N/mm	k_4 N/mm	F_0 N	F_1 N	Δ_y mm	Δ_{ult} mm	Δ_{fail} mm	α	β
M10 Bolt	**Double**	7200	35	100000	8350	11500	3000	1.6	21.0	21.8	0	1.1
M10 Bolt	**Triple**	6600	280	1600	7000	13000	3700	2.5	13	15.0	0	1.1
M12 Bolt	**Double**	7200	150	100000	7400	16500	4200	2.5	28	30	0.70	1.1
M12 Bolt	**Triple**	6000	150	1600	6400	15800	3500	3.0	28	30	0.15	1.0
M10 C. Screw	**Double**	4410	150	500	5220	10000	1700	2.2	20	21.0	0	1.1
M10 C. Screw	**Triple**	4250	150	1000	7050	10000	2000	2.8	20.5	21.0	0.2	1.0
M12 C. Screw	**Double**	2800	150	50000	5500	13200	1500	6.0	28.9	29	0.85	1.1
M12 C. Screw	**Triple**	3800	160	50000	6000	14000	1700	6.0	26	26.5	0	1.1

Note:

t_p = Plywood thickness, mm

k_1 = Initial stiffness, N/mm

k_2 = Plastic stiffness, N/mm

k_3 = Degradation stiffness, N/mm

k_4 = Unloading stiffness, N/mm

4.2.2.3 *F_0 = Yield Force, N*

F_1 = Pinching Force, N

α = Reloading degradation factor

β = Stiffness degradation factor

Connection structural representation

When subjected to lateral loads, nail fasteners in plywood infill walls tend to deform along different directions, and will not be restricted to only horizontal or vertical movement. Therefore, the oriented spring pairs proposed by Judd (2005) were also used to model the coupling behavior of the nailed connections along the original motion direction and the perpendicular to the original direction.

For the bolted timber-steel interface connections, Li et al (2014b) suggested that these connections should be strong enough and avoid any premature failure before the failure of the infill wall. For these connections, the bolt fasteners are restrained by the flanges of steel members and the timber framing members under lateral loading. Therefore, it was assumed that these connections only deform in lateral and axial directions. Non-oriented (uncoupled) spring pairs were adopted to represent the connection behavior under shear loading and axial loading. The Q-pinch algorithm was used to model the connection behavior under shear loads. Elastic springs were used to model the connection behavior under axial loads.

4.2.3 Finite Element model validation

The response of a 2/3 scale timber-steel hybrid wall with infilled OSB-sheathed shear wall tested by Dong (2017) (Figure 4-3) was used to validate the numerical model. The height and width of the wall specimen was 2.4m and 1.65m respectively. The FE model used in this thesis simply adopted material and section properties of the timber framing, steel framing and OSB sheathing in the tested wall, as summarised in

Table 4-7. The experimental test specimen and FE model were both subjected to the ISOI6670:2003 cyclic protocol. The load-drift hysteresis of the FE hybrid wall model was compared against the experimental results, as shown in Figure 4-4. The overall model predictions agreed well with the experimental results.

Figure 4-3: Two-third scale test on hybrid shear wall (Dong, 2017)

Table 4-7: Finite element representation and materal & section properties used in Dong (2017)

Structural Component	Finite-Element representation (ABAQUS)	Material and Section properties
Steel framing	Beam element: 2-node (B21)	E = 210GPa, ρ = 7850 kg/m^3, σ_y = 235MPa, σ_{yp} = 260MPa, ε_p = 0.001 Steel frame sections: UB150 and UC150
Timber framing	Beam element: 2-node (B21)	E = 8.23GPa, ρ = 450 kg/m^3 Cross-sectional area = 140x38mm
Sheathing	Solid element: 8-node plain stress, reduced integration (CPS8R)	E_x = 5.16GPa, E_y = 2.64GPa, G = 1000MPa, ρ = 650 kg/m^3 OSB thicknesses (t_p) = 9.5mm
Timber-sheathing connections	User defined element pair: 2-node, non-linear (U1)	Nail sizes = Φ3.3x82.5mm Plain shank, Q-Pinch parameters
Timber-steel connections	User defined element pair: 2-node, non-linear (U1)	Q-Pinch parameters
Steel-frame base connections	Spring element: 2-nodes, linear (SPRING2)	k_{rot} = 760kNm/rad

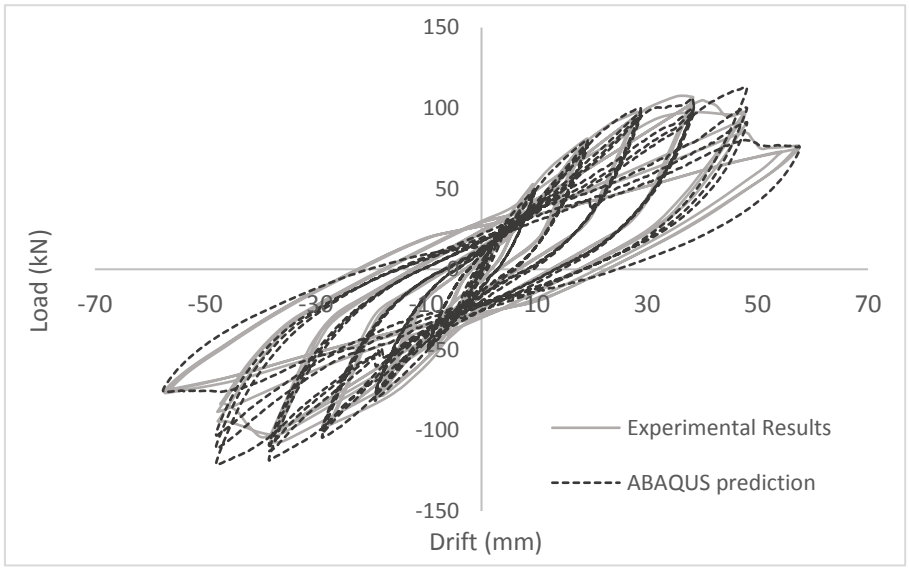

Figure 4-4: FE model predicitons vs. experimental results

4.3 Parametric Analysis

70 different wall configurations were simulated by the validated FE hybrid wall model in ABAQUS. The simulated wall configurations have been listed in Table 4-1 and Table 4-2.

4.3.1 Structural configuration

Conventional materials and dimensions following New Zealand contruction practice were used in this study. These also include nail spacings in accordance with NZS3603. For this study, nailing pattern of 50/100 was used in study, meaning the nail spacing of 50 mm along perimeters of plywood sheets and 100 mm in field. The total length of the infill wood frame wall is 3.6m long and 2.4m high. The benchmark wall configurations are shown in Figure 4-5.

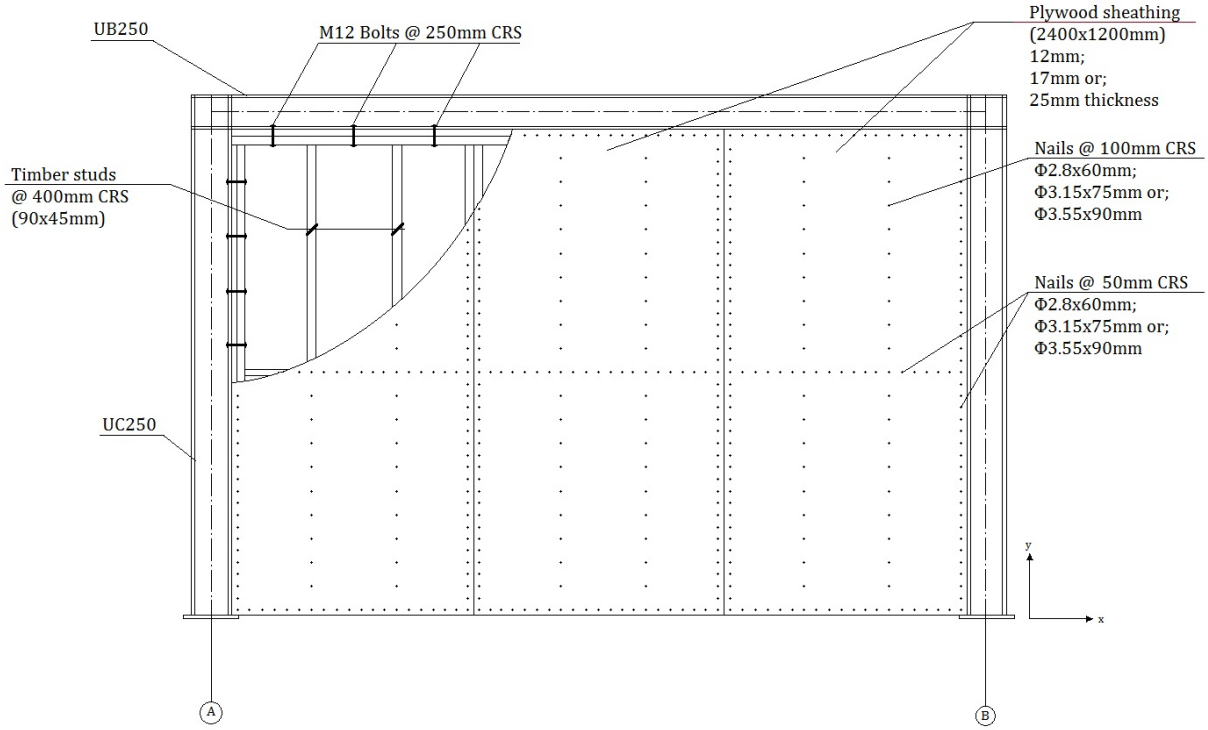

Figure 4-5: Structural configurations of the FE hybrid model

4.3.2 Methodology

The hybrid wall was subjected to displacement controlled loading shown in Figure 4-6. The load was applied to the top left beam column joint. To calculate the load-carrying contribution of the infill wall, the bottom nodes of the infill wall were tracked. The load-carrying contribution of the steel frame is the difference between the total base shear and the load carried by the infill wall.

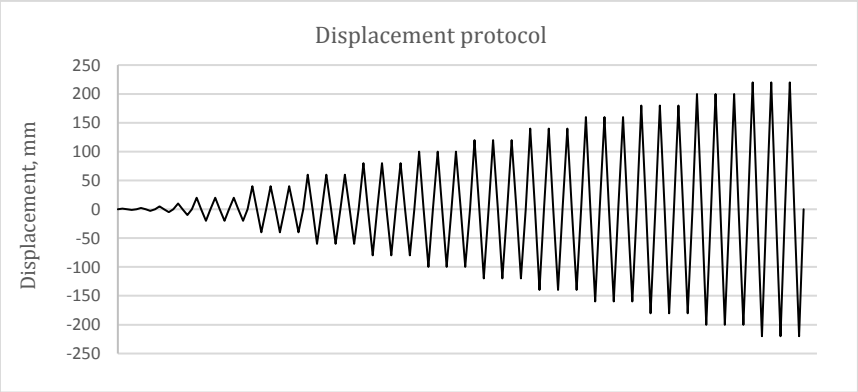

Figure 4-6: Cyclic displacement protocol

ASTM E2126 was used to assess the hybrid wall behavior, as shown in Figure 4-7. The ciritical wall performance parameters are listed as follows:

- Peak Load resisted by hybrid system, P_{peak}, kN.
- Peak load resisted by infill wall, $P_{peak,infill}$, kN
- Initial stiffness of hybrid system, k_{hybrid}, kN/m

$$k_{hybrid} = \frac{0.4P_{peak}}{\Delta_{0.4Ppeak}} \quad (7)$$

- Initial stiffness of infill wall, k_{infill}, kN/m

$$k_{infill} = \frac{0.4P_{peak,infill}}{\Delta_{0.4Ppeak,infill}} \quad (8)$$

- Relative infill-to-frame ratio, R ratio

$$\mathrm{R} = \frac{k_{infill}}{k_{bareframe}} \quad (9)$$

- Yield force of the hybrid shear wall, P_{yield}, kN

$$P_{yield} = \frac{F_o}{(1-\frac{k_{post-yield}}{k_{initial}})} \quad (10)$$

Where, F_o is the y-intercept of the post-yield stiffness line ($k_{post\text{-}yield}$).

- Yield displacement, Δ_y, mm

$$\Delta_y = \frac{P_{yield}}{k_{hybrid}} \quad (11)$$

- Ultimate displacement, Δ_{ult}, mm, the displacement corresponding to the point of th envelope curve of attaining a residual strength equal to $0.8P_{peak}$.
- Ductility, μ

$$\frac{\Delta_{ult}}{\Delta_y} \quad (12)$$

- Total energy dissipation, E_{diss} (kJ), calculated in accordance with ASTM E2126

$$E_{diss} = \left(\frac{1}{2}P_{yield}\Delta_y\right) + [P_{yield}(\Delta_{ult} - \Delta_y)] \quad (13)$$

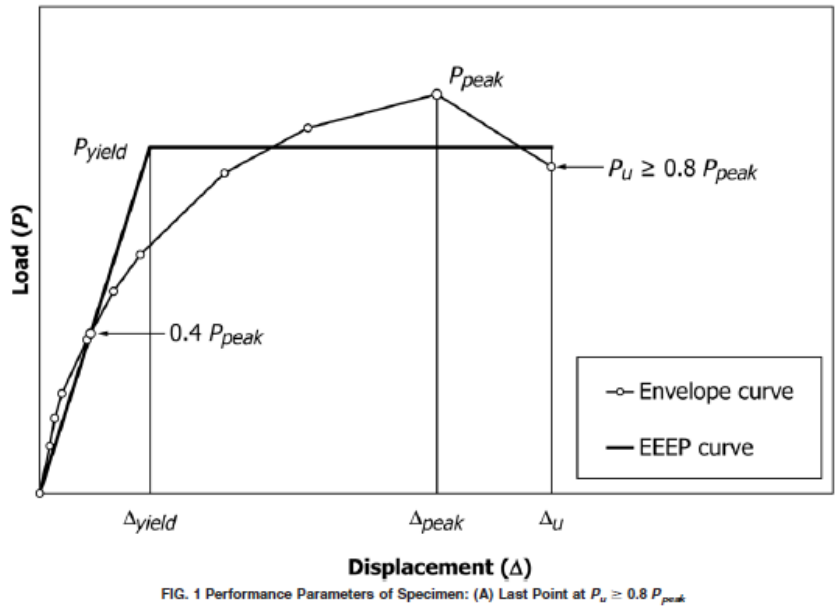

FIG. 1 Performance Parameters of Specimen: (A) Last Point at $P_u \geq 0.8\ P_{peak}$

Figure 4-7: Idealised envelope curve to determine energy dissipation following ASTM E2126

4.4 Numerical Results

A typical load-deformation curve of the timber-steel hybrid system obtained from the numerical cyclic analysis is shown in Figure 4-8. Full tabulated results are presented below, and are presented according to different types of timber-steel interface connections for readability.

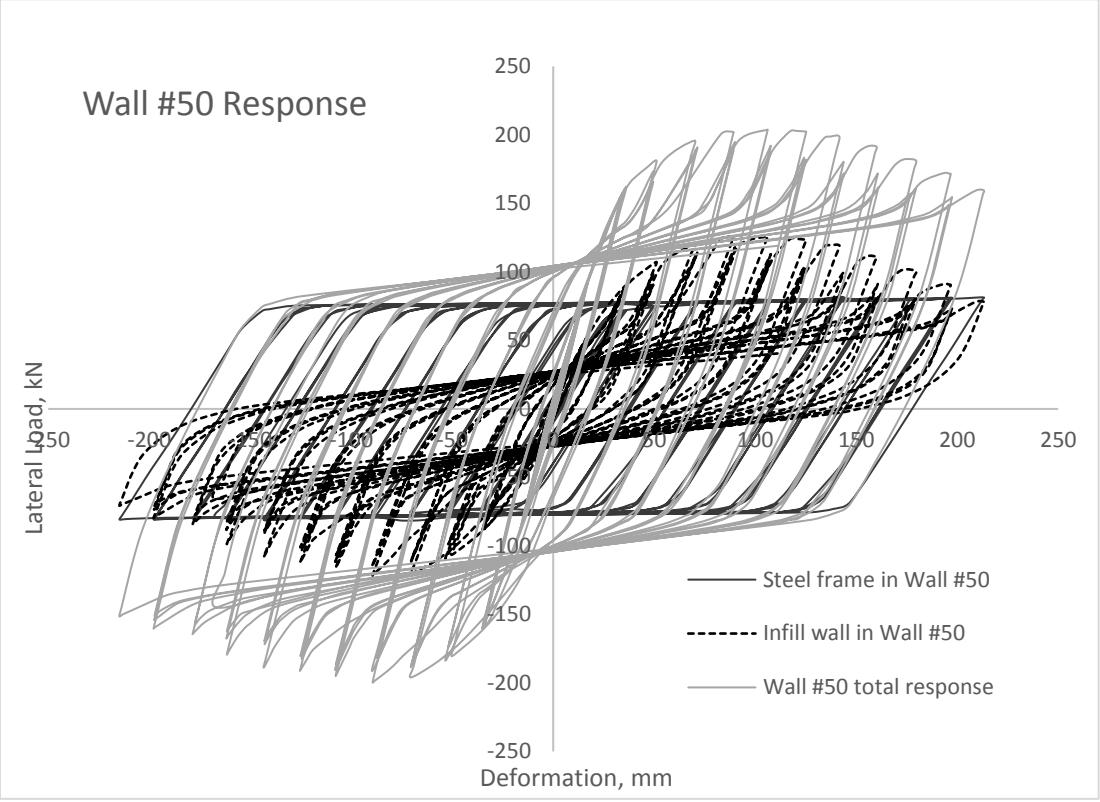

Figure 4-8: Typical hysteretic response of the timber-steel hybrid shear wall, with load carrying contributions from the infill wall and bare frame shown.

Table 4-8: Results of the hybrid wall configurations using M10 Coach Screws

Wall #	Timber-steel	Nail size	Plywood thickness	P_{peak}, kN	P_{yield}, kN	$P_{infill,peak}$, kN	k_{hybrid}, kN/m	k_{infill}, kN/m	R	Δ_y, mm	Δ_{ult}, mm	μ	E_{diss} (kJ)
1	M10 Coach (2x Studs)	Φ2.8 x 60	12mm	182	149	105	4.61	2.99	1.8	24	149	6.3	18.7
2		Φ3.15 x 75	12mm	203	175	126	4.26	2.62	1.6	30	180	6.0	26.6
3		Φ3.55 x 90	12mm	224	178	146	5.06	3.50	2.2	26	194	7.5	29.2
4		Φ2.8 x 60	17mm	179	146	103	5.08	3.52	2.3	21	105	5.0	12.5
5		Φ3.15 x 75	17mm	221	177	143	5.50	3.96	2.6	24	220	9.3	34.5
6		Φ3.55 x 90	17mm	218	175	136	5.31	3.75	2.4	24	176	7.3	26.1
7		Φ3.15 x 75	25mm	203	167	122	5.05	3.29	1.9	24	148	6.1	20.6
8		Φ3.55 x 90	25mm	248	191	167	5.21	3.49	2.0	27	162	6.0	25.3
9	M10 Coach (3x Studs)	Φ2.8 x 60	12mm	175	149	97	4.60	2.92	1.7	24	138	5.8	17.3
10		Φ3.15 x 75	12mm	203	171	124	4.25	2.56	1.5	30	196	6.7	28.3
11		Φ3.55 x 90	12mm	224	179	147	5.05	3.43	2.1	26	189	7.3	28.7
12		Φ2.8 x 60	17mm	179	148	103	5.08	3.43	2.1	21	106	5.0	12.8
13		Φ3.15 x 75	17mm	217	173	138	5.49	3.85	2.3	23	215	9.3	32.7
14		Φ3.55 x 90	17mm	217	172	136	5.30	3.65	2.2	24	180	7.6	26.3
15		Φ3.15 x 75	25mm	203	168	121	5.04	3.17	1.7	24	145	5.9	20.4
16		Φ3.55 x 90	25mm	249	191	167	5.21	3.37	1.8	27	162	6.0	25.3

Table 4-9: Results of the hybrid wall configurations using M12 Coach Screws

Wall #	Timber-steel connection	Nail size	Plywood thickness	P_{peak}, kN	P_{yield}, kN	P_{infill}, kN	k_{hybrid}, kN/m	k_{infill}, kN/m	R	Δ_y, mm	Δ_{ult}, mm	μ	E_{diss} (kJ)
17	M12 Coach Screw (2x Studs)	Φ2.8 x 60	12mm	182	152	104	4.55	2.88	1.7	24.5	142	5.8	18.3
18		Φ3.15 x 75	12mm	203	169	126	4.21	2.52	1.5	29.4	210	7.0	30.1
19		Φ3.55 x 90	12mm	224	182	146	4.99	3.38	2.1	26.7	191	7.1	29.7
20		Φ2.8 x 60	17mm	178	174	102	5.01	3.38	2.1	22	108	4.9	13.4
21		Φ3.15 x 75	17mm	219	174	141	5.4	3.79	2.4	23.5	217	9.2	33.4
22		Φ3.55 x 90	17mm	218	174	136	5.22	3.59	2.2	24.4	180	7.4	26.7
23		Φ3.15 x 75	25mm	203	166	121	4.96	3.09	1.7	24.6	150	6.1	20.6
24		Φ3.55 x 90	25mm	246	191	165	5.12	3.31	1.8	27.3	161	5.9	25.2
25	M12 Coach Screw (3x Studs)	Φ2.8 x 60	12mm	182	152	104	4.59	2.93	1.8	24.3	148	6.1	19.2
26		Φ3.15 x 75	12mm	204	175	126	4.24	2.56	1.5	30.2	210	7.0	31.4
27		Φ3.55 x 90	12mm	224	189	146	5.04	3.43	2.1	27.4	191	6.9	31.1
28		Φ2.8 x 60	17mm	179	150	102	5.06	3.44	2.1	21.7	106	4.9	13.1
29		Φ3.15 x 75	17mm	219	174	140	5.4	3.79	2.4	23.5	217	9.2	33.4
30		Φ3.55 x 90	17mm	222	174	144	5.28	3.65	2.2	24.1	180	7.5	26.7
31		Φ3.15 x 75	25mm	203	167	122	5.02	3.17	1.7	24.4	148	6.1	20.6
32		Φ3.55 x 90	25mm	249	196	167	5.18	3.37	1.9	27.6	162	5.9	26.2

Table 4-10: Results of the hybrid wall configurations using M10 Bolts

Wall #	Timber-steel	Nail size	Plywood thickness	P_{peak}, kN	P_{yield}, kN	$P_{infill, peak}$, kN	k_{hybrid}, kN/m	k_{infill}, kN/m	R	Δ_{y}, mm	Δ_{ult}, mm	μ	E_{diss} (kJ)
33	M10 Bolt (2x Studs)	Φ2.8 x 60	12mm	182	151	105	4.66	3.01	1.8	23.7	150	6.3	19.2
34		Φ3.15 x 75	12mm	202	165	125	4.3	2.64	1.6	28	216	7.7	29.6
35		Φ3.55 x 90	12mm	224	184	146	5.13	3.52	2.2	26.3	192	7.3	30.6
36		Φ2.8 x 60	17mm	179	147	103	5.15	3.53	2.2	20.8	106	5.1	12.6
37		Φ3.15 x 75	17mm	222	179	144	5.59	3.97	2.5	23.5	214	9.1	34.5
38		Φ3.55 x 90	17mm	220	179	140	5.39	3.77	2.3	24.2	181	7.5	27.9
39		Φ3.15 x 75	25mm	203	170	120	5.13	3.34	1.9	24.2	147	6.1	21.0
40		Φ3.55 x 90	25mm	245	192	167	6.67	5.08	3.2	21.1	162	7.7	26.8
41	M10 Bolt (3x Studs)	Φ2.8 x 60	12mm	182	152	105	4.65	3.04	1.9	23.9	152	6.4	19.7
42		Φ3.15 x 75	12mm	203	175	126	4.29	2.66	1.6	29.8	210	7.0	31.4
43		Φ3.55 x 90	12mm	225	182	147	5.12	3.54	2.3	26	192	7.4	29.9
44		Φ2.8 x 60	17mm	179	148	103	5.14	3.56	2.2	21	108	5.1	13.0
45		Φ3.15 x 75	17mm	221	182	142	5.57	4.00	2.5	23.8	217	9.1	35.4
46		Φ3.55 x 90	17mm	220	171	141	5.38	3.79	2.4	23.3	182	7.8	26.6
47		Φ3.15 x 75	25mm	203	171	120	5.11	3.38	1.9	24.5	144	5.9	20.6
48		Φ3.55 x 90	25mm	250	192	167	5.29	3.55	2.1	26.6	156	5.9	24.7

Table 4-11: Results of the hybrid wall configurations using M12 Bolts

Wall #	Timber-steel	Nail size	Plywood thickness	P_{peak}, kN	P_{yield}, kN	$P_{infill,peak}$,	k_{hybrid}, kN/m	k_{infill}, kN/m	R	Δ_{y}, mm	Δ_{ult}, mm	μ	E_{diss} (kJ)
49	M12 Bolt (2x Studs)	Φ2.8 x 60	12mm	182	151	105	4.66	3.03	1.8	23.7	142	6.0	19.6
50		Φ3.15 x 75	12mm	204	171	126	4.30	2.67	1.6	29.1	195	6.7	28.2
51		Φ3.55 x 90	12mm	224	176	147	5.13	3.55	2.3	25.1	190	7.6	28.1
52		Φ2.8 x 60	17mm	179	146	102	5.16	3.57	2.3	20.7	105	5.1	12.3
53		Φ3.15 x 75	17mm	223	182	145	5.59	4.01	2.5	23.8	216	9.1	35.2
54		Φ3.55 x 90	17mm	222	182	143	5.39	3.78	2.3	24.8	182	7.4	29.0
55		Φ3.15 x 75	25mm	201	165	123	6.30	4.72	3.0	19.2	142	7.4	20.3
56		Φ3.55 x 90	25mm	242	192	162	6.64	5.11	3.4	21.2	155	7.3	25.5
57	M12 Bolt (3x Studs)	Φ2.8 x 60	12mm	182	149	104	4.64	3.03	1.9	23.5	151	6.4	19.0
58		Φ3.15 x 75	12mm	203	171	126	4.28	2.65	1.6	29.2	207	7.1	30.1
59		Φ3.55 x 90	12mm	223	178	145	5.10	3.54	2.3	25.5	192	7.5	28.9
60		Φ2.8 x 60	17mm	179	151	102	5.13	3.55	2.3	21.5	106	4.9	13.2
61		Φ3.15 x 75	17mm	220	173	139	5.56	4.00	2.6	22.8	215	9.4	33.1
62		Φ3.55 x 90	17mm	222	180	145	5.36	3.79	2.4	24.5	198	8.1	30.8
63		Φ3.15 x 75	25mm	203	167	120	5.10	3.37	1.9	23.9	145	6.1	20.2
64		Φ3.55 x 90	25mm	249	196	167	5.27	3.55	2.1	27.3	160	5.9	26.0

Table 4-12: Results of the hybrid wall configurations with various steel section sizes

Wall #	Timber steel	Nail size	Plywood thickness	Steel column	Steel beam	P_{peak}, kN	P_{yield}, kN	$P_{infill,peak}$, kN	k_{hybrid}, kN/m	$k_{bareframe}$, kN/m	k_{infill}, kN/m	R	$\Delta_{y,}$ mm	$\Delta_{ult,}$ mm	μ	E_{diss} (kJ)
65	M12 Bolt (2x Studs)	ϕ3.55x90	25mm thick ply	UC200	UB150	202	167	163	7.7	0.97	6.73	6.92	21.7	132	6.1	18.4
66				UC200	UB180	203	167	166	7.7	0.88	6.8	7.71	21.8	152	7	21.4
67				UC250	UB200	214	199	168	7.8	0.87	6.95	7.98	25.5	155	6.1	25.9
68				UC250	UC250	247	195	167	9.6	2.66	6.9	2.6	20.4	155	7.6	26.2
69				UC310	UB200	214	193	167	8.4	1.86	6.57	3.53	22.9	156	6.8	25.5
70				UC310	UC250	247	195	168	9.9	3.13	6.75	2.15	19.7	161	8.2	27.4

4.4.1 Effect of plywood thickness

Given the nail size, Figure 4-9 through to Figure 4-11 show load-drift hystereses of the hybrid walls with different plywood thicknesses. In general, using larger nails and thicker plywood tends to increase the load carrying capacity of the hybrid walls given the same steel frame configuration. However, this is not always the case. In the wall configurations using ϕ3.15x75mm nails where the peak load decreased when the plywood thickness increased from 17mm to 25mm. This is because the hybrid wall capacity is affected by the timber-plywood connections and the connection capacity is dependent upon nail size, plywood thickness, and nail penetration depth, etc.. The increase of plywood thickness from 17 to 25 mm will cause the reducution of nail penetration length into timber members from 58 mm to 50 mm, which may cause reduced capacity.

The infill wall-to-bare frame stiffness ratio R has a positive trend with increases in plywood thickness. In this study, R ratios increased between 9% – 56% as plywood thickness is incrementally increased, regardless of the nail size combination. This translated to 9.8% – 30.2% increases in the initial stiffness of the hybrid system. An R ratio greater than 1 will allow the infill walls will carry higher lateral loads than the bare steel frame during the intial stages of loading.

It was also found that the highest ductility factors were provided by the timber-sheathing connections using 17mm thick plywood in combination with larger nails (ϕ3.15x75mm and ϕ3.55x90mm). 17mm thick plywood with smaller nails (ϕ2.8x60mm) is not advised due to insufficent nail penetration length.

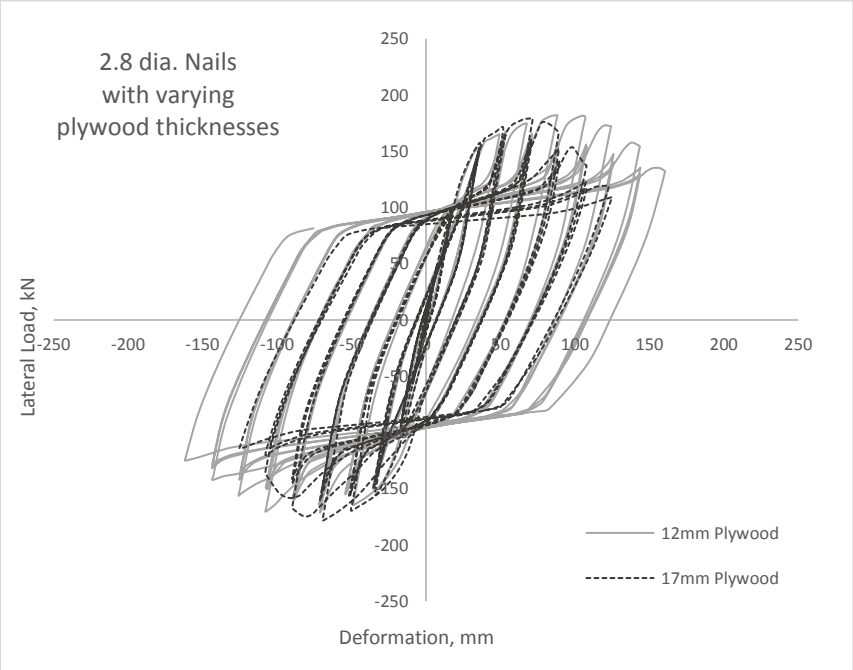

Figure 4-9: Hysteresis curves for hybrid shear walls with ϕ2.8x60mm nails with varying plywood thicknesses

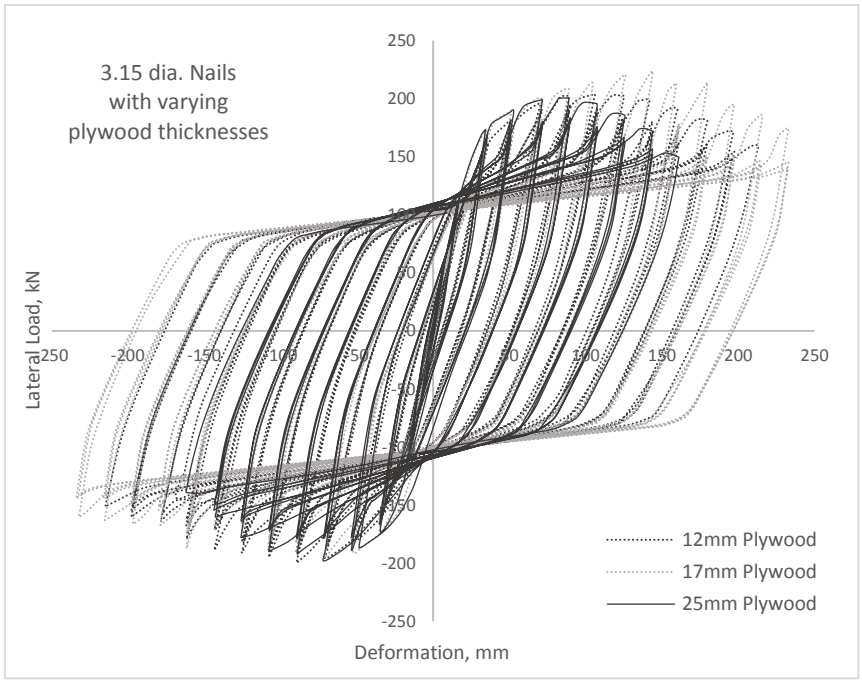

Figure 4-10: Hysteresis curves for hybrid shear walls with ϕ3.15x75mm nails with varying plywood thicknesses

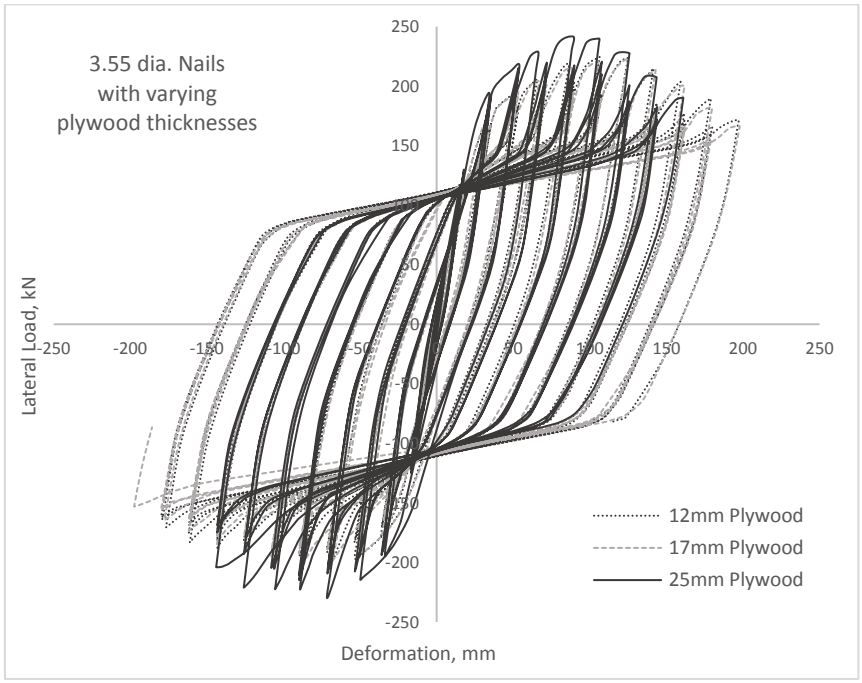

Figure 4-11: Hysteresis curves for hybrid shear walls with ϕ3.55x90mm nails with varying plywood thicknesses

4.4.2 Effect of nail size

Given the plywood thickness, Figure 4-12 through to Figure 4-14 show the load-drift hystereres of the hybrid walls. It was found that the increased nail size generally increased the load carrying capacity by 10% – 24%. Increasing nail size generally increases the ductility as well. The results also showed that using the timber-plywood connections with ϕ3.15x75mm nails in combination with either 12mm or 17mm thick plywood

seemed to provide the largest ductility factors. Larger nails are recommended to meet requirements for higher loads. ϕ3.15x75mm nails seemed to provide the greatest ductility while providing comparable strengths to the larger ϕ3.55x90mm nails.

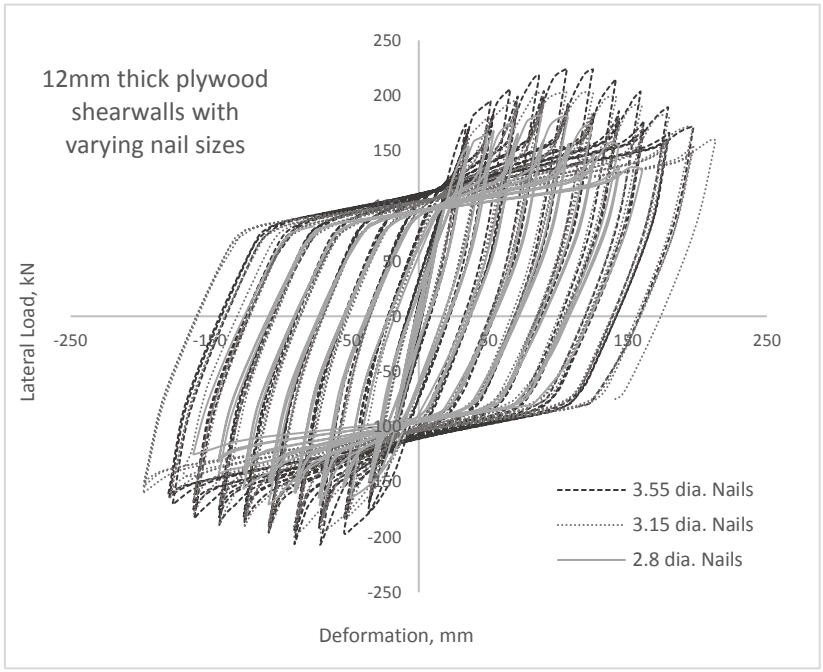

Figure 4-12: Hysteresis curves for hybrid shear walls with 12mm plywood thickness with varying nail sizes

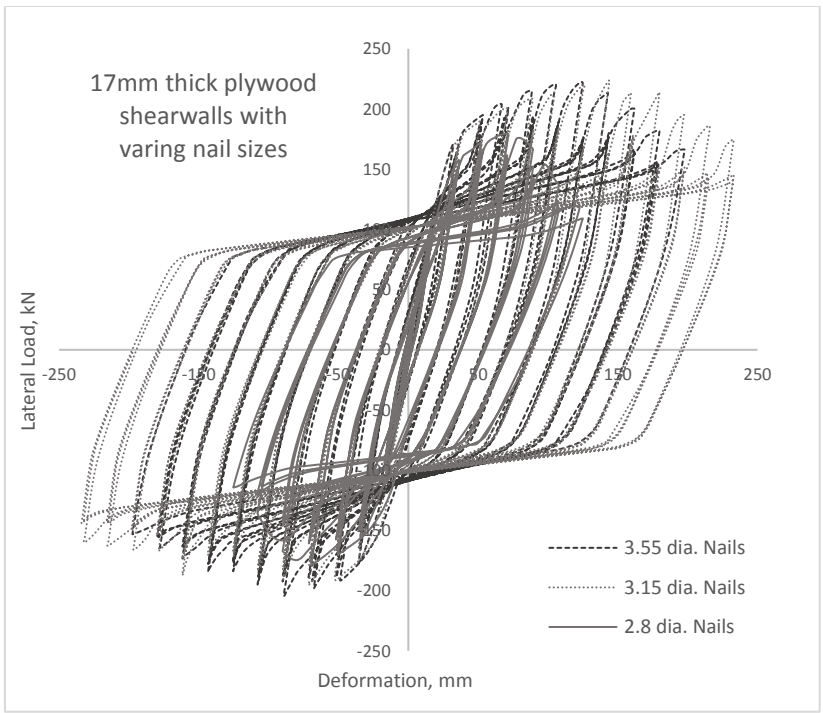

Figure 4-13: Hysteresis curves for hybrid shear walls with 17mm plywood thickness with varying nail sizes

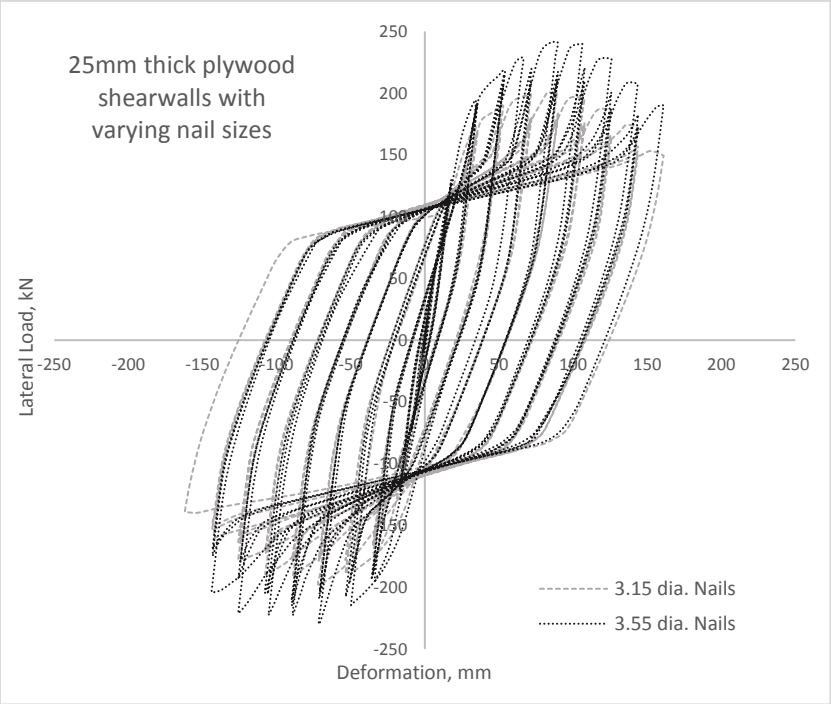

Figure 4-14: Hysteresis curves for hybrid shear walls with 25mm plywood thickness with varying nail sizes

4.4.3 Effect of timber-steel fasteners

Given that timber-steel fasteners are stiff and strong enough to transfer the load between the steel frame and the infill walls, the numerical results indicated that the timber-steel connections did not have significant effect on the overall hybrid wall performance.

Of the four types of metal fasteners (M10 bolts, M12 bolts, M10 coach screws, and M12 coach screws) used in this parametric study, the spacing of 200mm was sufficient to transfer a lateral force equal to or greater than the shear capacity of the plywood infill wall configurations tested.

4.4.4 Effect of steel framing member sizes

Figure 4-15 shows the load-drift hystereses of the hybrid walls with varing steel beam and column sizes. Given the infill wall configurations, larger steel frame sections led to expected increases in peak load, yield load and stiffness. The stiffness of the hybrid system was increased as well. Energy dissipation increases due to the more steel material available for yielding.

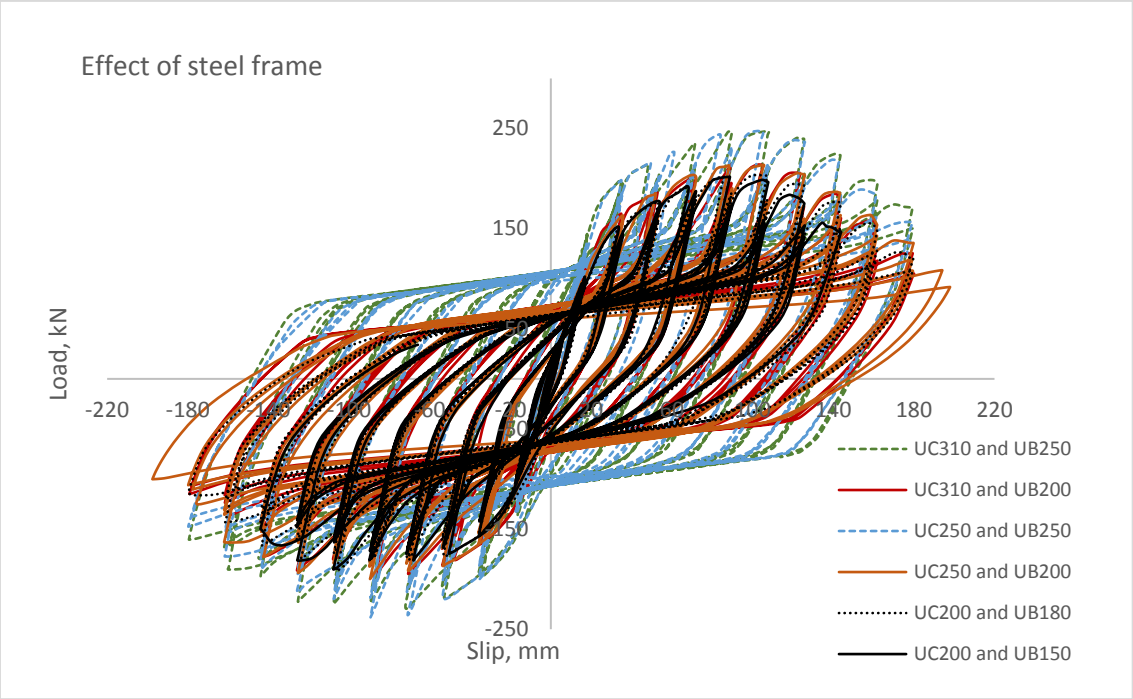

Figure 4-15: Hysteresis curves for timber-steel hybrid shear walls with varying steel member sizes

Incrementally increasing steel beam and column sections results in 11% when other structural parameters are kept constant. However, the ductility remains unchanged. Because a bilinear plastic model for steel is used in modelling, the post-peak strength reduction was mainly governed by the infill shear wall. It is also noticed that similar sizes for the beam and column cross sections can achieved higher strength as the formation of the beam-column plastic hinges may limit the further increase of the hybrid wall strength. Also choosing similar beam and column cross section sizes may lead to more economic design.

4.5 Recommended ductility factors

In New Zealand, a ductility factor of μ=4 for plywood shear walls is used. For ductile steel moment frames, a ductility factor of 6 can be used (NZS3404: Appendix C). Based on a statistical analysis of the ductlity factors derived from the 70 hybrid wall configurations, the average ductility ratio was μ=6.8 with standard deviations of 1.2. Thus, the estimated fifth percentile value was about μ=5.0, which is inbetween the ductility factor of plywood shear walls and ductile steel moment frames. Therefore, a conservative value μ=5.0 is recommended for the hybrid wall systems. This value will be used in the force-based design example in Chapter 5.

4.6 Viscous damping ratio determination

The equivalent viscous damping ratio (ξ_{eq}), is required for displacement-based seismic design. It can be obtained by:

$$\xi_{eq} = \xi_{el} + \xi_{hyst} \qquad (14)$$

where ξ_{el} is the elastic damping ratio, which can be assumed to be 2 – 3% for light timber framed buildings (Pang and Rosowsky, 2008). For steel structures, 2% elastic damping ratio is commonly used. The hysteretic

damping (ξ_{hyst}) can be determined for load-drift hysteresis curves of the hybrid wall systems. In this study, ξ_{hyst} was derived at various wall drift levels (0.5%, 1.0%, 2.0%. 2.5%, 3.0% and 4.0%).

The hysterstic damping can be calculated by:

$$\xi_{hyst} = \frac{1}{4\pi}\frac{E_{loop}}{E_{so}} = \frac{1}{2\pi}\frac{E_{loop}}{K_s\Delta_t^2} \qquad (15)$$

where E_{loop} is the energy dissipated by the actual nonlinear shear wall (i.e. the area enclosed by load-drift loops). E_{so} is the strain energy of the linear-elastic system at the target displacement, Δ_t. K_s is the secant stiffness determined at Δ_t. In this study, E_{loop} was calculated using a MATLAB function "trapz".

Given strong bolted or coach screwed timber-steel interface connections, the hysteretic damping at different target displacements was evaluated for the hybrid wall configurations with different nailed timber-plywood connection types. The results are presented in Figure 4-16.

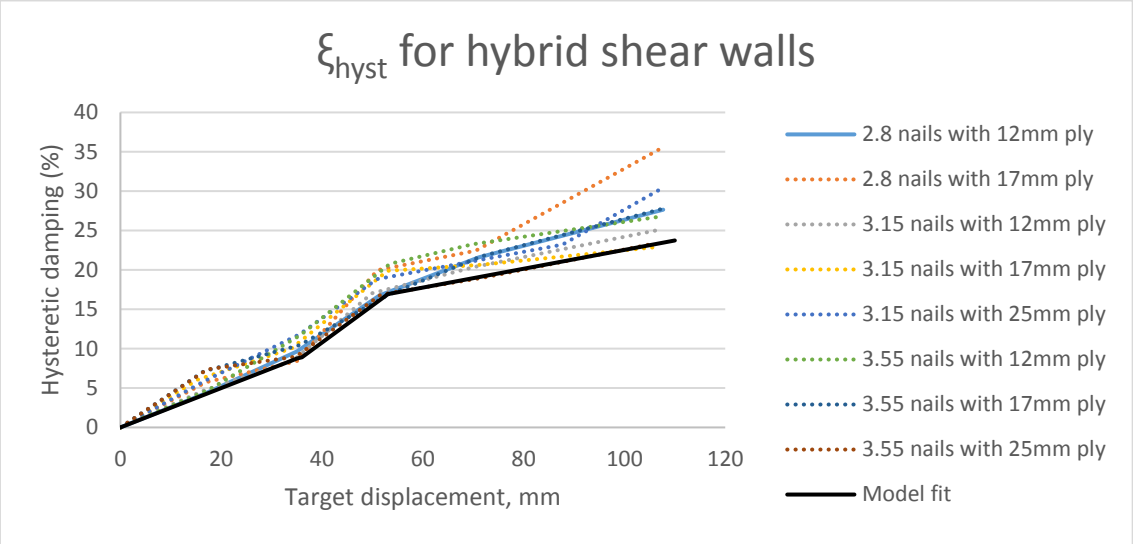

Figure 4-16: Experimental determination and equivalent model of the hysteretic damping for hybrid shear walls

By fitting the lower-bound curves in Figure 4-16, a conservative estimation of ξ_{hyst} can be characterised by the trilinear expression Eq. (16) at various target displacement Δ_t:

$$\xi_{hyst}(\%) = \begin{cases} 0.25\Delta_t & for\ \Delta_t < 36mm \\ 8.9 + 0.47(\Delta_t - 36) & for\ 36mm < \Delta_t < 53mm \\ 16.9 + 0.12((\Delta_t - 53) & for\ \Delta_t > 53mm \end{cases} \qquad (16)$$

4.7 Conclusion

This chapter presents a finite element model developed in ABAQUS to represent the structural response of the hybrid shear wall under lateral loading. Special attention was given to the numerical and structural representation of the critical interface connections. The FE model was validated using the experimental results provided by Dong (2017).

The validated FE model was then used to conduct a parametric investigation for the purposes of optimizing the hybrid wall configuration. A total of 70 different wall configurations were simulated. Based on the results of the parametric study, the main findings are listed as follows:

- Given sufficently small spacing provided for the timber-steel interface connections (200mm used in this study), the use of M10 or M12 bolts and coach screws had negligible effects on the hybrid wall response.
- Proper nail size and plywood thickness should be specified because the nailed timber-plywood connections provide one main source of engery dissipation and governs the behavior of the infill walls. The combination of ϕ3.15x75mm nails and 17mm thick plywood seemed to provide better performance compared with other combinations.
- Larger steel frame sections led to the increase of the hybrid wall capacity and stiffness and energy dissipation. However, further research is needed to optimize the steel member size and achieve more econonic design.
- A ductility factor μ=5.0 is recommended for the timber-steel hybrid walls.
- The parametric study also has its limitations. A few other important design parameters have not been considerd, for example, double-sheathed plywood for the infill walls, the influence of possible window/door openings in the infill walls and different nailing spacing, etc.

5 DESIGN EXAMPLE

This chapter presents a seismic design example of the timber-steel hybrid wall systems following a displacment-based design approach.

5.1 Lateral force design for timber-steel hybrid systems

In New Zealand, force-based seismic design is widely used for multi-storey buildings following NZS1170:5 (Standards New Zealand, 2004). Force-based design can be found in literature by Buchanan et al (2008) and in Multistorey Timber Buildings Manual (2001). Priestley et al (2007) provides detailed introduction of the state of the art art displacement-based seismic design. The displacement based design approaches have also been used by Filiatrault et al (2002), Pang and Rosowsky (2007; 2009) in the research of light timber framed buildings.

In this study, a five-storey timber-steel hybrid wall system was selected to demonstate the design process. There are two walls carrying the design base shear. Figure 5-1 shows the wall geometry. The interstorey height is 2.8m and the wall length is 3.75m, similar the wall dimensions used in the parametric study. The tributary area of each wall is roughly 175m^2, with a seismic mass of 350kN.

For the displacement based design, the structure needs to be convert to an equivalent single-degree-of-freedom (SDOF) system, shown in Figure 5-2, with equivalent elastic lateral stiffness and viscous damping properties representative of the global behaviour of the actual structure at target displacements.

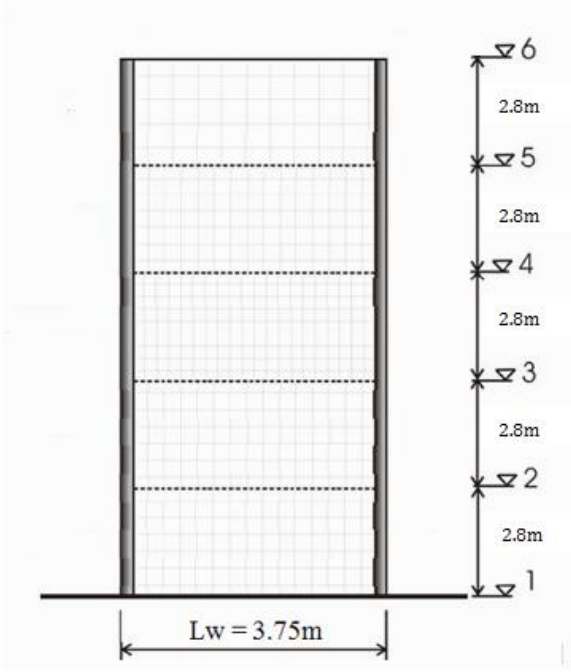

Figure 5-1: Elevation view of the timber-steel hybrid shear wall to be analysed for design forces.

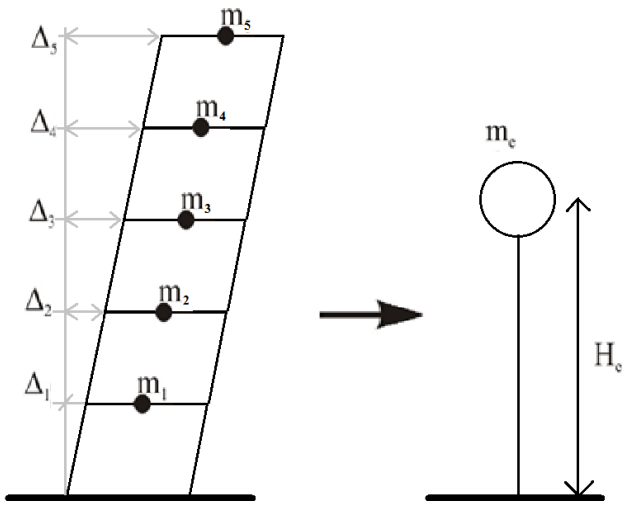

Figure 5-2: SDOF idealization of multi-storey structure for displacement-based design.

The following design assumptions were used:

- The wall shall be designed to have a characteristic displacement profile defined by Pettinga & Preistley (2005), given in Equation (17) and (18).
- Seismic weight of 300kN was assumed for each floor and the floor-type roof.
  The building was designed according to NZS1170.5 acceleration and displacement spectra for 500 year return period earthquakes (Soil D, Christchurch City). The design acceleration and displacement spectrum are shown in Figure 5-3 and Figure 5-4 respectively.

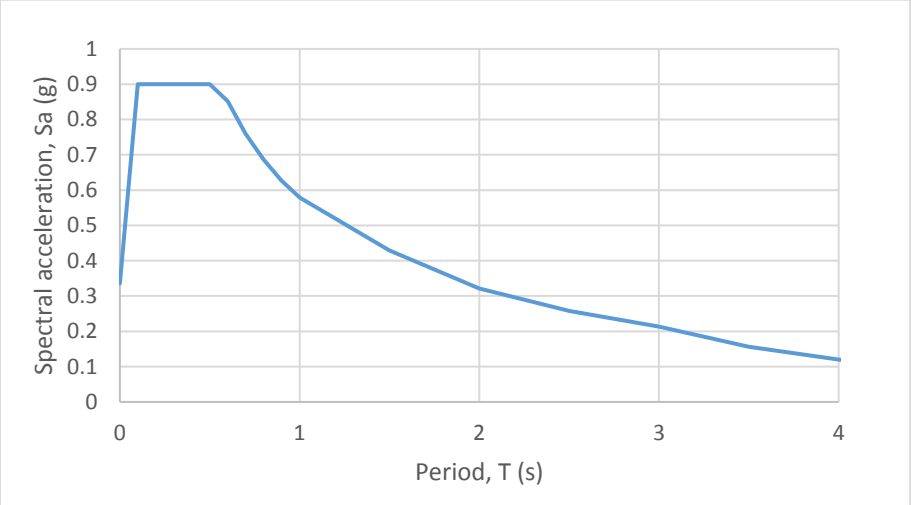

Figure 5-3: Design acceleration spectrum

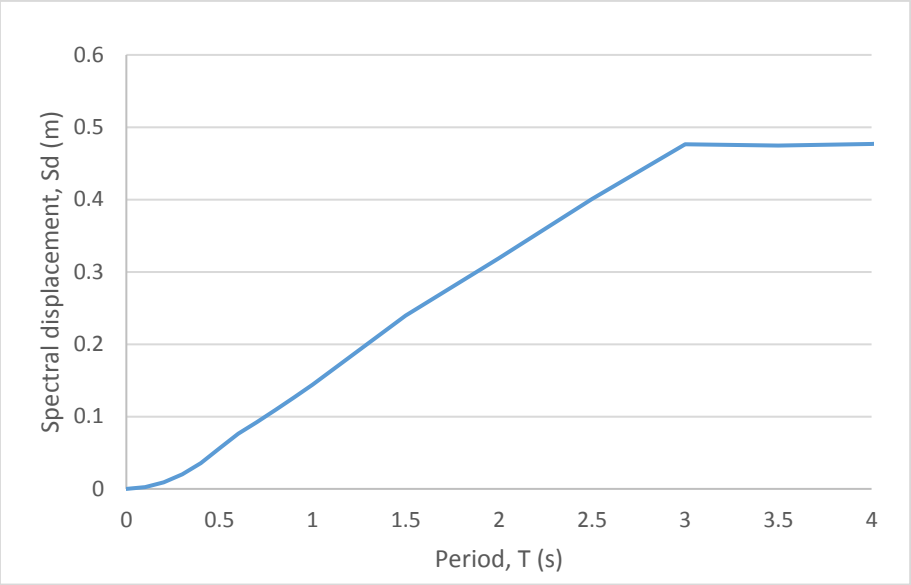

Figure 5-4: Design displacement spectrum

5.1.1 Force-based design

Step 1: Estimate the natural period, T_1 following C4.1.2.2 (NZS1770.5, Supp. 1:2004).

For ultimate limit state,

$$T_1 = 1.25 k_t h_n^{0.75}$$

$$T_1 = 1.25(0.05)(14.0^{0.75})$$

$$T_1 = 0.45 secs$$

where: $k_t = 0.05$ $(for\ structural\ wall\ buildings)$ and $h_n =$ building height

Step 2: Obtain the elastic site hazard spectrum for horizontal loading, $C(T_1)$

$$C(T_1) = C_h(T) Z R N(T, D)$$

$$C(T_1) = (3.0)(0.3)(1.0)(1.0)$$

$$C(T_1) = 0.9$$

A 2% elastic damping may be assumed for timber-steel hybrid systems. It is the designer's responsibilty to choose a correct a elastic damping value.

$$C_d(T_1) = \frac{C(T_1) s_p}{k_u}$$

For ultimate limit state, structural performance factor, $s_p = 0.7$ and the ductility factor $\mu=5.0$ derived from the parametric study were used. For site subsoil class D and natural period $(T_1) < 0.7s$,

$$k_u = \frac{(\mu-1)T_1}{0.7} + 1$$

$$k_u = \frac{(5.0-1)0.45}{0.7} + 1$$

$$k_u = 3.59$$

Therefore:

$$C_d(T_1) = \frac{(0.9)(0.7)}{3.59}$$

$$C_d(T_1) = 0.176$$

Step 3: Determine design base shear, V_b:

$$V_b = C_d(T_1)W_{tot}$$

$$V_b = (0.176)(350kN)(5\ storeys)$$

$$V_b = 307.54kN$$

Step 4: Distribute the base shear:

$$F_i = F_t + 0.92V_b \frac{(m_i H_i)}{\sum_{i=1}^{n}(m_i H_i)}$$

Where: $F_t = 0.08V_b$ when $i = n$ (at the roof)

= 0 when $i \neq n$ (all floors except the roof)

Using a spreadsheet:

Storey	m_i (kN)	H_i (m)	mi*Hi (kNm)	Ft (kN)	F_i (kN)
6	350	14.0	4900	24.60	118.92
5	350	11.2	3920	0	75.45
4	350	8.4	2940	0	56.59
3	350	5.6	1960	0	37.73
2	350	2.8	980	0	18.86
1	0	0	0	0	0.00
		V_b	**14700**	**ΣV_b**	**307.54**

5.1.2 Displacement-based design

Step 2: Determine displacement profile.

The displacement of each critical mass (or level) is given by:

$$\Delta_i = \delta_i \frac{\Delta_c}{\delta_c} \tag{17}$$

$$\delta_i = \begin{cases} \frac{4}{3}\left(\frac{H_i}{H_n}\right)\left(1 - \frac{H_i}{4H_n}\right), & for\ frames \\ \frac{h_i}{h_n} + \left[\frac{3}{2}\frac{h_i^2}{h_n^2}\left(1 - \frac{h_i}{3h_n}\right) - \frac{h_i}{h_n}\right]\left(0.075 + \frac{0.7}{\mu}\right), & for\ walls \end{cases} \tag{18}$$

Where:

δ_i is the elastic mode shape, and Δ_c is the design displacement at the critical mass. c (49.5mm for a 2.0% drift limit, and δ_c is the value of the mode shape at mass c.

The average value for δ_i between frames and walls for was taken for the hybrid system, as it contains both frames and walls. Using a spreadsheet:

Storey, i	H_i (m)	normalised height	δi (frame)	δi (wall)	δi (average)	δi.Δc(m)	Δi (m)
6	14.0	1.0	1.00	0.88	0.94	0.053	0.210
5	11.2	0.8	0.85	0.78	0.82	0.046	0.183
4	8.4	0.6	0.68	0.63	0.65	0.037	0.146
3	5.6	0.4	0.48	0.43	0.45	0.025	0.102
2	2.8	0.2	0.25	0.21	0.23	0.013	0.052
1	0	0	0.00	0.00	0.00	0.000	0.000

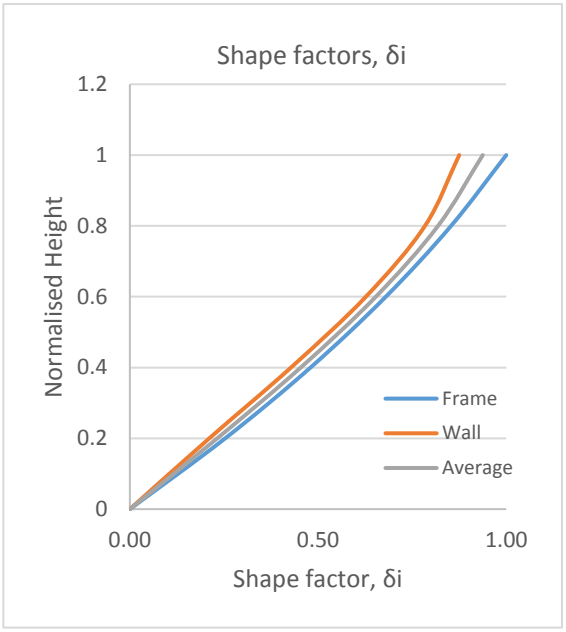

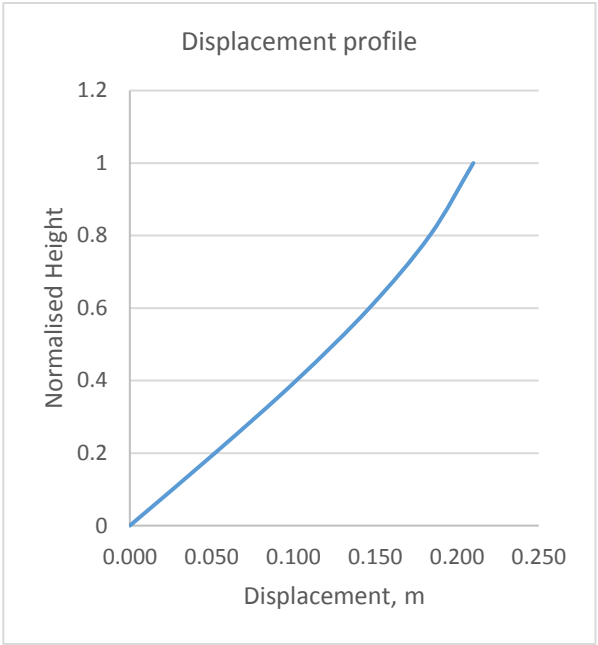

Step 2: The design displacement, the effective mass and the effective height must be determined.

The peak design displacment for the SDOF representation:

$$\Delta_d = \sum_{1=1}^{n}(m_i\Delta_i^2)/\sum_{i=1}^{n}(m_i\Delta_i) \quad (19)$$

The effective mass:

$$m_e = \sum_{i=1}^{n}(m_i\Delta_i)/\Delta_d) \quad (20)$$

The effective height:

$$H_e = \sum_{i=1}^{n}(m_i\Delta_i H_i)/\sum_{i=1}^{n}(m_i\Delta_i) \quad (21)$$

Using a spreadsheet:

Storey	W_i (kN)	H_i (m)	m_i (kg)	Δi (m)	mi*Δi	mi*Δi^2	mi*Δi*Hi
6	350	14.0	35678	0.210	7492	1573	104893
5	350	11.2	35678	0.183	6543	1200	73278
4	350	8.4	35678	0.146	5223	765	43870
3	350	5.6	35678	0.102	3628	369	20318
2	350	2.8	35678	0.052	1855	96	5195
1	0	0	0	0	0	0	0
					24741	**4003**	**247555**

Therefore:

$$\Delta_d = \sum_{1=1}^{n}(m_i\Delta_i^2)/\sum_{i=1}^{n}(m_i\Delta_i)$$

$$\Delta_d = \frac{24741}{4003} = 0.162m$$

$$m_e = \sum_{i=1}^{n}(m_i\Delta_i)/\Delta_d)$$

$$m_e = \frac{24741}{0.162} = 152912.6\text{k}g$$

$$H_e = \sum_{i=1}^{n}(m_i\Delta_i H_i)/\sum_{i=1}^{n}(m_i\Delta_i)$$

$$H_e = \frac{247555}{24741} = 10.0m$$

Step 3: Calculate the equivalent viscous damping.

$$\xi_{eq} = \xi_{el} + \xi_{hyst}$$

The elastic damping can be assumed to be 2.0% (Pang and Rosowsky, 2008). The hysteretic damping based on experimental studies can be obtained from Figure 4-16. At a design displacement of 162mm, the hysteretic damping, ξ_{hyst} = 16%.

Therefore, the equivalent viscous damping is:

$$\xi_{eq} = 2 + 16 = 18\%$$

Step 4: Determine the effective period from the reduced design displacement spectrum:

The displacement spectrum, S_d, can be calaculated from the acceleration spectrum.

$$S_d = \frac{T^2}{4\pi^2}S_a$$

The scale factor to be applied to the design displacement spectrum (with 18% damping) is:

$$R_{eq} = \left(\frac{7}{2+\xi_{eq}}\right)^{0.5}$$

$$R_{eq} = \left(\frac{7}{2+18}\right)^{0.5}$$

$$R_{eq} = 0.59$$

The scaled displacement becomes:

$$S_d(\xi_{eq}) = R_{eq}S_d(16\%)$$

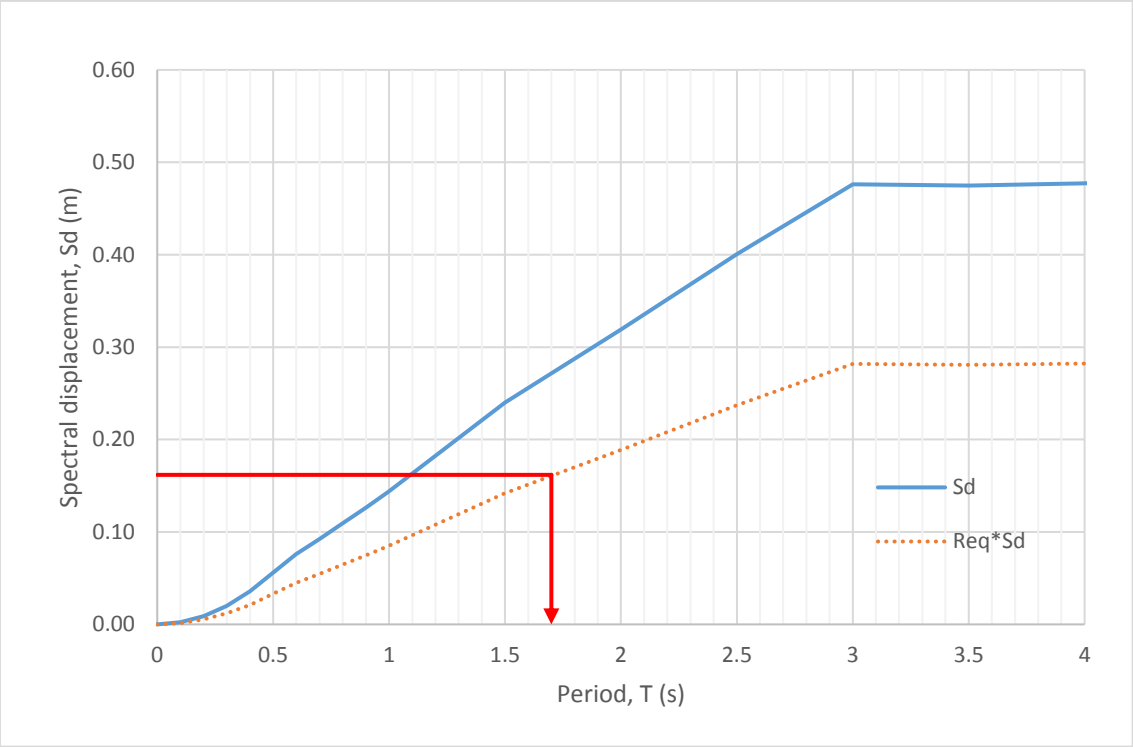

The effective period is obtained from the scaled displacement spectrum: $T_e = 1.7s$

Step 5: Obtain the equivalent lateral stiffness:

$$K_e = \frac{4\pi^2 m_e}{T_e^2}$$

$$K_e = \frac{4\pi^2 \times 152912.6\text{kg}}{1.7^2} = 2088.84kN/m$$

Step 6: Determine design base shear:

$$V_b = K_e \Delta_d$$

$$V_b = 2088.84 \times 0.162 = 337.98kN$$

Step 6: Distribute base shear up the structure:

Assuming a sinusoidal, first-mode response at the peak displacement, the base shear can be distributed in proportion to mass and displacement.

$$F_i = F_t + 0.92V_b \frac{(m_i \Delta_i)}{\sum_{i=1}^{n}(m_i \Delta_i)}$$

Using a spreadsheet:

Storey, i	Fi (kN)
6	121.20
5	82.23
4	65.64
3	45.60
2	23.32
1	0.00
Σ V_b	**337.98**

5.1.3 Comparison of force-based and displacement-based designs

Storey, i	Floor Force, kN	
	FBD	DBD
6	118.92	121.20
5	75.45	82.23
4	56.59	65.64
3	37.73	45.60
2	18.86	23.32
1	0.00	0.00
Sum (V_b)	**307.54**	**337.98**

For this example, the base shear according to FBD is 10% less than DBD. This is mainly due to the force-reduction factor assumed for FBD ($1/k_u$) and DBD (R_{eq}).

5.2 Design Tables

Table 5-1: Design table for timber-steel hybrid shear walls (with UC250 and UB250 steel members and rigid beam column joints)

HYBRID WALL #ID		Nail size (50/100mm CRS)	Plywood thickness	For a 3.75x2.48m hybrid wall	drift (% of storey height)					
					0.5%	1.0%	1.5%	2.0%	2.5%	3.0%
				Displacement	12.4mm	24.8mm	37.1mm	49.5mm	61.9mm	74.3mm
H1	M12 Bolt (2x Studs) @ ~200mm CRS	2.8 x 60	12mm	Force (kN)	70	126	155	165	171	177
				K_{eq} (kN/mm)	5.66	5.09	4.18	3.33	2.76	2.38
H2			17mm	Force (kN)	74	128	159	171	176	178
				K_{eq} (kN/mm)	5.98	5.17	4.28	3.45	2.84	2.40
H3		3.15 x 75	12mm	Force (kN)	72	126	163	181	190	197
				K_{eq} (kN/mm)	5.82	5.09	4.39	3.66	3.07	2.65
H4			17mm	Force (kN)	83	144	177	188	194	203
				K_{eq} (kN/mm)	6.71	5.82	4.77	3.80	3.14	2.73
H5			25mm	Force (kN)	88	146	177	188	196	200
				K_{eq} (kN/mm)	7.11	5.90	4.77	3.80	3.17	2.69
H6		3.55 x 90	12mm	Force (kN)	81	145	180	193	201	205
				K_{eq} (kN/mm)	6.55	5.86	4.85	3.90	3.25	2.76
H7			17mm	Force (kN)	81	145	179	191	201	210
				K_{eq} (kN/mm)	6.55	5.86	4.82	3.86	3.25	2.83
H8			25mm	Force (kN)	96	163	198	213	226	234
				K_{eq} (kN/mm)	7.76	6.59	5.33	4.30	3.65	3.15

Table 5-2: Design table for plywood infill shear walls

INFILL WALL #ID		Nail size (50/100 mm CRS)	Plywood thickness	For a 3.6x2.4m plywood infill wall	drift (% of storey height)					
					0.5%	1.0%	1.5%	2.0%	2.5%	3.0%
				Displacement	12.4mm	24.8mm	37.1mm	49.5mm	61.9mm	74.3mm
I1	M12 Bolt (2x Studs) @ ~200mm CRS	2.8 x 60	12mm	Force (kN)	43	69	81	89	94	100
				K_{eq} (kN/mm)	3.47	2.79	2.18	1.80	1.52	1.35
I2			17mm	Force (kN)	48	72	85	94	100	102
				K_{eq} (kN/mm)	3.88	2.91	2.29	1.90	1.62	1.37
I3		3.15 x 75	12mm	Force (kN)	38	71	91	105	114	122
				K_{eq} (kN/mm)	3.07	2.87	2.45	2.12	1.84	1.64
I4			17mm	Force (kN)	55	88	104	112	117	125
				K_{eq} (kN/mm)	4.44	3.56	2.80	2.26	1.89	1.68
I5			25mm	Force (kN)	61	59	103	112	119	122
				K_{eq} (kN/mm)	4.93	2.38	2.77	2.26	1.92	1.64
I6		3.55 x 90	12mm	Force (kN)	51	87	107	118	124	135
				K_{eq} (kN/mm)	4.12	3.52	2.88	2.38	2.00	1.82
I7			17mm	Force (kN)	52	88	104	117	125	131
				K_{eq} (kN/mm)	4.20	3.56	2.80	2.36	2.02	1.76
I8			25mm	Force (kN)	68	98	125	139	151	157
				K_{eq} (kN/mm)	5.49	3.96	3.37	2.81	2.44	2.11

Table 5-3: Structural properties of steel moment frames (with bilinear model properties)

Steel moment frame		**Structural properties**	
Steel Column	**Steel Beam**	**F_y (kN)**	**k_i (kN/mm)**
UC200	UB150	35.6	0.97
UC200	UB180	37.4	0.88
UC250	UB200	43.9	0.87
UC250	UC250	77.9	2.66
UC310	UB200	45.5	1.86
UC310	UB250	79.7	3.13

5.3 Displacement-based design procedure – design example

This section presents a design example of an ultimate limit state and a servicability limit state design for the timber-steel hybrid shear wall system shown in

Figure 5-1. The design method proposed in this thesis only requires the SDOF idealisation (obtaining equivalent viscous damping, mass, height and lateral elastic stiffness) and shear wall design tables.

For the purposes of this example, it may be assumed that earthquake loads govern lateral load design.

- It is assumed that the wall chords and studs have been designed based on the gravity load design.
- The plywood wall is part of a building with a 50 year year design working life and an importance level of 2 under NZS1170.0. Therefore, the ultimate limit state design earthquake has an annual probability of exceedance 1/500 years and the servicability limit state design has an annual probability of exceedance of 1/25 years.
- The design forces have been calculated using a DBD approach.
- Following the 1170.5 inter-storey deflection limits, for ULS design, the drift limit should not exceed 2.5%. This translates to 70mm lateral deformation for a hybrid shear wall with 2.8m height. However, to improve performance of the structure, a drift limit of 2.0% will be used, so a interstorey drift of 49.5mm should not be exceeded.

Design for Strength

Step 1: Determine the design actions:

The interstorey shear:

$$V_i^* = \sum_{i=1}^{n} F_i$$

The interstorey moment:

$$M_i^* = \sum_{i=1}^{n} F_i(H_{i+1} - H_i)$$

The chord force:

$$N_i^* = \frac{M_i^*}{L_w}$$

Storey	F_i (kN)	H_i (m)	V^*_I (kN)	M^*_I (kN)	N^*_I (kN)
6	121.20	14.0	121.20	0	0
5	82.23	11.2	203.42	339.36	90.49
4	65.64	8.4	269.06	908.94	242.38
3	45.60	5.6	314.66	1662.31	443.28
2	23.32	2.8	337.98	2543.35	678.23
1	0.00	0	337.98	3489.69	930.58

Using the Design Tables (Table 5-1 and Table 5-2):

Storey	**V^*_l (kN)**	**Configuration**	**F_{prov} (kN)**
6	121.20	2x I1	178
5	203.42	2x I3	210
4	269.06	2x H1	330
3	314.66	2x H1	330
2	337.98	2x H2	342
1	337.98	-	-

Anchor connections can be designed as per standard design procedures, accounting for uplift forces at the base.

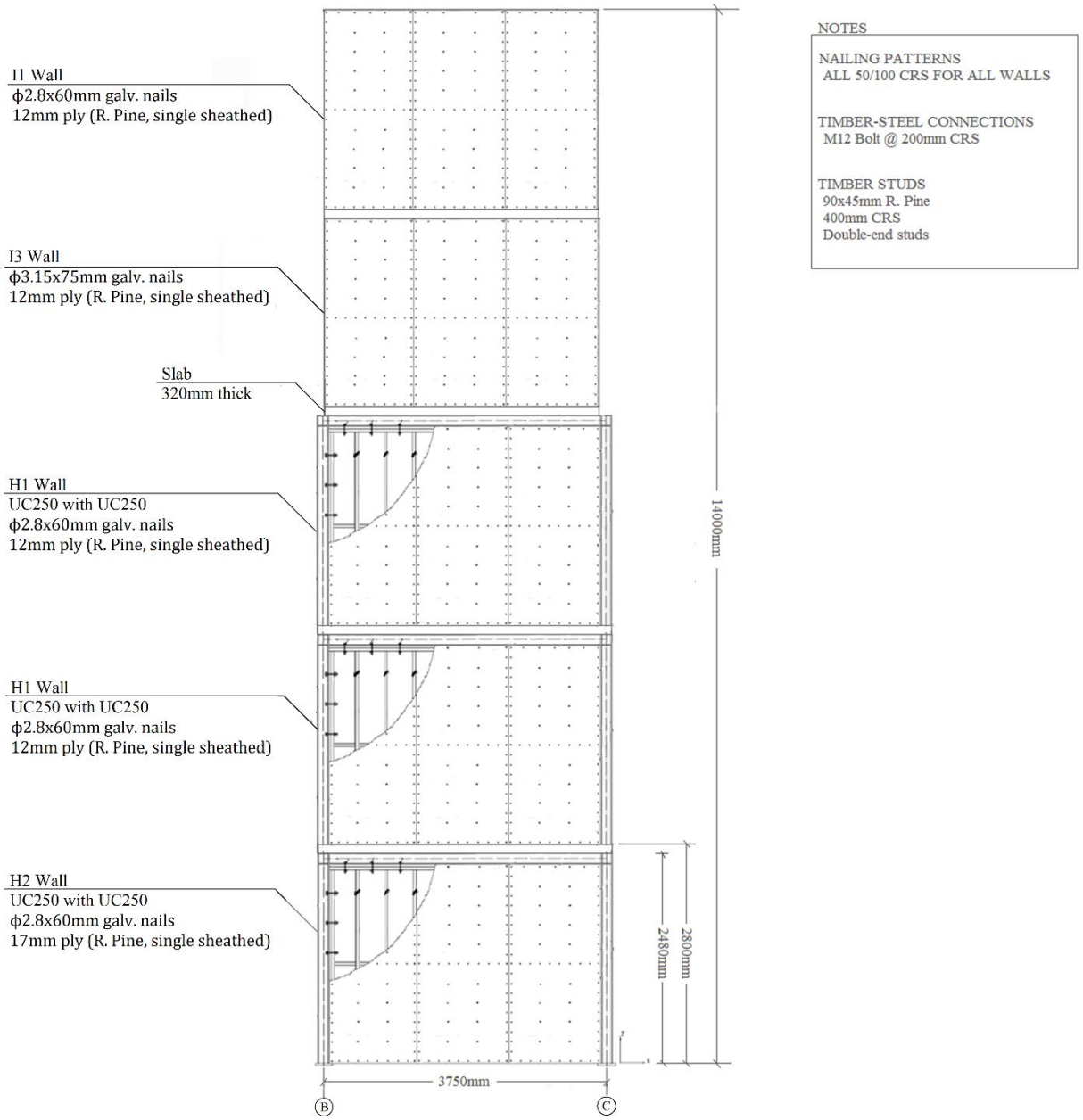

Figure 5-5: Final design for one shear wall for the five-storey structure using timber-steel hybrid shear wall and plywood infill walls.

6 CONCLUSIONS

6.1 Summary

This thesis presents a combined experimental and numerical study on the cyclic performance of a type of timber-steel hybrid shear walls which can be used as an alternative lateral load resisting system for multi-storey timber buildings.

In Chpater 2, a literature review of previous research on the timber-steel hybrid systems was conducted. The need for the adaptation of the timber-steel hybrid system to the NZ market was highlighted, using local materials and design practices.

In Chapter 3, experimental investigations were conducted on the critical timber-steel interface connections and nailed timber-plywood interface connections. Their structural performance under cyclic loading was evaluated. Connections with various configurations were investigated. These includes different fastener sizes, plywood thicknesses, fasterner types and number of timber studs.

In Chapter 4, a finite element model of a single storey timber-steel hybrid shear wall was developed in ABAQUS software. The model incorporated the critical connection data and the structural performance of the hybrid system under cyclic loading was studied. Key structural parameters such as peak load, initial stiffness and ductility were derived from the wall load-drift hystereses. The effect of nail size, plywood thickness, timber-steel connections and steel frame sections on the overall hybrid wall performance were evaluated. Based on the results, ductility factors and hysteretic damping values were also derived and suggested for this type of hybrid wall system.

In Chapter 5,the data from the parametric analysis has been collated in the form of design tables for practicing engineers to use as an aid to lateral load design. Design examples (Force-based and Displacement-based) were presented to show the applications of the hybrid system a 5-storey building. The proposed design methodology ultilises design tables to select appropriate timber-steel hybrid shear wall configurations to meet the lateral load demand.

6.2 Key research findings

- The addition of steel moment resisting frames signficantly increases the strength and stiffness of the plywood infill wall, in some cases doubling the peak loads and initial stiffnesses.
- Given the timber-steel interface connections are strong enough to transfer the load between the steel frame and the infill shear wall, the full capacity of the infill wall can be achieved.
- Adoption of thicker plywood thicknesses generally leads to the increase of lateral load capacity of the infill plywood shear walls. However, care must be taken to provide sufficient nail penetration depth into timber members. It was found that the combination of Φ3.15x75 nails with 17mm thick plywood used in infill walls seemed to give best performance compared with the other combinations. The connection test results also showed that the ϕ3.15x75mm were able to provide the greatest ductility while providing comparable strength to the larger ϕ3.55x90mm nails
- Overall the hybrid systems showed very ductile behavior. A ductility factor of 5.0 is recommended based on the results of 70 hybrid wall simulations.
- Given the explict load-drift responses of the hybrid walls, it is straightforward to use the displacement-based seismic design approach to design these hybrid walls in multi-storey buildings.

6.3 Future research

In this thesis, only one hybrid wall geometry was studied. Other influential design variables may also affect the hybrid wall performance. The variables include different wall geometries (length and height), whether or not openings exist in the infill walls, nailing patterns/spacing, etc. To further validate the design concept and check against the numerical models, experimental testing on full-scale hybrid wall systems should be conducted. In the numerical modeling, the steel beam-column joints were assumed to be rigid moment resisitng connections. This assumption should also be checked carefully in the full-scale wall testing.

7 REFERENCES

AS/NZS1748:2011. "Timber – Solid – Stress-graded for structural purposes." Standards New Zealand.

AS/NZS2269:2012. "*Plywood – Structural*." Standards New Zealand.

AS/NZS 2465:1999. "*Unified hexagon bolts, screws and nuts (UNC and UNF threads)*." Joint Technical Committee ME/29.

ASTM E2126. 2011. "Standard test methods for cyclic (reversed) load test for shear resistance of vertical element of lateral force resisting systems for buildings". ASTM International.

Buchanan, A. "*Timber Design Guide, New Zealand Timber Industry Federation Inc. 3rd edition*," 2007.

Carradine, D. "*Guiding multi-storey timber buildings*". BRANZ Build 141 April/May 2014

Dickof C., Stiemer S. F., Tesfamariam S. 2012. "*Wood-steel hybrid seismic force resisting systems: seismic ductility*". Proc. 12th World Conference on Timber Engineering, Auckland, New Zealand

Dong, W. 2017. "*Lateral behavior of connections between steel moment-resisting frame and wood-frame shear wall in the hybrid system*." Tongji University.

Folz, B. and Filiatrault, A., 2001. "*Cyclic analysis of wood shear walls*." Journal of Structural Engineering, 127(4), 433-441.

Folz, B., Filiatrault, A., 2002. "*Performance-Based Seismic Design of Wood Framed Buildings.* Journal of Structural Engineering, 128(1):39-47.

Harding, N., Fowkes, A. H. R., 1984. "*Bolted Timber Joints".* Volume 111 Wood Science, Proceedings of Pacific Timber Engineering Conference, N.Z. Timber Design Society, I.P.E.N.Z.

He M., Li Z., Lam F., Ma R., Ma Z. 2014. "*Experimental investigation on lateral performance of timber-steel hybrid shear wall systems*". Journal of Structural Engineering, 140(6): 04014029-1~12

Heine, C. P., and Dolan, J. D. (2001). "*A new model to predict the load–slip relationship of bolted connections in timber.*" Wood and Fiber Science, Society of Wood Science and Technology, Vol. 33, No. 4.

ISO16670. 2003. "*Timber Structures – Joints made with mechanical fasteners – Quasi-static reversed-cyclic test method*." The International Organization for Standardization, Geneva.

Johansen, K. W. (1949) "*Theory of Timber Connections."* Int. Assn of Bridge & Struct. ENg., Publ. No. 9, pp. 249-262, Bern, Switzerland.

Judd, J. P. 2005. "Analytical modeling of wood-frame shear walls and diaphragms." Brigham Young University.

Li Z., He M., Li M., Lam F. 2014a. "Damage assessment and performance-based seismic design of timber-steel hybrid shear wall systems" Earthquakes and Structures. 7(1): 101-117.

Li Z., He M., Li M., Lam F. 2014c. "*Finite element modelling and parametric analysis of timber-steel hybrid structures*". The Structural Design of Tall and Special Buildings. 23(14): 1045-1063.

Li, Z., He, M., Lam, F., and Li, M 2015 "*Load-sharing mechanism in timber-steel hybrid shear wall systems.*" Front. Struct. Civ. Eng 9(2): 203–214

Li, Z. Dong, H., Wang, X., and He, M. 2017 "*Experimental and numerical investigations into seismic performance of timber-steel hybrid structure with supplemental dampers*". Engineering Structures, 151:33-43.

Newcombe, M., Pampanin, S., Buchanan, A., "*Multi-Storey Timber Buildings Seismic Design Guide, 7th Edition."* Department of Natural and Civil Resources Engineering, University of Canterbury.

Ministry for Primary Industries (MPI). *2014 Facts & Figures, New Zealand Plantation Forest Industry,* http://www.mpi.govt.nz/news-and-resources/open-data-and-forecasting/forestry/ - *accessed November 2016.*

NZS3404:1997. "*Steel Structures Standard*." Standards New Zealand.

NZS3604:2011 – "*Timber-framed buildings.*" Standards New Zealand.

Pang, W., Rosowsky, D. V., Pei, S., Lindt, J.W., (2010) "*Simplified Direct Displacement Design of Six-Story Woodframe Building and Pretest Seismic Performance Assessment*". Journal of Structural Engineering, 136(7): 813-825.

Pettinga, J. D., Priestley, M. J. N., (2005) "*Dynamic behaviour of reinforced concrete frames designed with direct displacment-based design*". Journal of Earthquake Engineering, Vol. 9, Special Issue 2 (2005) 309-330.

Porteous, J., Kermani, A., 2003. "Structural Timber Design to Eurocode 5, 2nd Edition" Wiley.

Sawata, K. (2015). *"Strength of bolted timber joints subjected to lateral force."* The Japan Wood Research Society, 61: 221-229.

Structural Steel Properties & Design Charts Book, March 2016. Easy Steel, Fletcher Building Ltd.

Wang, Y., Rosowsky, D. V., Pang, W., (2010), "*Performance-based Procedure for Direct Displacement Design of Engineered Wood-Frame Structures".* Journal of Structural Engineering, 136(8): 978-988.

Quenneville, P. (2008) "*Design of Bolted Connections: A Comparison of a Proposal and Various Existing Standards*." NZ Timber Design Journal, Volume 17, Issue 2.

8 APPENDICES

APPENDIX A: TIMBER-STEEL CONNECTIONS: DERIVED CYCLIC DISPLACEMENT PROTOCOLS

Bolted Connections

Table 8-1: Cyclic Displacement protocol for M10 Bolts with Double Studs.

Steps	No. of cycles	Amplitude	
1	1	1.25%	-0.6 mm
2	1	2.5%	1.3 mm
3	1	5%	-2.6 mm
4	1	7.5%	3.8 mm
5	1	10%	-5.1 mm
6	3	20%	10.2 mm
7	3	40%	-20.4 mm
8	3	60%	30.6 mm
9	3	80%	-40.8 mm
10	3	100%	51 mm
11	3	increments of 20% v_{ult}	

Table 8-2: Cyclic Displacement protocol for M10 Bolts with Triple Studs.

Steps	No. of cycles	Amplitude	
1	1	1.25%	-0.8 mm
2	1	2.5%	1.6 mm
3	1	5%	-3.2 mm
4	1	7.5%	4.8 mm
5	1	10%	-6.5 mm
6	3	20%	12.9 mm
7	3	40%	-25.8 mm
8	3	60%	38.7 mm
9	3	80%	-51.6 mm
10	3	100%	64.5 mm
11	3	increments of 20% v_{ult}	

Table 8-3: Cyclic Displacement protocol for M12 Bolts with Double Studs.

Steps	No. of cycles	Amplitude	
1	1	1.25%	-0.6 mm
2	1	2.5%	1.3 mm
3	1	5%	-2.6 mm
4	1	7.5%	3.9 mm
5	1	10%	-5.2 mm
6	3	20%	10.2 mm
7	3	40%	-20.6 mm
8	3	60%	30.9 mm
9	3	80%	-41.2 mm
10	3	100%	51.5 mm
11	3	increments of 20% v_{ult}	

Table 8-4: Cyclic Displacement protocol for M12 Bolts with Triple Studs.

Steps	No. of cycles	Amplitude	
1	1	1.25%	-0.9 mm
2	1	2.5%	1.8 mm
3	1	5%	-3.6 mm
4	1	7.5%	5.3 mm
5	1	10%	-7.1 mm
6	3	20%	14.2 mm
7	3	40%	-28.5 mm
8	3	60%	42.7 mm
9	3	80%	-57 mm
10	3	100%	71.2 mm
11	3	increments of 20% v_{ult}	

Table 8-5: Cyclic Displacement protocol for M10 Coach Screws with Double Studs.

Steps	No. of cycles	Amplitude	
1	1	1.25%	-0.6 mm
2	1	2.5%	1.3 mm
3	1	5%	-2.6 mm
4	1	7.5%	3.8 mm
5	1	10%	-5 mm
6	3	20%	10 mm
7	3	40%	-20 mm
8	3	60%	30 mm
9	3	80%	-40 mm
10	3	100%	50 mm
11	3	increments of 20% v_{ult}	

Table 8-6: Cyclic Displacement protocol for M10 Coach Screws with Triple Studs.

Steps	No. of cycles	Amplitude	
1	1	1.25%	-0.5 mm
2	1	2.5%	0.9 mm
3	1	5%	-1.7 mm
4	1	7.5%	2.6 mm
5	1	10%	-3.4 mm
6	3	20%	6.8 mm
7	3	40%	-13.6 mm
8	3	60%	20.6 mm
9	3	80%	-27.5 mm
10	3	100%	34.4 mm
11	3	increments of 20% v_{ult}	

Table 8-7: Cyclic Displacement protocol for M12 Coach Screws with Double Studs.

Steps	No. of cycles	Amplitude	
1	1	1.25%	-0.6 mm
2	1	2.5%	1.2 mm
3	1	5%	-2.4 mm
4	1	7.5%	3.6 mm
5	1	10%	-4.8 mm
6	3	20%	9.5 mm
7	3	40%	-19 mm
8	3	60%	28.6 mm
9	3	80%	-38.1 mm
10	3	100%	47.6 mm
11	3	increments of 20% v_{ult}	

Table 8-8: Cyclic Displacement protocol for M12 Coach Screws with Triple Studs.

Steps	No. of cycles	Amplitude	
1	1	1.25%	-0.5 mm
2	1	2.5%	1.1 mm
3	1	5%	-2.2 mm
4	1	7.5%	3.2 mm
5	1	10%	-4.3 mm
6	3	20%	8.7 mm
7	3	40%	-17.3 mm
8	3	60%	26 mm
9	3	80%	-34.6 mm
10	3	100%	43.3 mm
11	3	increments of 20% v_{ult}	

APPENDIX B TIMBER-STEEL CONNECTIONS: INDIVIDUAL TEST RESULTS (CYCLIC)

Individual test results for every Timber-Steel connection tested are shown in the Tables below.

Variability in the structural properties are likely a result of the inherent imperfections of sawn timber materials, however, results show that the structural properties of the Timber-Steel connections are quite consistent.

Bolted Connections

Table 8-9: Individual test results for M10 Bolts with Double Studs under cyclic loading.

		TEST 1	TEST 2	TEST 3	TEST 4	TEST 5	TEST 6	AVERAGE
POSITIVE	k_i (kN/mm)	6.4	4.9	4.9	8.7	4.8	4.1	5.6
	F_y (kN)	9.4	7.5	5.9	8.9	9.0	8.7	8.2
	F_{max} (kN)	18.4	12.6	12.6	14.0	14.6	17.4	14.9
	F_{ult} (kN)	14.8	12.6	9.4	14.0	11.6	17.4	13.3
	Δ_y (mm)	1.4	1.4	1.0	1.2	1.5	1.8	1.4
	Δ_{max} (mm)	31.0	20.9	20.9	20.4	11.6	27.7	22.1
	Δ_{ult} (mm)	31.0	20.9	22.9	23.8	16.8	27.7	23.9
	u	22.0	14.8	22.5	20.4	11.5	15.4	17.8
	$F_{(1-3)}$	17.2 - 62.3%	43.7 - 100%	59.6 - 100%	34.5 - 100%	19.9 - 47.3%	100 - 100%	45.8-84.9%
NEGATIVE	k_i (kN/mm)	7.3	5.6	5.6	6.2	5.7	7.6	6.3
	F_y (kN)	10.8	10.8	8.6	10.8	10.5	10.5	10.3
	F_{max} (kN)	16.4	17.1	17.1	16.2	17.3	17.2	16.9
	F_{ult} (kN)	13.2	17.1	17.1	16.2	17.3	10.7	15.3
	Δ_y (mm)	1.5	2.5	1.6	2.2	1.9	1.8	1.9
	Δ_{max} (mm)	25.9	20.8	20.9	20.4	20.5	21.0	21.6
	Δ_{ult} (mm)	25.9	20.8	20.9	20.4	20.5	24.1	22.1
	u	17.7	8.3	13.4	9.4	10.6	13.8	12.2
	$F_{(1-3)}$	42.5 - 100%	44.6 - 100%	50.6 - 100%	44.4 - 100%	100-100%	17.9-100%	50-100%

Table 8-10: Individual test results for M10 Bolts with Triple Studs under cyclic loading.

		TEST 1	TEST 2	TEST 3	TEST 4	TEST 5	TEST 6	AVERAGE
POSITIVE	k_i (kN/mm)	4.3	6.4	3.7	4.2	4.2	5.6	4.7
	F_y (kN)	9.5	10.0	10.0	8.6	10.2	10.7	9.8
	F_{max} (kN)	17.3	17.4	16.1	15.6	15.6	16.1	16.3
	F_{ult} (kN)	10.8	12.4	11.0	12.9	13.0	13.1	11.4
	Δ_y (mm)	2.2	1.8	2.6	2.1	2.9	2.4	2.3
	Δ_{max} (mm)	14.2	13.2	13.0	13.0	13.0	13.1	13.2
	Δ_{ult} (mm)	20.4	21.0	13.0	22.3	22.3	22.0	20.2
	u	9.2	11.7	5.1	10.7	7.8	9.1	8.9
	$F_{(1-3)}$	17.2 - 62.3%	17.2 - 62.3%	12.4-67.1%	6.8-40.2%	9.3-44.7%	12.4-67.1%	12-46.4%
NEGATIVE	k_i (kN/mm)	9.1	6.6	4.6	4.6	4.6	5.3	5.8
	F_y (kN)	10.0	10.5	10.7	10.2	10.2	10.2	10.3
	F_{max} (kN)	20.7	21.3	18.7	19.4	19.4	18.9	19.7
	F_{ult} (kN)	20.7	21.3	18.7	19.4	19.4	18.9	19.7
	Δ_y (mm)	1.3	1.8	2.4	2.3	2.3	2.4	2.1
	Δ_{max} (mm)	25.7	25.8	25.8	25.8	25.8	25.8	25.8
	Δ_{ult} (mm)	25.7	25.8	25.8	25.8	25.8	25.8	25.8
	u	19.6	14.8	10.8	11.3	11.3	10.6	13.1
	$F_{(1-3)}$	42.5 - 100%	42.5 - 100%	100-100%	100-100%	100-100%	100-100%	100-100%

Table 8-11: Individual test results for M12 Bolts with Double Studs under cyclic loading.

		TEST 1	TEST 2	TEST 3	TEST 4	TEST 5	TEST 6	AVERAGE
POSITIVE	k_i (kN/mm)	4.5	4.0	3.6	4.3	5.0	5.2	4.4
	F_y (kN)	14.2	14.0	12.0	13.2	15.0	15.0	13.9
	F_{max} (kN)	21.7	19.1	20.7	21.3	20.0	20.2	20.5
	F_{ult} (kN)	21.7	19.1	20.7	21.3	20.0	20.2	20.5
	Δ_y (mm)	3.8	3.9	3.1	3.8	4.0	3.1	3.6
	Δ_{max} (mm)	30.9	30.9	30.9	29.5	29.5	20.6	28.7
	Δ_{ult} (mm)	30.9	30.9	30.9	29.5	29.5	20.6	28.7
	u	8.2	7.9	10.1	7.8	7.4	6.7	8.0
	$F_{(1-3)}$	6.8-40.2%	6.8-40.2%	6.8-40.2%	6.8-40.2%	6.8-40.2%	6.8-40.2%	90.1 - 100%
NEGATIVE	k_i (kN/mm)	6.6	8.1	5.5	9.5	7.3	9.2	7.7
	F_y (kN)	13.05	14.0	12.4	15.5	14.7	14.7	14.1
	F_{max} (kN)	22.4	20.8	20.5	23.1	22.7	23.8	22.2
	F_{ult} (kN)	7.8	18.6	18.6	23.1	22.7	23.8	19.1
	Δ_y (mm)	2.6	2.8	2.0	1.9	2.2	1.8	2.2
	Δ_{max} (mm)	20.2	20.2	20.6	20.6	20.6	20.6	20.5
	Δ_{ult} (mm)	20.2	30.9	26.8	20.6	20.6	20.6	23.3
	u	7.7	11.0	13.1	10.9	9.4	11.8	10.7
	$F_{(1-3)}$	100-100%	100-100%	100-100%	100-100%	100-100%	100-100%	29.2 - 76.6%

Table 8-12: Individual test results for M12 Bolts with Triple Studs under cyclic loading.

		TEST 1	TEST 2	TEST 3	TEST 4	TEST 5	TEST 6	AVERAGE
POSITIVE	k_i (kN/mm)	2.5	3.1	3.8	3.8	3.1	3.0	3.2
	F_y (kN)	12.1	12.1	12.1	12.1	12.1	13.8	12.3
	F_{max} (kN)	19.9	18.3	21.1	19.6	20.3	19.6	19.8
	F_{ult} (kN)	7.5	17.0	21.1	17.5	20.3	14.0	16.2
	Δ_y (mm)	3.9	3.4	2.9	2.6	3.5	17.3	5.6
	Δ_{max} (mm)	28.5	28.5	28.5	14.2	14.2	14.2	21.4
	Δ_{ult} (mm)	28.5	28.5	28.5	28.5	28.5	19.5	27.0
	u	7.3	8.5	9.8	10.9	8.3	1.1	7.7
	$F_{(1-3)}$	62.2 - 100%	12.6 - 31.7%	14.7- 100%	13.1 - 36.1%	18.9 - 38.5%	15.7 - 43.8%	22.9 - 58.4%
NEGATIVE	k_i (kN/mm)	5.6	5.6	3.8	7.7	7.4	6.9	6.2
	F_y (kN)	14.0	14.0	13.5	15.2	13.98	13.1	14.0
	F_{max} (kN)	25.5	22.8	27.9	25.0	25.2	22.3	24.8
	F_{ult} (kN)	25.5	10.0	27.9	8.5	11.0	22.3	17.6
	Δ_y (mm)	2.7	3.2	3.1	2.4	1.9	1.9	2.5
	Δ_{max} (mm)	28.2	28.2	27.0	28.2	28.2	28.2	28.0
	Δ_{ult} (mm)	28.2	28.2	27.0	28.2	28.2	28.2	28.0
	u	10.6	9.0	8.7	11.6	14.9	14.5	11.5
	$F_{(1-3)}$	43.2 - 100%	56.1 - 100%	100 - 100%	66 - 100%	56.4 - 100%	100 - 100%	70.3 - 100%

Coach Screwed Connections

Table 8-13: Individual test results for M10 Coach Screws with Double Studs under cyclic loading.

		TEST 1	TEST 2	TEST 3	TEST 4	TEST 5	TEST 6	AVERAGE
POSITIVE	k_i (kN/mm)	2.4	2.1	2.3	1.1	4.5	3.0	2.5
	F_y (kN)	7.0	8.8	6.8	7.2	6.1	7.0	7.1
	F_{max} (kN)	13.3	12.2	12.5	11.8	12.3	12.9	12.5
	F_{ult} (kN)	13.1	8.0	7.9	6.6	7.3	7.2	8.4
	Δ_y (mm)	2.8	3.8	2.7	4.6	1.4	2.4	3.0
	Δ_{max} (mm)	20.0	10.0	20.0	20.0	12.0	20.0	17.0
	Δ_{ult} (mm)	30.0	30.0	37.5	30.0	30.0	30.0	31.3
	u	10.7	7.9	13.8	6.5	22.1	12.3	12.2
	$F_{(1-3)}$	43.8 - 100%	42.5 - 100%	43.8 - 63.9%	40.8 - 49.3%	22.5 - 59.2%	53.6 - 61.4%	41.2 - 72.3%
NEGATIVE	k_i (kN/mm)	2.5	4.0	2.5	3.7	3.4	2.5	3.1
	F_y (kN)	7.5	8.9	7.8	7.8	7.2	7.2	7.7
	F_{max} (kN)	13.5	16.3	14.4	15.6	15.3	15.1	15.0
	F_{ult} (kN)	7.1	8.5	8.8	7.0	9.0	8.0	8.1
	Δ_y (mm)	3.0	2.8	3.4	2.2	2.3	3.0	2.8
	Δ_{max} (mm)	30.0	20.0	20.0	20.0	20.0	20.0	21.7
	Δ_{ult} (mm)	30.0	30.0	30.0	35.4	30.0	30.0	30.9
	u	10.1	10.7	8.8	15.9	12.9	10.1	11.4
	$F_{(1-3)}$	40.7 - 48.1%	44.9 - 57.1%	41.1 - 51.5%	45.4 - 55.1%	44.3 - 47.6%	33.6 - 46.9%	41.7 - 51.1%

Table 8-14: Individual test results for M10 Coach Screws with Triple Studs under cyclic loading.

		TEST 1	TEST 2	TEST 3	TEST 4	TEST 5	TEST 6	AVERAGE
POSITIVE	k_i (kN/mm)	2.0	2.1	2.0	2.8	1.6	2.3	2.1
	F_y (kN)	7.5	7.0	7.1	8.8	8.5	8.0	7.8
	F_{max} (kN)	14.2	14.6	13.5	14.0	14.1	13.7	14.0
	F_{ult} (kN)	14.2	6.9	5.8	6.3	14.1	13.7	10.2
	Δ_y (mm)	2.8	2.6	2.7	2.8	3.4	2.8	2.8
	Δ_{max} (mm)	20.6	20.6	20.6	20.6	20.6	20.6	20.6
	Δ_{ult} (mm)	27.5	26.0	26.0	24.5	20.6	28.0	25.4
	u	9.9	9.9	9.6	8.8	6.1	10.0	9.0
	$F_{(1-3)}$	21.3 - 100%	55.4 - 100%	55.6 - 100%	57.2 - 100%	39.6 - 100%	26.8 - 48.8%	42.7 - 91.5%
NEGATIVE	k_i (kN/mm)	4.2	3.5	4.6	3.9	6.5	5.3	4.7
	F_y (kN)	8.5	8.2	7.2	8.1	9.0	8.5	8.3
	F_{max} (kN)	14.2	13.4	14.0	14.0	14.8	18.8	14.9
	F_{ult} (kN)	14.2	7.0	10.0	7.5	6.0	19.0	10.6
	Δ_y (mm)	1.8	2.6	1.6	2.0	1.6	1.7	1.9
	Δ_{max} (mm)	20.6	20.6	13.6	20.6	20.6	20.6	19.4
	Δ_{ult} (mm)	20.6	28.0	20.6	28.0	28.0	20.6	24.3
	u	11.4	10.7	13.3	14.1	17.5	12.1	13.2
	$F_{(1-3)}$	15.7 - 22.7%	17.7 - 25.2%	21.7 - 28.8%	13.8 - 28.8%	18.5 - 32.6%	60.5 - 100%	24.6 - 39.7%

Table 8-15: Individual test results for M12 Coach Screws with Double Studs under cyclic loading.

		TEST 1	TEST 2	TEST 3	TEST 4	TEST 5	TEST 6	AVERAGE
POSITIVE	k_i (kN/mm)	1.6	1.0	2.0	1.5	2.1	1.2	1.6
	F_y (kN)	16.0	11.5	11.5	11.0	11.0	12.0	12.2
	F_{max} (kN)	19.2	17.8	19.2	17.6	17.7	19.0	18.4
	F_{ult} (kN)	11.0	11.0	7.2	17.6	17.7	19.0	13.9
	Δ_y (mm)	11.2	7.9	5.1	5.6	5.0	7.2	7.0
	Δ_{max} (mm)	19.0	28.6	28.6	28.6	28.6	28.6	27.0
	Δ_{ult} (mm)	28.6	28.6	28.6	28.6	28.6	28.6	28.6
	u	2.6	3.6	5.7	5.1	5.8	4.0	4.5
	$F_{(1-3)}$	27.1 - 100%	21.2 - 100%	62.6 - 100%	43.3 - 100%	29.5 - 100%	42.1 - 100%	37.6 - 100%
NEGATIVE	k_i (kN/mm)	3.0	4.7	1.8	2.3	2.5	2.3	2.8
	F_y (kN)	13.0	13.5	10.5	11.0	11.5	12.2	12.0
	F_{max} (kN)	20.2	19.1	18.7	17.5	18.7	19.5	18.9
	F_{ult} (kN)	8.0	16.4	15.1	8.5	8.5	8.5	10.8
	Δ_y (mm)	4.4	3.9	4.8	4.9	4.9	4.7	4.6
	Δ_{max} (mm)	19.0	19.0	19.0	19.0	19.0	19.0	19.0
	Δ_{ult} (mm)	30.0	28.6	28.6	28.6	28.6	28.6	28.8
	u	6.8	7.4	6.0	5.9	5.9	6.1	6.3
	$F_{(1-3)}$	28.1 - 77.7%	16.1 - 31.9%	19.7 - 49.1%	16.9 - 45.6%	22.5 - 41.2%	25.7 - 43.6%	21.5 - 48.2%

Table 8-16: Individual test results for M12 Coach Screws with Triple Studs under cyclic loading.

		TEST 1	TEST 2	TEST 3	TEST 4	TEST 5	TEST 6	AVERAGE
POSITIVE	k_i (kN/mm)	2.9	1.5	2.2	1.9	1.9	1.6	2.0
	F_y (kN)	11.0	11.4	11.2	11.1	11.0	10.7	11.1
	F_{max} (kN)	21.7	20.6	20.6	18.1	21.4	20.3	20.5
	F_{ult} (kN)	9.2	20.6	9.0	10.0	8.5	9.5	11.1
	Δ_y (mm)	3.0	5.6	4.3	4.2	4.4	5.0	4.4
	Δ_{max} (mm)	17.3	26.0	26.0	26.0	26.0	26.0	24.6
	Δ_{ult} (mm)	26.0	26.0	26.0	26.0	26.0	26.0	26.0
	u	8.6	4.6	6.1	6.2	5.9	5.2	6.1
	$F_{(1-3)}$	19.4 - 100%	37 - 100%	56.4 - 100%	44.8 - 100%	60.2 - 100%	53.2 - 100%	45.1 - 100%
NEGATIVE	k_i (kN/mm)	4.5	4.7	3.6	4.6	4.9	4.7	4.5
	F_y (kN)	12.09	12.0	10.5	12.0	11.8	11.5	11.6
	F_{max} (kN)	26.5	22.3	18.4	19.1	19.7	21.9	21.3
	F_{ult} (kN)	11.5	7.0	9.0	9.0	10.0	8.5	9.2
	Δ_y (mm)	3.0	3.2	4.3	3.5	3.3	2.4	3.2
	Δ_{max} (mm)	17.3	17.3	17.3	17.3	17.3	17.3	17.3
	Δ_{ult} (mm)	26.0	26.0	26.0	26.0	26.0	26.0	26.0
	u	8.8	8.3	6.1	7.5	8.0	10.9	8.3
	$F_{(1-3)}$	24.5 - 52.8%	30.4 - 46.1%	18.4 - 34.7%	21.5 - 45.1%	24 - 46.8%	31.5 - 52.1%	25.1 - 46.3%

APPENDIX C: TIMBER-SHEATHING CONNECTIONS: INDIVIDUAL TEST RESULTS (MONOTONIC) AND DERIVED CYCLIC DISPLACEMENT PROTOCOLS

ϕ2.8x60mm Nails

Table 8-17: Cyclic Displacement protocol for φ2.8 nails with 12mm Ply loaded parallel to grain.

Steps	**No. of cycles**	**Amplitude**	
1	1	1.25%	-0.3 mm
2	1	2.5%	0.6 mm
3	1	5%	-1.2 mm
4	1	7.5%	1.8 mm
5	1	10%	-2.4 mm
6	3	20%	4.9 mm
7	3	40%	-9.7 mm
8	3	60%	14.6 mm
9	3	80%	-19.4 mm
10	3	100%	24.3 mm
11	3	increments of 20% v_{ult}	

Table 8-18: Cyclic Displacement protocol for φ2.8 nails with 12mm Ply loaded perpendicular to grain.

Steps	No. of cycles	Amplitude	
1	1	1.25%	-0.3 mm
2	1	2.5%	0.6 mm
3	1	5%	-1.2 mm
4	1	7.5%	1.7 mm
5	1	10%	-2.3 mm
6	3	20%	4.6 mm
7	3	40%	-9.3 mm
8	3	60%	14 mm
9	3	80%	-18.6 mm
10	3	100%	23.2 mm
11	3	increments of 20% v_{ult}	

Table 8-19: Cyclic Displacement protocol for φ2.8 nails with 17mm Ply loaded parallel to grain.

Steps	No. of cycles	Amplitude	
1	1	1.25%	-0.2 mm
2	1	2.5%	0.5 mm
3	1	5%	-0.9 mm
4	1	7.5%	1.4 mm
5	1	10%	-1.8 mm
6	3	20%	3.7 mm
7	3	40%	-7.3 mm
8	3	60%	10.9 mm
9	3	80%	-14.6 mm
10	3	100%	18.3 mm
11	3	120%	-21.9 mm
12	3	140%	25.6 mm

Table 8-20: Cyclic Protocol for φ2.8 Nails with 17mm Ply loaded perpendicular to grain.

Steps	No. of cycles	Amplitude	
1	1	1.25%	-0.2 mm
2	1	2.5%	0.3 mm
3	1	5%	-0.6 mm
4	1	7.5%	0.8 mm
5	1	10%	-1.1 mm
6	3	20%	2.2 mm
7	3	40%	-4.4 mm
8	3	60%	6.6 mm
9	3	80%	-8.8 mm
10	3	100%	11 mm
11	3	120%	-13.2 mm
12	3	140%	15.4 mm
13	3	160%	-17.6 mm
14	3	180%	19.8 mm
15	3	200%	22 mm
16	3	220%	-24.2 mm
17	3	240%	26.4 mm

ϕ3.15x75mm Nails

Table 8-21: Cyclic Protocol for φ3.15 Nails with 12mm Ply loaded parallel to grain.

Steps	No. of cycles	Amplitude	
1	1	1.25%	-0.3 mm
2	1	2.5%	0.7 mm
3	1	5%	-1.3 mm
4	1	7.5%	2.0 mm
5	1	10%	-2.6 mm
6	3	20%	5.3 mm
7	3	40%	-10.6 mm
8	3	60%	15.8 mm
9	3	80%	-21.1 mm
10	3	100%	26.4 mm
11	3	120%	31.7 mm
12	3	140%	37 mm
13	3	160%	-42.2 mm

Table 8-22: Cyclic Protocol for φ3.15 Nails with 12mm Ply loaded perpendicular to grain.

Steps	No. of cycles	Amplitude	
1	1	1.25%	-0.2 mm
2	1	2.5%	0.4 mm
3	1	5%	-0.9 mm
4	1	7.5%	1.3 mm
5	1	10%	-1.7 mm
6	3	20%	3.5 mm
7	3	40%	-7 mm
8	3	60%	10.4 mm
9	3	80%	-13.9 mm
10	3	100%	17.4 mm
11	3	120%	-20.9 mm
12	3	140%	24.4 mm
13	3	160%	-27.8 mm
14	3	180%	31.3 mm

Table 8-23: Cyclic Protocol for φ3.15 Nails with 17mm Ply loaded parallel to grain.

Steps	No. of cycles	Amplitude	
1	1	1.25%	-0.3 mm
2	1	2.5%	0.7 mm
3	1	5%	-1.3 mm
4	1	7.5%	2.0 mm
5	1	10%	-2.6 mm
6	3	20%	5.2 mm
7	3	40%	-10.4 mm
8	3	60%	15.6 mm
9	3	80%	-20.8 mm
10	3	100%	26 mm
11	3	120%	-31.2 mm
12	3	140%	36.4 mm
13	3	160%	-41.6 mm
14	3	180%	46.8 mm

Table 8-24: Cyclic Protocol for φ3.15 Nails with 17mm Ply loaded perpendicular to grain.

Steps	No. of cycles	Amplitude	
1	1	1.25%	-0.4 mm
2	1	2.5%	0.7 mm
3	1	5%	-1.3 mm
4	1	7.5%	2.1 mm
5	1	10%	-2.6 mm
6	3	20%	5.2 mm
7	3	40%	-10.4 mm
8	3	60%	15.6 mm
9	3	80%	-20.8 mm
10	3	100%	26 mm
11	3	120%	-31.2 mm
12	3	140%	36.4 mm
13	3	160%	-41.6 mm

Table 8-25: Cyclic Protocol for φ3.15 Nails with 25mm Ply loaded parallel to grain.

Steps	No. of cycles	Amplitude	
1	1	1.25%	-0.3 mm
2	1	2.5%	0.5 mm
3	1	5%	-1.0 mm
4	1	7.5%	1.6 mm
5	1	10%	-2.1 mm
6	3	20%	4.2 mm
7	3	40%	-8.4 mm
8	3	60%	12.6 mm
9	3	80%	-16.2 mm
10	3	100%	21 mm
11	3	120%	-25.2 mm
12	3	140%	29.4 mm
13	3	160%	-32.4 mm
14	3	180%	37.8 mm

Table 8-26: Cyclic Protocol for φ3.15 Nails with 25mm Ply loaded perpendicular to grain.

Steps	No. of cycles	Amplitude	
1	1	1.25%	-0.2 mm
2	1	2.5%	0.4 mm
3	1	5%	-0.7 mm
4	1	7.5%	1.0 mm
5	1	10%	-1.4 mm
6	3	20%	2.8 mm
7	3	40%	-5.5 mm
8	3	60%	8.3 mm
9	3	80%	-11 mm
10	3	100%	13.8 mm
11	3	120%	-16.6 mm
12	3	140%	19.3 mm
13	3	160%	-22.1 mm
14	3	180%	24.8 mm
15	3	200%	-27.6 mm
16	3	220%	30.4 mm

ϕ3.55x90mm Nails

Table 8-27: Cyclic Protocol for φ3.55 Nails with 12mm Ply loaded parallel to grain.

Steps	No. of cycles	Amplitude	
1	1	1.25%	-0.3 mm
2	1	2.5%	0.5 mm
3	1	5%	-1.0 mm
4	1	7.5%	1.5 mm
5	1	10%	-2 mm
6	3	20%	4 mm
7	3	40%	-8 mm
8	3	60%	11.9 mm
9	3	80%	-15.8 mm
10	3	100%	19.8 mm
11	3	120%	-23.8 mm
12	3	140%	27.7 mm
13	3	160%	-31.7 mm
14	3	180%	35.6 mm
15	3	200%	-39.6 mm
16	3	220%	43.8 mm
17	3	240%	-47.5 mm
18	3	260%	51.5 mm

Table 8-28: Cyclic Protocol for φ3.55 Nails with 12mm Ply loaded perpendicular to grain.

Steps	No. of cycles	Amplitude	
1	1	1.25%	-0.3 mm
2	1	2.5%	0.5 mm
3	1	5%	-1.0 mm
4	1	7.5%	1.5 mm
5	1	10%	-2 mm
6	3	20%	4 mm
7	3	40%	-8 mm
8	3	60%	12 mm
9	3	80%	-16 mm
10	3	100%	20 mm
11	3	120%	-24 mm
12	3	140%	28 mm
13	3	160%	-32 mm
14	3	180%	36 mm

Table 8-29: Cyclic Protocol for φ3.55 Nails with 17mm Ply loaded parallel to grain.

Steps	No. of cycles	Amplitude	
1	1	1.25%	-0.3 mm
2	1	2.5%	0.6 mm
3	1	5%	-1.2 mm
4	1	7.5%	1.6 mm
5	1	10%	-2.4 mm
6	3	20%	4.8 mm
7	3	40%	-9.6 mm
8	3	60%	12.9 mm
9	3	80%	-17.2 mm
10	3	100%	21.5 mm
11	3	120%	-25.8 mm
12	3	140%	30.1 mm
13	3	160%	-34.4 mm
14	3	180%	38.7 mm
15	3	200%	-43 mm
16	3	220%	47.8 mm

Table 8-30: Cyclic Protocol for φ3.55 Nails with 17mm Ply loaded perpendicular to grain.

Steps	No. of cycles	Amplitude	
1	1	1.25%	-0.3 mm
2	1	2.5%	0.5 mm
3	1	5%	-1.0 mm
4	1	7.5%	1.5 mm
5	1	10%	-2 mm
6	3	20%	4.1 mm
7	3	40%	-8.2 mm
8	3	60%	12.2 mm
9	3	80%	-16.4 mm
10	3	100%	20.4 mm
11	3	120%	-24.5 mm
12	3	140%	28.6 mm
13	3	160%	-32.6 mm
14	3	180%	36.7 mm

Table 8-31: Cyclic Protocol for φ3.55 Nails with 25mm Ply loaded parallel to grain.

Steps	No. of cycles	Amplitude	
1	1	1.25%	-0.3 mm
2	1	2.5%	0.6 mm
3	1	5%	-1.2 mm
4	1	7.5%	1.7 mm
5	1	10%	-2.3 mm
6	3	20%	4.6 mm
7	3	40%	9.2 mm
8	3	60%	13.8 mm
9	3	80%	-18.4 mm
10	3	100%	23 mm
11	3	120%	-27.6 mm
12	3	140%	32.2 mm
13	3	160%	-36.8 mm
14	3	180%	41.4 mm
15	3	200%	-46 mm

Table 8-32: Cyclic Protocol for φ3.55 Nails with 25mm Ply loaded perpendicular to grain.

Steps	No. of cycles	Amplitude	
1	1	1.25%	-0.2 mm
2	1	2.5%	0.3 mm
3	1	5%	-0.6 mm
4	1	7.5%	0.9 mm
5	1	10%	-1.2 mm
6	3	20%	2.4 mm
7	3	40%	-4.8 mm
8	3	60%	7.2 mm
9	3	80%	-9.6 mm
10	3	100%	12 mm
11	3	120%	-14.4 mm
12	3	140%	16.8 mm
13	3	160%	-19.2 mm
14	3	180%	21.6 mm
15	3	200%	-24 mm
16	3	220%	26.4 mm
17	3	240%	-28.8 mm
18	3	260%	31.2 mm

APPENDIX D: TIMBER-SHEATHING CONNECTIONS: INDIVIDUAL TEST RESULTS

Individual test results for every Timber-Sheathing connection tested are shown in the Tables below.

Variability in the structural properties are likely a result of the inherent imperfections of sawn timber materials. Results show that the displacements and ductility of the Timber-Sheathing connections can be quite variable.

ϕ2.8x60mm Nails

Table 8-33: Test results for φ2.8 Nails with 12mm Ply loaded parallel to grain (single nail).

		TEST 1	TEST 2	TEST 3	TEST 4	TEST 5	TEST 6	AVERAGE
POSITIVE	k_i (kN/mm)	0.47	1.15	1.40	1.13	1.07	0.87	1.01
	F_y (kN)	0.70	0.68	0.68	0.68	0.68	0.70	0.68
	F_{max} (kN)	0.92	0.92	0.89	0.90	0.89	0.85	0.89
	F_{ult} (kN)	0.73	0.74	0.71	0.72	0.71	0.68	0.71
	Δ_y (mm)	1.8	1.8	1.8	1.8	1.8	2.2	1.9
	Δ_{max} (mm)	9.7	4.9	9.7	9.7	14.2	9.7	9.7
	Δ_{ult} (mm)	14.7	18.0	17.0	14.0	34.1	18.3	19.4
	u	8.0	9.8	9.2	7.6	19.5	8.2	10.4
	$F_{(1-3)}$	17.6 – 50.5%	14.4 – 39.2%	12.8 – 53.5%	10.6 – 44.1%	11.4 – 20.0%	7.4 – 38.7%	12.4 - 41%
NEGATIVE	k_i (kN/mm)	1.41	0.71	0.60	0.61	0.68	0.74	0.79
	F_y (kN)	0.77	0.58	0.55	0.61	0.60	0.65	0.63
	F_{max} (kN)	1.13	0.92	0.88	0.89	0.89	0.89	0.93
	F_{ult} (kN)	0.90	0.74	0.70	0.71	0.71	0.71	0.75
	Δ_y (mm)	2.9	1.2	0.9	1.4	1.6	2.1	1.7
	Δ_{max} (mm)	9.7	14.6	9.7	9.7	14.0	9.7	11.2
	Δ_{ult} (mm)	13.2	21.0	17.0	13.0	34.1	18.0	19.4
	u	4.6	17.4	19.5	9.3	21.3	8.4	13.4
	$F_{(1-3)}$	35.8 – 55.8%	23.9 – 26.6%	22.9 – 65.7%	37.5 – 65.7%	32.6 – 57.9%	28.6 – 48.6%	30.2 - 52%

Table 8-34: Test results for φ2.8 Nails with 12mm Ply loaded perpendicular to grain (single nail).

		TEST 1	TEST 2	TEST 3	TEST 4	TEST 5	TEST 6	AVERAGE
POSITIVE	k_i (kN/mm)	1.56	0.83	1.77	0.92	1.19	0.88	1.19
	F_y (kN)	0.70	0.83	0.66	0.66	0.66	0.60	0.68
	F_{max} (kN)	0.99	1.08	1.12	1.05	0.96	1.29	1.08
	F_{ult} (kN)	0.79	0.86	0.90	0.84	0.76	1.03	0.86
	Δ_y (mm)	1.3	1.3	1.2	1.3	1.7	1.7	1.4
	Δ_{max} (mm)	4.6	4.6	4.6	14.0	8.0	12.0	8.0
	Δ_{ult} (mm)	11.2	12.0	16.2	24.0	12.0	23.2	16.4
	u	8.8	9.4	13.8	18.5	7.0	13.5	11.8
	$F_{(1-3)}$	16.2 - 37.2%	11.6 - 25.6%	15.2 - 33%	27.2 - 29.6%	26.3 - 47.4%	30.9 - 43.1%	21.1 - 36
NEGATIVE	k_i (kN/mm)	0.89	2.34	0.88	1.06	1.23	0.89	1.21
	F_y (kN)	0.63	0.73	0.63	0.80	0.63	0.60	0.67
	F_{max} (kN)	1.01	1.09	1.12	1.20	0.99	1.16	1.09
	F_{ult} (kN)	0.81	0.87	0.90	0.96	0.79	0.92	0.87
	Δ_y (mm)	1.2	1.2	1.0	1.2	1.1	0.7	1.1
	Δ_{max} (mm)	8.5	9.3	9.3	9.3	8.0	9.3	9.0
	Δ_{ult} (mm)	18.3	13.0	20.0	18.2	12.0	23.2	17.5
	u	15.1	10.9	19.6	15.2	11.2	31.8	17.3
	$F_{(1-3)}$	37.5 - 45%	14.3 - 28.6%	7.8 - 21.7%	12.2 - 52.2%	18.4 - 26.3%	18.2 - 45.5%	18.1 - 36.5%

Table 8-35: Test results for φ2.8 Nails with 17mm Ply loaded parallel to grain (single nail).

		TEST 1	TEST 2	TEST 3	TEST 4	TEST 5	TEST 6	AVERAGE
POSITIVE	k_i (kN/mm)	1.03	0.45	0.81	1.27	1.30	0.88	0.96
	F_y (kN)	0.75	0.65	0.68	0.77	0.58	0.65	0.68
	F_{max} (kN)	1.00	0.94	0.92	1.02	0.83	1.00	0.95
	F_{ult} (kN)	0.80	0.75	0.74	0.81	0.66	0.80	0.76
	Δ_y (mm)	1.3	1.6	1.8	1.2	1.4	1.4	1.4
	Δ_{max} (mm)	7.3	10.8	7.3	3.7	7.3	7.3	7.3
	Δ_{ult} (mm)	10.9	12.9	12.2	11.0	17.0	14.0	13.0
	u	8.5	8.1	6.8	9.3	12.5	10.3	9.2
	$F_{(1-3)}$	7.5 - 47.5%	10.5 - 28.9%	8.1 - 27%	10 - 25%	6.1 - 27.3%	7.5 -40%	8.3 - 32.6%
NEGATIVE	k_i (kN/mm)	3.05	0.30	1.25	1.65	1.09	1.94	1.55
	F_y (kN)	0.70	0.73	0.68	0.70	0.55	0.55	0.65
	F_{max} (kN)	1.02	0.94	1.00	1.05	0.87	0.91	0.96
	F_{ult} (kN)	0.81	0.75	0.80	0.84	0.70	0.72	0.77
	Δ_y (mm)	1.2	1.8	1.2	1.0	1.0	1.0	1.2
	Δ_{max} (mm)	8.5	10.8	10.8	8.5	8.5	8.5	9.3
	Δ_{ult} (mm)	12.0	12.6	17.0	12.0	12.0	16.0	13.6
	u	9.9	7.2	14.0	12.0	12.0	16.0	11.9
	$F_{(1-3)}$	10 - 42.5%	18.9 - 51.4%	20 -40%	28.6 - 35.7%	14.3 - 22.9%	5.6 - 11.1%	16.2 - 33.9%

Table 8-36: Test results for φ2.8 Nails with 17mm Ply loaded perpendicular to grain (single nail).

		TEST 1	TEST 2	TEST 3	TEST 4	TEST 5	TEST 6	AVERAGE
POSITIVE	k_i (kN/mm)	0.94	0.69	0.74	0.66	0.78	1.36	0.86
	F_y (kN)	0.50	0.60	0.58	0.65	0.65	0.45	0.57
	F_{max} (kN)	0.91	1.12	1.22	1.08	1.02	1.09	1.07
	F_{ult} (kN)	0.72	0.90	0.97	0.86	0.81	0.87	0.86
	Δ_y (mm)	1.3	1.3	1.3	1.2	1.4	1.4	1.3
	Δ_{max} (mm)	9.2	2.2	2.3	2.1	9.2	9.2	5.7
	Δ_{ult} (mm)	13.0	15.0	20.0	9.5	11.2	10.0	13.1
	u	10.2	11.7	15.6	7.9	8.0	7.1	10.1
	$F_{(1-3)}$	2.4 -5.3%	6.8 - 9.1%	2.6 -14.3%	5.3 - 10.2%	2.5 -20.5%	4.6 -13.3%	4 - 12%
NEGATIVE	k_i (kN/mm)	1.24	1.02	0.86	0.74	0.92	0.92	0.95
	F_y (kN)	0.45	0.80	0.55	0.60	0.60	0.55	0.59
	F_{max} (kN)	1.00	1.43	1.20	1.03	1.05	1.05	1.12
	F_{ult} (kN)	0.80	1.14	0.96	0.82	0.84	0.84	0.90
	Δ_y (mm)	9.2	1.1	1.1	1.8	0.7	0.7	2.4
	Δ_{max} (mm)	13.8	13.8	13.8	13.8	4.6	4.6	10.7
	Δ_{ult} (mm)	16.0	26.1	18.0	14.5	14.0	10.4	16.5
	u	1.7	23.1	15.9	8.3	21.5	16.0	6.8
	$F_{(1-3)}$	12.1 - 14.6%	21.3 - 28.3%	5.3 - 9.5%	3 - 8.9%	3.6 - 23.9%	3.7 -9.1%	8.2 - 15.7%

ϕ3.15x75mm Nails

Table 8-37: Test results for φ3.15 Nails with 12mm Ply loaded parallel to grain (single nail).

		TEST 1	TEST 2	TEST 3	TEST 4	TEST 5	TEST 6	AVERAGE
POSITIVE	k_i (kN/mm)	1.26	0.73	0.85	0.88	1.82	0.63	1.03
	F_y (kN)	0.91	0.85	0.80	0.85	1.05	0.85	0.88
	F_{max} (kN)	1.26	1.09	1.22	1.26	1.31	1.88	1.34
	F_{ult} (kN)	1.01	0.87	0.98	1.01	1.04	1.50	1.07
	Δ_y (mm)	1.9	1.8	2.9	2.9	2.9	2.9	2.5
	Δ_{max} (mm)	15.8	10.3	10.3	10.3	5.3	26.4	13.1
	Δ_{ult} (mm)	28.0	22.0	22.0	20.0	15.0	29.0	22.7
	u	14.8	12.2	7.6	6.9	5.2	10.0	8.9
	$F_{(1-3)}$	18 - 47.2%	13.8 - 35%	22.2 - 41.3%	27.7 - 53.8%	6.1 - 13.8%	30.7 - 46.7%	19.8 -39.6%
NEGATIVE	k_i (kN/mm)	0.90	1.56	1.42	0.49	1.41	0.54	1.05
	F_y (kN)	0.76	0.76	0.80	1.03	0.85	0.80	0.83
	F_{max} (kN)	1.20	1.09	1.25	1.29	1.32	1.86	1.34
	F_{ult} (kN)	0.96	0.87	1.00	1.03	1.06	1.49	1.07
	Δ_y (mm)	1.8	1.9	4.7	4.7	4.7	4.7	3.8
	Δ_{max} (mm)	8.5	8.5	8.5	8.5	8.5	31.7	12.4
	Δ_{ult} (mm)	18.0	22.0	22.0	21.0	15.0	31.7	21.6
	u	9.8	11.6	4.7	4.5	3.2	6.7	5.8
	$F_{(1-3)}$	21.7 50%	20.5 - 47.7%	21.6 - 40%	7.7 - 42.3%	7.7 -42.3%	66.3 -100%	24.2 - 53.7%

Table 8-38: Test results for φ3.15 Nails with 12mm Ply loaded perpendicular to grain (single nail).

		TEST 1	TEST 2	TEST 3	TEST 4	TEST 5	TEST 6	AVERAGE
POSITIVE	k_i (kN/mm)	0.55	0.79	0.83	1.05	0.99	0.89	0.85
	F_y (kN)	0.60	0.86	0.80	0.88	0.73	0.65	0.75
	F_{max} (kN)	1.25	1.54	1.22	1.19	1.29	1.16	1.27
	F_{ult} (kN)	1.00	1.23	0.97	0.95	1.03	0.92	1.02
	Δ_y (mm)	1.2	1.3	1.1	1.5	1.0	1.1	1.2
	Δ_{max} (mm)	10.4	10.4	10.4	10.4	10.4	10.4	10.4
	Δ_{ult} (mm)	21.0	19.2	15.2	15.0	14.0	19.2	17.3
	u	17.9	14.8	13.8	10.0	13.7	17.1	14.4
	$F_{(1-3)}$	18.7 - 43.1%	14.5 - 35.9%	22.9 - 22.9%	21.3 - 31.9%	18.6 - 38%	28.6 - 30.7%	20.8 - 33.1%
NEGATIVE	k_i (kN/mm)	1.56	1.01	0.40	0.69	0.01	1.89	0.93
	F_y (kN)	0.73	0.75	0.62	0.69	0.75	0.73	0.71
	F_{max} (kN)	1.25	1.35	1.34	1.34	1.35	1.14	1.29
	F_{ult} (kN)	1.00	1.08	1.07	1.07	1.08	0.91	1.03
	Δ_y (mm)	0.6	1.5	1.3	1.5	1.2	0.9	1.2
	Δ_{max} (mm)	10.4	13.9	13.9	13.9	10.4	13.9	12.7
	Δ_{ult} (mm)	19.2	24.0	16.2	17.0	16.0	24.2	19.4
	u	33.1	16.0	12.4	11.6	13.0	26.3	16.7
	$F_{(1-3)}$	5.7 - 28.9%	23 - 28.1%	20.6 - 31.8%	20.6 - 28.6%	3.7 -27.4%	18.5 - 33%	16.6 - 29.6%

Table 8-39: Test results for φ3.15 Nails with 17mm Ply loaded parallel to grain (single nail).

		TEST 1	TEST 2	TEST 3	TEST 4	TEST 5	TEST 6	AVERAGE
POSITIVE	k_i (kN/mm)	0.91	0.78	1.09	1.37	1.04	0.65	0.97
	F_y (kN)	0.88	0.80	0.95	0.90	0.63	0.70	0.81
	F_{max} (kN)	1.60	1.25	1.85	1.19	1.42	1.57	1.48
	F_{ult} (kN)	1.28	1.00	1.48	0.95	1.13	1.25	1.18
	Δ_y (mm)	1.4	1.6	1.2	1.9	0.8	1.0	1.3
	Δ_{max} (mm)	15.6	5.2	15.6	10.4	15.6	15.6	13.0
	Δ_{ult} (mm)	29.7	19.0	29.7	21.0	36.4	29.5	27.6
	u	21.1	12.3	24.5	11.1	45.5	31.1	21.2
	$F_{(1-3)}$	37.5 - 56.3%	23.9 - 30%	7.6 -20.1%	4.2 - 12.5%	19.3 - 26.3%	25.8 - 27.4%	19.7 - 28.8%
NEGATIVE	k_i (kN/mm)	1.13	1.64	0.97	0.84	1.38	1.07	1.17
	F_y (kN)	0.80	0.80	0.90	0.80	0.78	0.85	0.82
	F_{max} (kN)	1.59	1.20	1.72	1.20	1.43	1.54	1.45
	F_{ult} (kN)	1.27	0.96	1.38	0.96	1.14	1.23	1.16
	Δ_y (mm)	0.8	1.1	1.3	1.4	1.0	1.2	1.1
	Δ_{max} (mm)	20.8	10.4	20.8	10.4	20.8	20.8	17.3
	Δ_{ult} (mm)	31.2	20.0	31.2	22.5	36.4	34.0	29.2
	u	37.6	17.9	24.8	16.5	38.3	28.8	26.2
	$F_{(1-3)}$	32.8 - 40.6%	8.3 -37.5%	20.7 - 27.6%	7.2 - 24.1%	22.8 - 33.3%	28.3 - 38.1%	20 - 33.5%

Table 8-40: Test results for φ3.15 Nails with 17mm Ply loaded perpendicular to grain (single nail).

		TEST 1	TEST 2	TEST 3	TEST 4	TEST 5	TEST 6	AVERAGE
POSITIVE	k_i (kN/mm)	1.45	1.13	1.21	1.54	2.05	1.93	1.55
	F_y (kN)	0.75	0.68	0.90	0.81	0.73	0.70	0.76
	F_{max} (kN)	1.31	1.20	1.29	1.23	1.23	1.16	1.24
	F_{ult} (kN)	1.04	0.96	1.03	0.98	0.98	0.92	0.99
	Δ_y (mm)	0.8	0.8	1.6	1.3	1.2	1.2	1.2
	Δ_{max} (mm)	8.2	12.2	8.2	8.2	12.2	12.2	10.2
	Δ_{ult} (mm)	11.0	11.0	14.0	28.0	14.0	19.0	16.2
	u	13.3	13.3	9.0	21.4	11.7	15.8	14.0
	$F_{(1-3)}$	23.1 - 51.9%	12.8 - 22.6%	9.4 - 26%	7.7 - 12%	21.7 - 34.8%	8.3 - 22.7%	13.8 - 28.3%
NEGATIVE	k_i (kN/mm)	0.51	2.31	1.16	1.05	1.06	1.70	1.30
	F_y (kN)	0.60	0.81	0.73	0.66	0.63	0.75	0.70
	F_{max} (kN)	1.43	1.39	1.28	1.29	1.32	1.31	1.33
	F_{ult} (kN)	1.14	1.11	1.02	1.03	1.06	1.04	1.07
	Δ_y (mm)	1.3	0.8	1.1	1.4	0.8	1.1	1.1
	Δ_{max} (mm)	16.4	8.2	10.0	10.0	10.0	10.0	10.8
	Δ_{ult} (mm)	20.4	13.0	13.4	30.0	15.0	19.0	18.5
	u	15.6	15.7	11.9	21.3	19.2	17.0	16.9
	$F_{(1-3)}$	39.9 - 100%	16.4 - 23.6%	5.3 - 30.6%	16.3 - 20.8%	5.8 - 9.6%	7.7 - 11.5%	15.2 - 32.7%

Table 8-41: Test results for φ3.15 Nails with 25mm Ply loaded parallel to grain (single nail).

		TEST 1	TEST 2	TEST 3	TEST 4	TEST 5	TEST 6	AVERAGE
POSITIVE	k_i (kN/mm)	1.34	1.09	1.61	0.67	0.91	1.26	1.15
	F_y (kN)	0.80	0.83	0.80	0.83	0.83	1.00	0.85
	F_{max} (kN)	1.28	1.57	1.29	1.19	1.60	1.26	1.36
	F_{ult} (kN)	1.02	1.25	1.03	0.95	1.28	1.01	1.09
	Δ_y (mm)	1.1	1.0	1.2	1.5	1.0	1.5	1.2
	Δ_{max} (mm)	11.6	11.6	11.6	11.6	29.4	8.4	14.0
	Δ_{ult} (mm)	21.0	24.0	29.4	29.4	29.4	17.0	25.0
	u	18.8	23.5	24.3	19.6	30.3	11.3	20.5
	$F_{(1-3)}$	29.2 - 45.8%	29.6 - 45.8%	17.6 - 25.5%	9.1 - 24.2%	77.4 - 80.6%	11.6 - 22.5%	29.1 - 40.8%
NEGATIVE	k_i (kN/mm)	1.21	1.04	1.91	2.49	1.85	1.67	1.69
	F_y (kN)	0.93	0.91	1.03	1.03	1.03	0.90	0.97
	F_{max} (kN)	1.29	1.74	1.28	1.25	1.60	1.34	1.41
	F_{ult} (kN)	1.03	1.39	1.02	1.00	1.28	1.07	1.13
	Δ_y (mm)	1.3	1.0	1.4	2.2	1.1	1.5	1.4
	Δ_{max} (mm)	8.5	8.5	8.5	8.5	25.2	8.5	11.3
	Δ_{ult} (mm)	16.0	23.0	22.0	22.0	27.0	18.0	21.3
	u	12.7	22.5	15.6	10.1	24.1	12.0	15.1
	$F_{(1-3)}$	10.9 - 26.4%	11.5 - 21.2%	2.8 - 18.7%	7.6 - 27.7%	35 - 60%	21.5 - 38.7%	14.9 - 32.1%

Table 8-42: Test results for φ3.15 Nails with 25mm Ply loaded perpendicular to grain (single nail).

		TEST 1	TEST 2	TEST 3	TEST 4	TEST 5	TEST 6	AVERAGE
POSITIVE	k_i (kN/mm)	0.86	1.16	1.41	1.35	2.24	2.92	1.66
	F_y (kN)	0.65	0.90	1.00	0.92	0.85	1.03	0.89
	F_{max} (kN)	1.09	1.12	1.51	1.26	1.17	1.22	1.23
	F_{ult} (kN)	0.87	0.90	1.20	1.01	0.93	0.97	0.98
	Δ_y (mm)	1.5	1.6	1.8	1.6	1.3	25.1	5.5
	Δ_{max} (mm)	8.2	8.2	16.4	8.2	8.2	2.4	8.6
	Δ_{ult} (mm)	13.0	14.0	18.1	18.1	14.0	16.6	15.6
	u	8.9	9.0	10.1	11.3	10.7	8.3	9.7
	$F_{(1-3)}$	17.1 - 30.9%	6.7 - 33.3%	58.6 - 69%	15.7 - 37.3%	6.9 - 17.7%	11.5 - 21.8%	19.4 - 35.0%
NEGATIVE	k_i (kN/mm)	1.33	1.37	1.70	1.36	2.73	1.18	1.61
	F_y (kN)	0.83	0.90	0.85	0.80	0.75	0.70	0.80
	F_{max} (kN)	1.16	1.23	1.25	1.20	1.05	1.40	1.21
	F_{ult} (kN)	0.92	0.98	1.00	0.96	0.84	1.12	0.97
	Δ_y (mm)	1.4	1.8	1.3	1.2	1.3	1.1	1.3
	Δ_{max} (mm)	8.2	4.8	8.2	8.2	8.2	16.4	9.0
	Δ_{ult} (mm)	11.8	12.0	16.6	11.7	19.7	19.0	15.1
	u	8.7	6.9	13.2	10.0	15.0	17.8	11.5
	$F_{(1-3)}$	9.5 - 14%	14.3 - 22.4%	6.4 - 19.1%	7.2 - 19.8%	7.3 - 17.1%	13.9 - 51.3%	9.8 - 24%

ϕ3.55x90mm Nails

Table 8-43: Test results for φ3.55 Nails with 12mm Ply loaded parallel to grain (single nail).

		TEST 1	TEST 2	TEST 3	TEST 4	TEST 5	TEST 6	AVERAGE
POSITIVE	k_i (kN/mm)	1.12	0.94	1.74	1.02	0.98	2.13	1.32
	F_y (kN)	0.89	0.84	0.91	1.03	1.03	1.18	0.98
	F_{max} (kN)	1.46	1.51	1.28	1.63	1.51	1.49	1.48
	F_{ult} (kN)	1.17	1.20	1.02	1.30	1.20	1.19	1.18
	Δ_y (mm)	1.3	1.2	1.3	1.3	1.3	1.3	1.3
	Δ_{max} (mm)	11.9	11.9	11.9	11.9	11.9	8.0	11.3
	Δ_{ult} (mm)	24.0	21.5	21.0	23.0	19.0	19.8	21.4
	u	18.3	17.8	15.9	17.4	14.4	15.0	16.4
	$F_{(1-3)}$	24.1 - 58.6%	8.6 - 33.6%	21.8 - 38.5%	10.2 - 38.1%	11.7 - 33.3%	5.7 - 25.9%	13.7 - 38%
NEGATIVE	k_i (kN/mm)	0.20	1.78	-4.95	0.45	1.60	1.91	0.17
	F_y (kN)	0.89	0.91	0.86	1.03	0.99	0.80	0.91
	F_{max} (kN)	1.43	1.55	1.32	1.72	1.60	1.40	1.50
	F_{ult} (kN)	1.14	1.24	1.06	1.38	1.28	1.12	1.20
	Δ_y (mm)	1.0	1.2	1.3	1.1	1.2	0.9	1.1
	Δ_{max} (mm)	11.9	11.9	8.0	11.9	15.8	11.9	11.9
	Δ_{ult} (mm)	25.0	24.2	25.2	24.5	20.0	24.0	23.8
	u	24.5	20.7	20.0	21.9	17.1	26.1	21.5
	$F_{(1-3)}$	3.8 - 14.3%	4.5 - 28.8%	19.6 - 25.5%	2.6 - 28.8%	27.4 - 38.5%	25 - 32.1%	13.8 - 28%

Table 8-44: Test results for φ3.55 Nails with 12mm Ply loaded perpendicular to grain (single nail).

		TEST 1	TEST 2	TEST 3	TEST 4	TEST 5	TEST 6	AVERAGE
POSITIVE	k_i (kN/mm)	0.82	3.11	1.18	1.16	1.05	4.25	1.93
	F_y (kN)	1.03	1.04	0.96	1.09	1.09	0.98	1.03
	F_{max} (kN)	1.29	1.56	1.18	1.32	1.59	1.42	1.39
	F_{ult} (kN)	1.03	1.24	0.94	1.06	1.27	1.13	1.11
	Δ_y (mm)	1.8	1.1	5.1	1.7	4.0	1.3	2.5
	Δ_{max} (mm)	4.8	9.6	9.6	9.6	12.9	12.9	9.9
	Δ_{ult} (mm)	12.0	13.0	14.1	18.2	18.1	15.0	15.1
	u	6.6	11.5	2.7	10.5	4.5	11.5	6.0
	$F_{(1-3)}$	11.5 - 17.3%	13.1 - 34.4%	9.3 - 15.6%	2.7 - 23.4%	16.1 - 41.9%	10.8 - 30.1%	10.6 - 27.1%
NEGATIVE	k_i (kN/mm)	0.76	1.55	0.56	0.79	1.07	3.06	1.30
	F_y (kN)	0.95	1.03	0.70	0.80	1.05	0.90	0.90
	F_{max} (kN)	1.43	1.55	1.10	1.42	1.60	1.43	1.42
	F_{ult} (kN)	1.14	1.24	0.88	1.13	1.28	1.14	1.14
	Δ_y (mm)	1.8	1.5	2.4	1.7	1.9	1.9	1.9
	Δ_{max} (mm)	8.2	8.0	8.0	8.0	9.6	8.0	8.3
	Δ_{ult} (mm)	14.1	12.8	24.0	18.0	24.0	19.0	18.7
	u	7.7	8.8	9.9	10.6	12.4	10.0	9.9
	$F_{(1-3)}$	18.4 - 22%	22.6 - 29.7%	16.8 - 27.3%	16.4 - 33.8%	7.3 - 25%	26.6 - 30.1%	18 - 28%

Table 8-45: Test results for φ3.55 Nails with 17mm Ply loaded parallel to grain (single nail).

		TEST 1	TEST 2	TEST 3	TEST 4	TEST 5	TEST 6	AVERAGE
POSITIVE	k_i (kN/mm)	0.44	0.92	0.67	0.58	1.10	1.37	0.85
	F_y (kN)	1.15	0.85	0.80	0.80	0.78	0.85	0.87
	F_{max} (kN)	1.74	1.37	1.34	1.39	1.34	1.57	1.45
	F_{ult} (kN)	1.39	1.09	1.07	1.11	1.07	1.25	1.16
	Δ_y (mm)	1.7	1.8	1.9	1.5	1.0	1.0	1.5
	Δ_{max} (mm)	12.9	12.9	12.9	12.9	12.9	12.9	12.9
	Δ_{ult} (mm)	20.0	20.0	27.0	26.0	25.0	24.0	23.7
	u	11.6	11.1	14.2	17.8	25.8	24.7	16.1
	$F_{(1-3)}$	15 - 39.5%	9.7 - 20.6%	5.3 - 16.7%	9.7 - 20.6%	17.6 - 25.1%	23.3 - 29.7%	13.5 - 25.4%
NEGATIVE	k_i (kN/mm)	0.28	1.86	2.06	2.38	1.37	1.59	1.59
	F_y (kN)	1.15	1.03	1.00	1.00	0.80	0.90	0.98
	F_{max} (kN)	1.77	1.34	1.45	1.43	1.34	1.54	1.47
	F_{ult} (kN)	1.41	1.07	1.16	1.14	1.07	1.23	1.18
	Δ_y (mm)	1.7	1.5	1.6	2.1	1.3	1.1	1.5
	Δ_{max} (mm)	9.6	9.6	9.6	9.6	17.2	17.2	12.1
	Δ_{ult} (mm)	23.8	21.4	26.0	26.0	27.0	22.0	24.4
	u	14.4	14.7	16.8	12.1	21.4	20.6	16.0
	$F_{(1-3)}$	14.3 - 28.6%	8.2 - 17.6%	6.6 - 17%	12.6 - 19.6%	21.3 - 25.1%	12.8 - 32.9%	12.6 - 23.4%

Table 8-46: Test results for φ3.55 Nails with 17mm Ply loaded perpendicular to grain (single nail).

		TEST 1	TEST 2	TEST 3	TEST 4	TEST 5	TEST 6	AVERAGE
POSITIVE	k_i (kN/mm)	0.90	0.96	1.08	2.19	0.65	0.47	1.04
	F_y (kN)	0.91	1.00	1.00	1.00	0.80	0.90	0.93
	F_{max} (kN)	1.35	1.54	1.25	1.46	1.26	1.25	1.35
	F_{ult} (kN)	1.08	1.23	1.00	1.17	1.01	1.00	1.08
	Δ_y (mm)	1.7	1.5	1.5	1.4	1.7	1.8	1.6
	Δ_{max} (mm)	12.2	12.2	8.2	8.2	8.2	12.2	10.2
	Δ_{ult} (mm)	15.5	15.0	15.9	14.8	21.6	19.0	17.0
	u	9.4	10.3	10.9	10.5	12.6	10.6	10.7
	$F_{(1-3)}$	14.3 - 27.1%	16.1 - 41%	7.6 - 17.7%	13.5 - 22.8%	6.5 - 16.7%	18.8 - 28%	12.8 - 25.5%
NEGATIVE	k_i (kN/mm)	0.97	1.66	1.28	0.80	2.08	0.95	1.29
	F_y (kN)	0.81	0.95	0.90	0.90	0.80	0.83	0.86
	F_{max} (kN)	1.37	1.39	1.45	1.37	1.25	1.43	1.37
	F_{ult} (kN)	1.10	1.11	1.16	1.09	1.00	1.14	1.10
	Δ_y (mm)	1.5	1.1	1.0	1.6	0.9	1.3	1.2
	Δ_{max} (mm)	8.2	8.2	8.2	8.2	8.2	12.2	8.9
	Δ_{ult} (mm)	18.0	21.3	11.3	18.0	18.0	18.5	17.5
	u	12.3	19.9	11.0	11.3	20.7	14.7	14.4
	$F_{(1-3)}$	8.9 - 21.4%	7.9 - 20.6%	21.1 - 23.9%	15.6 - 18.5%	11.6 - 24.9%	11.7 - 25.8%	12.8 - 22.5%

Table 8-47: Test results for φ3.55 Nails with 25mm Ply loaded parallel to grain (single nail).

		TEST 1	TEST 2	TEST 3	TEST 4	TEST 5	TEST 6	AVERAGE
POSITIVE	k_i (kN/mm)	1.00	0.87	0.76	0.64	1.11	0.59	0.83
	F_y (kN)	1.10	1.00	0.88	0.88	1.00	0.98	0.97
	F_{max} (kN)	1.60	1.39	1.48	1.59	1.34	1.60	1.50
	F_{ult} (kN)	1.28	1.11	1.18	1.27	1.07	1.28	1.20
	Δ_y (mm)	1.6	1.7	1.7	1.6	1.6	1.8	1.6
	Δ_{max} (mm)	9.2	9.2	13.8	13.8	9.2	9.2	10.7
	Δ_{ult} (mm)	20.0	22.0	20.0	20.0	19.0	17.8	19.8
	u	12.9	13.3	12.1	12.9	12.3	9.9	12.2
	$F_{(1-3)}$	6.3 - 12.5%	2.5 - 9.7%	12.3 - 14%	9.7 - 24.2%	2.6 - 8.2%	4.7 - 12.5%	6.3 - 13.5%
NEGATIVE	k_i (kN/mm)	1.94	2.38	1.30	1.50	1.20	1.23	1.59
	F_y (kN)	1.03	1.13	0.98	1.10	1.00	0.98	1.03
	F_{max} (kN)	1.62	1.59	1.49	1.68	1.45	1.72	1.59
	F_{ult} (kN)	1.29	1.27	1.19	1.34	1.16	1.38	1.27
	Δ_y (mm)	1.5	1.7	1.7	1.5	1.6	1.3	1.5
	Δ_{max} (mm)	9.2	9.2	9.2	9.2	9.2	9.2	9.2
	Δ_{ult} (mm)	21.3	19.0	22.5	19.5	21.5	21.0	20.8
	u	14.2	11.5	13.6	13.0	13.9	16.2	13.6
	$F_{(1-3)}$	14.1 - 21.9%	5.4 - 8.5%	10 - 16.7%	10.3 - 13.4%	10.8 - 19.6%	7 - 18.6%	9.6 - 16.4%

Table 8-48: Test results for φ3.55 Nails with 25mm Ply loaded perpendicular to grain (single nail).

		TEST 1	TEST 2	TEST 3	TEST 4	TEST 5	TEST 6	AVERAGE
POSITIVE	k_i (kN/mm)	1.26	1.47	1.22	1.27	2.58	0.88	1.45
	F_y (kN)	1.10	1.20	0.95	1.15	1.35	1.15	1.15
	F_{max} (kN)	1.39	1.72	1.39	1.65	1.72	1.71	1.59
	F_{ult} (kN)	1.11	1.38	1.11	1.32	1.38	1.36	1.27
	Δ_y (mm)	3.5	1.2	1.8	1.7	1.4	1.8	1.9
	Δ_{max} (mm)	7.2	9.6	7.2	7.2	7.2	7.2	7.6
	Δ_{ult} (mm)	19.8	17.2	20.0	14.2	14.0	16.5	17.0
	u	5.6	14.7	11.1	8.6	10.3	9.4	9.0
	$F_{(1-3)}$	12.1 - 19.4%	4.7 - 15%	12.1 - 19.4%	5.8 - 8.8%	8.4 - 12.8%	6 - 10.4%	8.2 - 14.3%
NEGATIVE	k_i (kN/mm)	1.67	1.68	1.67	1.73	3.35	1.10	1.87
	F_y (kN)	1.03	0.89	0.75	1.00	1.05	0.95	0.94
	F_{max} (kN)	1.20	1.68	1.20	1.68	1.68	1.51	1.49
	F_{ult} (kN)	0.96	1.34	0.96	1.34	1.34	1.20	1.19
	Δ_y (mm)	3.7	1.7	1.5	1.0	1.1	1.5	1.7
	Δ_{max} (mm)	14.4	15.7	14.4	9.6	9.6	9.6	12.2
	Δ_{ult} (mm)	24.0	16.2	24.0	15.4	17.0	20.5	19.5
	u	6.4	9.5	16.4	15.1	15.9	14.1	11.2
	$F_{(1-3)}$	10.4 - 20.8%	2.6 - 7.9%	10.4 - 20.8%	6.9 - 25.4%	1.6 - 5.4%	10.3 - 20.3%	7 - 16.8%